Simulating Ship Motions in the Time Domain

by

Harry Bradford Bingham

BS, Applied and Engineering Physics, Cornell, 1984

MS, Ocean Engineering, Stevens Institute of Technology, 1988

Submitted to the Department of Ocean Engineering
in partial fulfillment of the requirements for the degree of

Doctor of Philosophy in Hydrodynamics

at the

MASSACHUSETTS INSTITUTE OF TECHNOLOGY

February 1994

Author .....
Department of Ocean Engineering
January 25th 1994

Certified by .....
J. Nicholas Newman
Professor of Naval Architecture
Thesis Supervisor

Accepted by .....
A. Douglas Carmichael
Chairman, Departmental Committee on Graduate Students

Simulating Ship Motions in the Time Domain

by

Harry Bradford Bingham

Submitted to the Department of Ocean Engineering
on January 25^{th} 1994, in partial fulfillment of the
requirements for the degree of
Doctor of Philosophy in Hydrodynamics

Abstract

A three-dimensional panel method is used to solve the Neumann-Kelvin linearized ship-motions problem. The initial-boundary-value problem is recast as an integral equation using the transient free-surface Green function. This integral equation is discretized in space using planar panels, on which the potential is assumed to be constant, and in time using the trapezoid rule. Collocation is performed at the centroids of each panel.

It is argued that the integral equation (in either its potential formulation or as a source-only formulation) has a Rankine-type kernal and therefore has a unique solution, in contrast to the analogous frequency-domain integral equation. Discrete solutions of the transient integral equation however, contain a non-physical oscillation which, at zero forward speed, persists indefinitely in time but has a frequency content which is localized around the irregular frequencies in a way which is nearly identical to what is observed in discrete frequency-domain solutions. At non-zero forward speed the oscillation becomes of finite duration in time, and of increasing bandwidth in frequency, as the speed is increased so that it is no longer clearly associated with the irregular frequencies. These errors are removed from the solution by refinement of the spatial and temporal discretizations.

A technique of asymptotic continuation is developed in order to extend a relatively short calculation to large time in a rational way. The asymptotics of the transient numerical solution are analyzed and found to support the theory that the linearized problem has a finite solution (in general) at the critical frequency corresponding to $\tau = \frac{\omega_e U}{g} = \frac{1}{4}$. A technique for improving the satisfaction of the body boundary condition without the need for numerical spatial derivatives is also presented.

Calculations of the steady and the unsteady hydrodynamic forces on two ship hulls are included and compared to experiments, as well as to calculations made in the frequency domain. The hydrodynamic coefficients are used in the transient equations of motion to perform a simulation of a ship traveling through a Pierson-Moskowitz sea.

Thesis Supervisor: J. Nicholas Newman
Title: Professor of Naval Architecture

Acknowledgments

I wish to express my gratitude to the many people who have supported, encouraged and directed me in this endevour. To Nancy for suffering my constant preoccupation and making everything worthwhile. To my parents Harry H. and Judy for their sacrifice and for instilling in me a desire to learn. To my grandparents Brad and Vera Wells; and Ernestine and Hilgard Pannes for for their love and for the examples they have set for me.

Working with Professor J. N. Newman over the last four years has been a tremendous pleasure and an inspiration. His guidance and patience have kept me firmly on course and I am deeply grateful for all that he has taught me. Special thanks are due to the other members of my committee: to Dr. F. T. Korsmeyer who was never too busy to discuss the details, and whose clear insight has kept me from capsizing many a time; and to Prof. P. D. Sclavounos for his unparalleled experience with this problem and his invaluable advice.

I would like to express my appreciation to all of the members of the Computational Hydrodynamics Facility and to the Department of Ocean Engineering for creating a very special atmosphere for hydrodynamic research. In particular to Prof. D. K. Yue for his stimulating guidance. Also to Dr. Polinsky, colleague and friend.

Financial support for this work was provided by the Office of Naval Research, contract #N00014-90-J1160.

Contents

1 Introduction 12

2 Mathematical Formulation 17

2.1 Equations of Motion 17

2.2 The Exact Boundary Value Problem 18

2.3 Linearization 20

2.4 An Integral Equation Representation 23

2.5 A Source-Only Integral Equation 24

2.6 Uniqueness of Solutions 25

2.6.1 The Transient Integral Equations 26

2.6.2 Time-Harmonic Oscillations at Zero Speed 28

2.7 Asymptotic Behavior of the Solution 30

2.8 The Radiation Problem 32

2.8.1 Impulse-Response Functions 34

2.8.2 Frequency-Response Functions 39

2.9 The Steady Problem 40

2.9.1 Impulsive Acceleration 40

2.9.2 Non-Impulsive Acceleration 42

2.10 The Diffraction Problem 42

2.11 Other Approximations of the m-terms 44

2.11.1 The Double-Body Flow 46

3 Numerical Solution 48

3.1 Evaluating the Waterline Integral 49
3.2 A Discrete Integral Equation 52
3.3 Computational Cost and Storage Requirements 54
3.4 Asymptotic Continuation at Forward Speed 55
3.5 Numerical Fourier Transform 64
3.5.1 Analytic Transform of the Asymptotics 64
3.6 Irregular Behavior of Solutions 66
3.7 Convergence of the Calculations 79
3.7.1 Wigley Hull 79
3.7.2 Series 60 Block 70 Hull 80

4 Results **90**
4.1 Hull Geometries for the Calculations 90
4.1.1 Wigley Hull 90
4.1.2 Series 60 Hull 91
4.2 Steady Forces 96
4.3 Unsteady Forces 96
4.4 Simulation 109

5 Discussion **112**

A Derivation of the integral equations **116**
A.1 An Integral Equation in Earth-Fixed Coordinates 117
A.2 Steady Forward Speed 120

B Derivation of Source-Only Formulations **122**
B.1 Source-Only Integral Equations 122
B.2 Decomposition of the Radiation Source Strength 124

C Absence of Homogeneous Solutions to the Integral Equation **125**
C.1 The Time-Harmonic Problem 125
C.2 The Transient Problem 127

List of Figures

2-1 The reference frames and surfaces of the problem. 19

3-1 The coordinate system tangent and normal to the hull surface. 51

3-2 Wigley hull at $F_n = 0.3$, added-mass coefficients calculated using both a $1/t$ and a $1/t^2$ continuation of the impulse-response function. . . . 58

3-3 Expanded view near $\tau = 1/4$ 58

3-4 Wigley hull at $F_n = 0.3$, damping coefficients calculated using both a $1/t$ and a $1/t^2$ continuation of the impulse-response function. 59

3-5 Expanded view near $\tau = 1/4$ 59

3-6 Wigley hull at $F_n = 0.3$, impulsive surge velocity potential on a bow-waterline panel. 60

3-7 Wigley hull at $F_n = 0.3$, potential on a panel and a least squares fitting of the data to two rates of decay. 60

3-8 Wigley hull at $F_n = 0.3$, a straight line least squares fit to the function $log(t \cdot f(t))$ where $f(t) =$ the values at the extrema of the potential. 61

3-9 Wigley hull at $F_n = 0.25$, impulsive surge velocity potential on a bow-waterline panel. 61

3-10 Wigley hull at $F_n = 0.2$, impulsive surge velocity potential on a bow-waterline panel. 62

3-11 Wigley hull at $F_n = 0.15$, impulsive surge velocity potential on a bow-waterline panel. 62

3-12 Wigley hull at $F_n = 0.1$, impulsive surge velocity potential on a bow-waterline panel. 63

3-13 Wigley hull at $F_n = 0.1$, expanded view of the large-time asymptotics of the potential and a least squares fit of the data to two rates of decay. 63
3-14 Impulsive acceleration heave-heave memory function for a Wigley hull at $F_n = 0.0$ 69
3-15 Expanded view of the effect of the irregular-frequencies, $F_n = 0.0$ . . 69
3-16 Heave-heave added-mass coefficients for a Wigley hull at $F_n = 0.0$ . . 70
3-17 Heave-heave damping coefficients for a Wigley hull at $F_n = 0.0$ . . . 70
3-18 Expanded view of the heave-heave added-mass coefficients for a Wigley hull at $F_n = 0.0$ 71
3-19 Expanded view of the heave-heave damping coefficients for a Wigley hull at $F_n = 0.0$ 71
3-20 Surge-surge memory function for a Wigley hull at $F_n = 0.0$ 72
3-21 Expanded view, $F_n = 0.0$ 72
3-22 Impulsive acceleration surge-surge memory function for a Wigley hull at $F_n = 0.1$ 73
3-23 Expanded view, $F_n = 0.1$ 73
3-24 Impulsive acceleration surge-surge memory function for a Wigley hull at $F_n = 0.2$ 74
3-25 Impulsive acceleration surge-surge memory function for a Wigley hull at $F_n = 0.3$ 74
3-26 Impulsive acceleration surge-surge memory function for a Wigley hull at $F_n = 0.4$ 75
3-27 Pitch-pitch damping coefficients for a Wigley hull at $F_n = 0.0$ 75
3-28 Pitch-pitch damping coefficients for a Wigley hull at Fn=0.1 76
3-29 Pitch-pitch damping coefficients for a Wigley hull at $F_n = 0.2$ 76
3-30 Pitch-pitch damping coefficients for a Wigley hull at $F_n = 0.3$ 77
3-31 Pitch-pitch damping coefficients for a Wigley hull at $F_n = 0.4$ 77
3-32 Pitch-pitch response of a Wigley hull at $F_n = 0.3$, showing how the the irregular behavior in the time domain is reduced with refinement of the discretization. 78

3-33 Pitch-pitch damping coefficients of a Wigley hull at $F_n = 0.3$, showing the corresponding reduction of the irregular behavior in the frequency domain. 78
3-34 Convergence with time step size of the steady wave resistance on a Wigley hull at $F_n = 0.3$, 64 panels. 81
3-35 Convergence with time step size of the steady wave resistance on a Wigley hull at $F_n = 0.3$, 144 panels. 81
3-36 Convergence with time step size of the steady wave resistance on a Wigley hull at $F_n = 0.3$, 256 panels. 82
3-37 Convergence of the steady wave resistance on a Wigley hull at $F_n = 0.3$. 82
3-38 Convergence with time step size of the steady sinkage force on a Wigley hull at $F_n = 0.3$, 64 panels. 83
3-39 Convergence with time step size of the steady sinkage force on a Wigley hull at $F_n = 0.3$, 144 panels. 83
3-40 Convergence with time step size of the steady sinkage force on a Wigley hull at $F_n = 0.3$, 256 panels. 84
3-41 Convergence of the steady sinkage force on a Wigley hull at $F_n = 0.3$. 84
3-42 Convergence with time step size of the steady trim moment on a Wigley hull at $F_n = 0.3$, 64 panels. 85
3-43 Convergence with time step size of the steady trim moment on a Wigley hull at $F_n = 0.3$, 144 panels. 85
3-44 Convergence with time step size of the steady trim moment on a Wigley hull at $F_n = 0.3$, 256 panels. 86
3-45 Convergence of the steady trim moment on a Wigley hull at $F_n = 0.3$. 86
3-46 Comparison of the steady wave resistance calculated using an impulsive and a gradual acceleration of the ship, Wigley hull at $F_n = 0.3$. . . . 87
3-47 Comparison of the steady sinkage force calculated using an impulsive and a gradual acceleration of the ship, Wigley hull at $F_n = 0.3$. . . . 87
3-48 Comparison of the steady trim moment calculated using an impulsive and a gradual acceleration of the ship, Wigley hull at $F_n = 0.3$. . . . 88

3-49 Convergence of the steady wave resistance on a Series 60 block 70 hull at $F_n = 0.3$. 88
3-50 Convergence of the steady sinkage force on a Series 60 block 70 hull at $F_n = 0.3$. 89
3-51 Convergence of the steady trim moment on a Series 60 block 70 hull at $F_n = 0.3$. 89

4-1 64 panel discretization of the Wigley hull. 92
4-2 144 panel discretization of the Wigley hull. 92
4-3 256 panel discretization of the Wigley hull. 93
4-4 576 panel discretization of the Wigley hull. 93
4-5 64 panel discretization of the Series 60 hull. 94
4-6 144 panel discretization of the Series 60 hull. 94
4-7 256 panel discretization of the Series 60 hull. 95
4-8 576 panel discretization of the Series 60 hull. 95
4-9 Wave resistance of the Wigley hull over a range of Froude numbers. . 98
4-10 Sinkage of the Wigley hull over a range of Froude numbers. 99
4-11 Trim angle of the Wigley hull over a range of Froude numbers. 99
4-12 Heave-heave added mass coefficients for a Wigley hull at $F_n = 0.3$ . . 100
4-13 Heave-heave damping coefficients for a Wigley hull at $F_n = 0.3$ 100
4-14 Heave-pitch added mass coefficients for a Wigley hull at $F_n = 0.3$ . . 101
4-15 Heave-pitch damping coefficients for a Wigley hull at $F_n = 0.3$ 101
4-16 Pitch-heave added mass coefficients for a Wigley hull at $F_n = 0.3$ . . 102
4-17 Pitch-heave damping coefficients for a Wigley hull at $F_n = 0.3$ 102
4-18 Pitch-pitch added mass coefficients for a Wigley hull at $F_n = 0.3$ . . . 103
4-19 Pitch-pitch damping coefficients for a Wigley hull at $F_n = 0.3$ 103
4-20 Heave exciting force coefficients for a Wigley hull at $F_n = 0.3$ 104
4-21 Heave exciting force phase angle for a Wigley hull at $F_n = 0.3$ 104
4-22 Pitch exciting force coefficients for a Wigley hull at $F_n = 0.3$ 105
4-23 Pitch exciting force phase angle for a Wigley hull at $F_n = 0.3$ 105

4-24 Heave-heave added mass coefficients for a Series 60 Block 70 hull at $F_n = 0.2$ 106
4-25 Heave-heave damping coefficients for a Series 60 hull at $F_n = 0.2$ . . . 106
4-26 Cross-coupling added mass coefficients for a Series 60 Block 70 hull at $F_n = 0.2$ 107
4-27 Cross-coupling damping coefficients in heave and pitch for a Series 60 Block 70 hull at $F_n = 0.2$ 107
4-28 Pitch-pitch added mass coefficients for a Series 60 Block 70 hull at $F_n = 0.2$ 108
4-29 Pitch-pitch damping coefficients for a Series 60 hull at $F_n = 0.2$ . . . 108
4-30 Time histories from a simulation of a Wigley hull at $F_n = 0.3, \beta = \pi$. From the top: incident wave elevation in the ship-fixed frame, heave response, pitch response. 110
4-31 Wigley hull at $F_n = 0.3, \beta = \pi$, the heave response-amplitude operator. 111
4-32 Wigley hull at $F_n = 0.3, \beta = \pi$, the pitch response-amplitude operator. 111

List of Tables

3.1 Estimates of the exponential decay rate α at various Froude numbers. 57

Chapter 1

Introduction

The classical problem of predicting the hydrodynamic forces on a ship as it travels through a seaway has been an active topic of investigation for over a century. William Froude [11] in 1861 appears to have been the first to tackle the unsteady oscillations of a ship in waves. 26 years later, Lord Kelvin [51] produced a mathematical explanation for the wave pattern observed behind a ship in steady translation through a calm sea. Since the turn of the century this approach, based on linearization along with the neglect of viscous and surface-tension forces, has been refined and applied to a variety of problems in Marine Hydrodynamics. An enlightening review of the Science of Naval Architecture from the time of Froude until the 1960's may be found in the Biographical Memoirs of Sir T. H. Havelock [47] (although the work of Krylov and Haskind [14] has been neglected). More detailed presentations of the modern theory of ship motions may be found in Ogilvie [46] or Newman [41].

With the advent of the high speed digital computer in the 1950's numerical solutions of the linearized formulations for general bodies began to appear, first using the two-dimensional strip theories [28] [45] [49] and more recently using three-dimensional methods. Several approaches have been followed in the effort to obtain three-dimensional numerical solutions to the sea-keeping problem and each exhibits its own advantages and limitations, in addition to those inherent in the mathematical statement itself. Typically these solutions are obtained using *boundary-element* (or *panel*) methods, where the boundary-value problem is recast as an integral equation

and solved at discrete points on the boundaries of the fluid domain. For solving problems where the mean position of the ship is traveling at a steady forward speed, the most promising panel methods fall into two categories: solutions using the transient free-surface Green function, where only the ship surface is discretized (*e.g.*: [24]; [30]; [23]; [3]; [33]; and [34]); and *Rankine* (or *Dawson-type*) methods, where simple source and dipole singularities are distributed on both the hull and a portion of the free surface. (*e.g.*: [39],[40],[4]).

The approach taken here is to use the transient free-surface Green function to derive a boundary-integral equation to be applied on the mean position of the body surface. This integral equation is discretized spatially using planar panels, upon which the potential is assumed to be constant, and enforced at the centroid of each panel, while the trapezoid rule is used for the integration in time. Linearization allows us to separate the effects of the ship's steady forward motion (the *steady problem*) from the scattering of the incident waves (the *diffraction problem*), and from the radiation of waves due to the unsteady motion of the ship (the *radiation problem*). Having been computed individually, the solutions to these three problems may be superimposed (and combined with an actual history of incident wave elevation) to construct a simulation of the ship's motion while traveling in a seaway.

In Chapter 2 the mathematical formulation of the problem is reviewed. Existence and uniqueness of solutions to the initial-boundary-value problem is assumed, and a proof is proposed for uniqueness of solutions to the integral equation. This is in contrast to the equivalent (zero speed) frequency-domain integral equation which does not have a unique solution at an infinite discrete set of frequencies (the irregular frequencies). The argument is based on showing that the kernel is formally of Rankine-type and therefore a non-trivial homogeneous solution to the integral equation does not exist. This argument applies equally well to the integral equation in either a potential or a source-only formulation.

The radiation problem is generalized using a series of canonical problems, related to each other through time derivatives, any of which can be used to obtain the impulse-response function. This generalization makes it clear that the steady problem can

be made identical to the surge radiation problem by regarding it as the steady-state limit of an impulsive acceleration of the ship to a forward speed U. The diffraction problem is discussed briefly, but emphasis is put on the forced motion problems.

Chapter 2 also contains a discussion of the asymptotic behavior of the solution at non-zero forward speed. This is intimately related to the resonance at the critical reduced frequency of $\tau = \frac{\omega_c U}{g} = 1/4$. The $\tau = 1/4$ resonance manifests itself in the time domain as a slowly decaying oscillation in the solution. The resonance is a physically observable phenomenon whose presence means that transients, at forward speed, require substantially more time to decay than they do at zero speed. At steady forward speed, the asymptotic behavior of the Green function is proportional to $\frac{1}{t} e^{i\omega_c t}$, corresponding to a logarithmic singularity at the critical frequency in Fourier-space [8]. It is known that the solution for an accelerating distribution of singularities, confined to the center-plane of a thin ship, behaves in the same way as $t \to \infty$ [52], and it is widely thought that the same behavior should be exhibited by three-dimensional solutions. Most of the numerical evidence also appears to support this view. It has been recently suggested however, that when singularities are distributed on the surface of a body of non-zero volume (which also satisfies certain geometric constraints) the solution in the frequency-domain is finite [13] [35], and that the decay rate of the transient solution is actually $\propto \frac{1}{t^2}$ [36]. In Chapter 3 a numerical experiment is presented which supports this theory.

Chapter 3 contains a description of the numerical implementation of the theory outlined in Chapter 2. Convergence of the calculations is shown using the computer code T$\bar{\text{I}}$MIT (TIme-domain wave analysis, MIT). T$\bar{\text{I}}$MIT was originally developed for bodies with zero forward speed as part of the dissertation by Korsmeyer [24]. It is based on efficient algorithms for calculating the transient free-surface Green function developed by Newman [42], and has been extended to bodies with a steady forward speed as part of this thesis. The tasks involved in this effort include inclusion of a waterline integral, repositioning the ship at each time step (either in a fixed or a moving coordinate system), and modification of the body boundary condition with the linearized effect of the steady forward velocity (the m-terms). This has been done in a

way which is essentially identical to what is described by Liapis [30]. In addition, the steady forces on the body are calculated both in an Earth-fixed coordinate system, as has been done by Lin and Yue [33] for example, and in the moving coordinate system using an impulsive acceleration. These two calculations are shown to agree to within 0.2%.

A technique of asymptotic continuation of the solution is developed which allows a truncated calculation to be extended to large time in a rational way. The Fourier transform of the asymptotic continuation is done analytically, and combined with a numerical transform of the calculated portion of the impulse-response function to obtain the complete frequency-response function.

Although the initial conditions prevent a non-trivial homogeneous solution from existing in the continuous integral equation (and this is shown in Appendix C), discrete numerical solutions show an irregular behavior when the discretizations are overly coarse. This irregular behavior manifests itself in the transient solution as a non-physical oscillation which, at zero forward speed, persists indefinitely and is the Fourier transform of the behavior which has been well documented in solutions obtained directly in the frequency domain. At non-zero forward speed the numerical irregularities are confined to a finite duration in time, and are absent from the solution after the ship has traveled approximately one ship length. This compression of the oscillation in time leads to an expansion in the frequency content until, at very high speed, the entire spectrum may become contaminated. This effect is removed by refining the discretizations in both space and time, but it may be desirable to attempt to reduce these effects by another means since they appear to be magnified by certain geometries and at high speeds. This is suggested as a topic of further research.

Chapter 4 presents calculations of the steady and the unsteady wave forces on two hulls traveling at steady forward speed. Calculations of the steady and the unsteady hydrodynamic forces agree well with experiment, and with calculations made using other linearized methods. Realistic ship forms, which usually have significant flare, are found to accentuate the numerical irregular effects in the solution, and the proper treatment of flare is suggested as another topic of further research. This chapter

also contains a transient simulation of the Wigley hull traveling through a Pierson-Moskowitz sea. A spectral analysis of this response produces response-amplitude operators which are in good agreement with experiment, as long as the equations of motion are solved accurately.

Chapter 5 contains some concluding remarks as well as suggestions for further research.

Chapter 2

Mathematical Formulation

2.1 Equations of Motion

During normal operating conditions the ship's weight, along with the steady hydrodynamic sinkage force and trim moment acting on it, are all balanced by the hydrostatic pressure acting on the hull, while its steady resistance is overcome by the propulsion. Assume these forces to be in balance, and consider small unsteady perturbations about this equilibrium condition. Through Newton's law, the dynamics of a ship's unsteady oscillations are governed by a balance between the inertia of the ship and the external forces acting upon it. This balance is complicated by the existence of radiated waves, as a consequence both of the ship's own motions and its scattering of the incident waves. This means that waves generated by the ship at any given time will persist indefinitely and, in principle, affect the ship at all subsequent times, a situation which is described mathematically by a convolution integral. As long as the unsteady perturbations to equilibrium are small, it is reasonable to consider the system to be linear, in which case the equations of motion may be written

$$\sum_{k=1}^{6} \Big[(M_{jk} + a_{jk})\ddot{x}_k(t) + b_{jk}\dot{x}_k(t) + (C_{jk} + c_{jk})x_k(t) + \int_{-\infty}^{t} d\tau\, K_{jk}^{(n)}(t-\tau)\frac{d^n x_k}{d\tau^n}(\tau)\Big] = X_j(t), \quad j = 1, 2, ..., 6. \tag{2.1}$$

This is essentially identical to the model proposed by Cummins [7] except that the radiation impulse-response function has been generalized (see Section 2.8.1). King [22] proposed an analogous form for the exciting forces on the right-hand side

$$X_j(t) = \int_{-\infty}^{\infty} d\tau \; K_{jD}(t-\tau)\zeta(\tau). \tag{2.2}$$

In equation (2.1), the ship's displacement from its mean position in each of its six rigid-body modes of motion is given by x_k, and the overdots indicate differentiation with respect to time. The excitation of the ship is provided by $\zeta(t)$, a time history of the incident wave elevation at some prescribed reference point on the free surface. The ship's inertia matrix is M_{jk}, and the linearized hydrostatic restoring force coefficients are given by C_{jk}. The hydrodynamic coefficients and the kernel of the convolution on the left-hand side of (2.1), and the kernel of the convolution on the right-hand side of (2.2), make up a set of radiation and diffraction impulse-response functions: the combination of a_{jk}, b_{jk}, c_{jk}, and $K_{jk}^{(n)}(t)$ is the force on the ship in the j^{th} direction due to an impulse in the nth derivative of the ship's motion in mode k. The function $K_{jD}(t,\beta)$ is the force on the ship in the j^{th} direction due to a uni-directional impulsive wave elevation incident from a heading angle of β.

In the following sections an integral representation of the hydrodynamic coefficients will be developed based on the assumptions of a potential flow, along with wave and body motions which are small enough that the boundary conditions can be linearized. With the hydrodynamic and hydrostatic coefficients in hand, a simulation of the ship translating in an ambient wave field may be carried out by integrating in time the above system of six coupled differential equations.

2.2 The Exact Boundary Value Problem

Consider a three-dimensional body in a semi-infinite fluid with a free surface, as shown in Figure 2-1. The ship moves through an incident wave field with velocity $\vec{U}(t)$, and is allowed to perform small unsteady oscillations about its mean position in any of

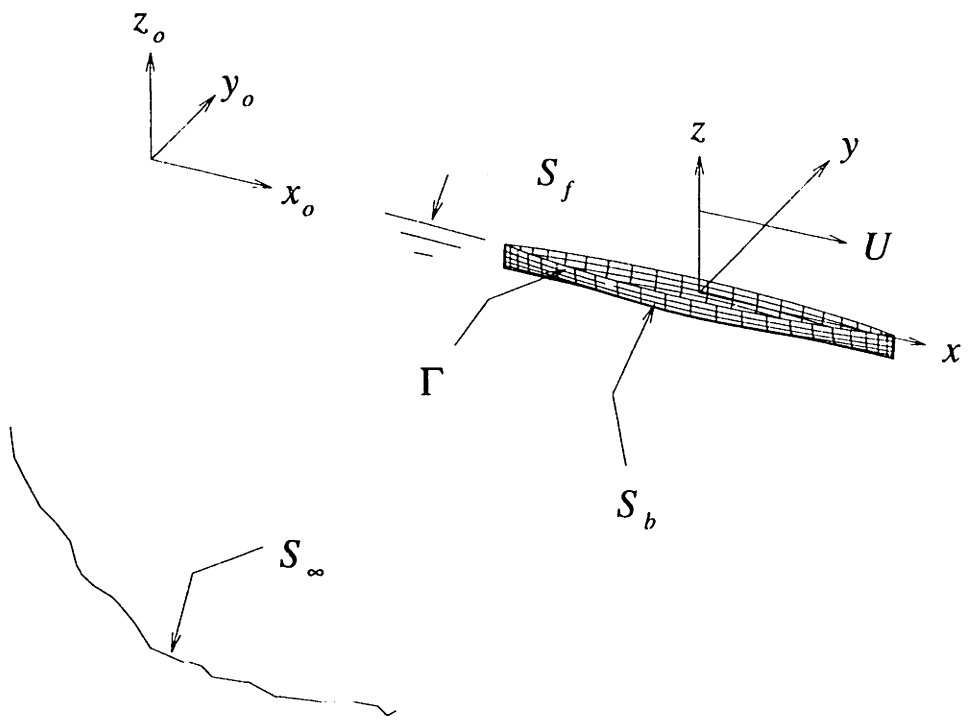

Figure 2-1: The reference frames and surfaces of the problem.

its six degrees of freedom. The fluid is assumed to be ideal and the flow irrotational, free of separation or lifting effects. Two coordinate systems will be employed in the ensuing derivations: the $\vec{x}_0$ system is fixed in space, and the $\vec{x}$ system is fixed to the mean position of the ship. At $t = 0$, these two coordinate systems coincide.

Subject to the above assumptions, the fluid velocity may be described by the gradient of a scalar velocity potential, $\vec{V}(\vec{x}_0, t) = \vec{\nabla}\Phi(\vec{x}_0, t)$. Conservation of mass requires that this potential satisfy the Laplace equation everywhere in the fluid:

$$\nabla^2\Phi = 0. \tag{2.3}$$

The pressure in the fluid, $p(\vec{x}_0, t)$, is given by Bernoulli's equation,

$$p = -\rho(\Phi_t + \frac{1}{2}V^2 + gz_0) + p_a, \tag{2.4}$$

where g is the acceleration due to gravity, ρ is the fluid density, and p_a is the atmo-

spheric pressure, which is assumed to be constant. (Partial differentiation is indicated when the independent variables x, y, z, t appear as subscripts.) If surface tension is neglected and the pressure on the free-surface is set equal to zero, a combined free-surface boundary condition may be written:

$$\Phi_{tt} + 2\nabla\Phi \cdot \nabla\Phi_t + \frac{1}{2}\nabla\Phi \cdot \nabla(\nabla\Phi \cdot \nabla\Phi) + g\Phi_{z_0} = 0 \quad \text{on } z_0 = \zeta, \tag{2.5}$$

where $\zeta(x_0, y_0, t)$ is the unknown free-surface elevation. Since the free-surface condition is second order in time, two initial conditions are required, and it will suffice to let

$$\left.\begin{aligned} \Phi &= 0 \\ \Phi_t &= 0 \end{aligned}\right\} \quad \text{on } z_0 = 0,\ t \leq t_0 \tag{2.6}$$

where t_0 is some arbitrary starting time for the fluid motions which will be taken to be zero in the radiation problems and $-\infty$ in the diffraction problem.

On the submerged portion of the hull the normal components of the fluid velocity and the ship's velocity must be equal:

$$\vec{n} \cdot \vec{\nabla}\Phi = \vec{V}_s \cdot \vec{n} \qquad \text{on } S_b(t), \tag{2.7}$$

where $S_b(t)$ is the exact position of the ship surface directed out of the fluid domain, $\vec{V}_s(\vec{x}_0, t)$, is the velocity of the point $\vec{x}_0$ on the ship, and $\vec{n}$ is the unit vector normal to the ship surface. Because of the initial conditions, fluid motions caused by the ship will go to zero at spatial infinity for all finite time,

$$\nabla\Phi \to 0, \qquad |\vec{x}| \to \infty \quad \text{for } t < \infty.$$

2.3 Linearization

In order to make further progress towards a solution, both the free-surface and the body boundary conditions, as well as the Bernoulli equation, will be linearized. Consider the coordinate system fixed to the mean position of the ship, which is traveling

along the x_0-axis with a constant speed U. We will think of the problem in two stages: First the ship is accelerated to a steady speed U, and all transients due to this initial acceleration are allowed to decay to zero; then the unsteady problem is solved, ideally with the ship in its equilibrium position (i.e. taking into account the sinkage and trim due to the steady forward speed). The total velocity potential, in the ship-fixed reference frame, is decomposed as follows:

$$\Phi = \bar{\Phi} + \bar{\phi} + \sum_{k=1}^{6} \phi_k + \phi_I + \phi_S. \tag{2.8}$$

The combination of $\bar{\Phi}(\vec{x})$ and $\bar{\phi}(\vec{x})$ is the potential due to the steady-state limit of the ship's uniform translation at forward speed U. This will be referred to as the *steady* problem. The *radiation* problem ensues when this translating ship is forced with some prescribed motion in a single rigid body mode k. The potential due to this motion is $\phi_k(\vec{x},t)$. If the steadily translating (but otherwise motionless) ship encounters an incident wave system with potential $\phi_I(\vec{x},t)$, the scattering of those waves by the ship will be described by the potential $\phi_S(\vec{x},t)$. The combination of ϕ_S and ϕ_I will be referred to as the diffraction potential, and solving for either the scattering or the diffraction potentials will be called the *diffraction* problem. Note that in the moving coordinate system, the fluid velocities in the far field will tend to those of the free stream and the undisturbed incident wave:

$$\vec{\nabla}\Phi \rightarrow -U\hat{\imath} + \vec{\nabla}\phi_I, \quad \text{as } |\vec{x}| \rightarrow \infty,$$

where $\hat{\imath}$ is the unit vector in the x-direction. Far from the ship the basis flow represented by $\bar{\Phi}$, must tend to the free stream, and this potential is assumed to represent the bulk of the steady flow around the ship. All of the remaining potentials represent flows which produce normal components of velocity at the ship which are small perturbations to those produced by the basis flow. The choice of $\bar{\Phi}$ is not unique, but the most common choices are the free-stream and the double-body flow.

If the decomposition of equation (2.8) is used in equations (2.7) and (2.5), the free-surface and body boundary conditions may be linearized about the mean positions

of the ship and free-surface boundaries. The simplest choice of a basis flow, and the one that will be used here, is the free-stream alone:

$$\bar{\Phi} = -Ux.$$

This choice leads to the familiar Neumann-Kelvin linearization of the pressure, the free-surface condition and the body boundary conditions:

$$p = -\rho\left(\phi_t - U\,\phi_x\right) \tag{2.9}$$

$$\left(\frac{\partial}{\partial t} - U\frac{\partial}{\partial x}\right)^2 \phi + g\frac{\partial \phi}{\partial z} = 0, \qquad \text{on } z = 0 \tag{2.10}$$

$$\begin{aligned} \vec{n}\cdot\nabla\bar{\phi} &= \quad U\,n_1 \qquad \text{on } \bar{S}_b \\ \vec{n}\cdot\nabla(\phi_I + \phi_S) &= \quad 0 \\ \vec{n}\cdot\nabla\phi_k &= \quad n_k\dot{x}_k + m_k x_k \quad . \end{aligned} \tag{2.11}$$

In equations (2.9) and (2.10), ϕ is again used to represent any of the perturbation potentials. The linearized body boundary conditions in equation (2.11) are to be applied on $\bar{S}_b$, the mean position of the ship surface, and the generalized unit normal n_k is defined by

$$\begin{aligned} (n_1, n_2, n_3) &= \quad \vec{n} \\ (n_4, n_5, n_6) &= \quad \vec{r}\times\vec{n}. \end{aligned} \tag{2.12}$$

The steady and the unsteady potentials are coupled through the presence of the so-called *m-terms* in the body boundary condition. For this linearization the m-terms simply reduce to

$$m_k = (0, 0, 0, 0, Un_3, -Un_2)$$

Other linearizations can be derived by making a different choice of basis flow, $\bar{\Phi}$. (See section 2.11 for example.)

2.4 An Integral Equation Representation

The foregoing initial-boundary-value problem can be recast as an integral equation by making use of the transient free-surface Green function. The three perturbation problems described above all satisfy the same boundary-value problem, with the exception of the body boundary condition. Consequently, the same integral equation may be used to solve for any of these potentials. The appropriate Green function is derived in Wehausen and Laitone [53] and can be written as

$$G(\vec{x};\vec{\xi},t) = G^{(0)}(\vec{x};\vec{\xi}) + H(\vec{x};\vec{\xi},t) \tag{2.13}$$

where

$$G^{(0)} = \left(\frac{1}{r} - \frac{1}{r'}\right), \qquad H = 2\int_0^\infty dk\,[1-\cos(\sqrt{gk}\,t)]\,e^{kZ}\,J_0(kR),$$

$$\left.\begin{matrix} r \\ r' \end{matrix}\right\} = \sqrt{(x-\xi)^2+(y-\eta)^2+(z\mp\zeta)^2},$$

$$Z = (z+\zeta), \qquad R = \sqrt{(x-\xi)^2+(y-\eta)^2},$$

and J_0 is the Bessel function of order zero. It is straightforward to verify that this function satisfies the initial-boundary-value problem without a body, except at the point $\vec{x} = \vec{\xi}$, and hence is a Green function for this problem. Applying Green's theorem to the time derivative of the potential, $\phi_\tau(\tau)$, and the Green function, $G(\vec{x},\vec{\xi},t-\tau)$, and integrating over the time history, results in the following integral equation for the potential at the present time

$$\begin{aligned} 2\pi\,\phi(\vec{x},t) &+ \int\!\!\int_{S_b} d\vec{\xi}\,\left(\phi(\vec{\xi},t)\,G^{(0)}_{n_\xi}(\vec{x},\vec{\xi}) - G^{(0)}(\vec{x},\vec{\xi})\,\phi_n(\vec{\xi},t)\right) \\ &- \int_{t_0}^t d\tau\,\int\!\!\int_{\bar{S}_t} d\vec{\xi}\,\left(\phi(\vec{\xi},\tau)\,G_{\tau n_\xi}(\vec{x},\vec{\xi},t-\tau) - G_\tau(\vec{x},\vec{\xi},t-\tau)\,\phi_n(\vec{\xi},\tau)\right) \\ &- \frac{U}{g}\int_{t_0}^t d\tau\,\int_\Gamma dl\,(\vec{n}_{2D}\cdot\hat{\imath})\,\Big[\phi(\vec{\xi},\tau)\,\left(G_{\tau\tau}(\vec{x},\vec{\xi},t-\tau) - UG_{\tau\xi}(\vec{x},\vec{\xi},t-\tau)\right) \\ &\qquad - G_\tau(\vec{x},\vec{\xi},t-\tau)\,\left(\phi_\tau(\vec{\xi},\tau) - U\phi_\xi(\vec{\xi},\tau)\right)\Big] = 0 \end{aligned} \tag{2.14}$$

where the ship waterline $\bar{\Gamma}$ is the intersection of $\bar{S}_b$ and the $z = 0$ plane, and $\vec{n}_{2D}$ is the two-dimensional normal to the body waterline lying in the plane of the free-surface. (The details of this derivation appear in Appendix A.) This equation is identical to that used by King *et al.* [23] among others.

2.5 A Source-Only Integral Equation

If fluid velocities are of interest, particularly on the body surface, then a source formulation may be preferred in order to avoid taking spatial derivatives of the potential numerically. The source formulation may be derived in the usual way by defining a flow in the region interior to the body specified by the scalar potential ϕ'. The integral equation for ϕ' is identical to the one for ϕ, except that the normal is defined in the opposite direction. These two equations may be added (the details are in Appendix B.1), and the source and dipole strengths defined as

$$\sigma = \frac{1}{4\pi}(\phi_n - \phi'_n), \qquad \mu = \frac{1}{4\pi}(\phi - \phi').$$

A source-only formulation is obtained by choosing $\phi' = \phi$ on the body boundary, and the result is a first-kind integral equation on $\bar{S}_b$ for σ if the potential is known (or an expression for the potential if the source strength is known):

$$\begin{aligned}\phi(\vec{x}) = & \iint_{\bar{S}_b} d\vec{\xi}\, G^{(0)}(\vec{x};\vec{\xi})\,\sigma(\vec{\xi},t) + \int_{t_0}^{t} d\tau \iint_{\bar{S}_b} d\vec{\xi}\, G_t(\vec{x};\vec{\xi},t-\tau)\,\sigma(\vec{\xi},\tau) \\ & -\frac{U^2}{g}\int_{t_0}^{t} d\tau \int_{\bar{\Gamma}} (\vec{n}_{2D}\cdot\hat{\imath})^2 dl\; G_t(\vec{x};\vec{\xi},t-\tau)\,\sigma(\vec{\xi},\tau) \end{aligned} \tag{2.15}$$

A more useful second-kind equation is obtained by operating on Equation (2.15) with $\vec{n}_x \cdot \vec{\nabla}_x$

$$\begin{aligned} 2\pi\sigma(\vec{x},t) + & \iint_{\bar{S}_b} d\vec{\xi} G^{(0)}_{n_x}(\vec{x};\vec{\xi})\,\sigma(\vec{\xi},t) + \int_{t_0}^{t} d\tau \iint_{\bar{S}_b} d\vec{\xi} G_{tn_x}(\vec{x};\vec{\xi},t-\tau)\,\sigma(\vec{\xi},\tau) \\ & -\frac{U^2}{g}\int_{t_0}^{t} d\tau \int_{\bar{\Gamma}} (\vec{n}_{2D}\cdot\hat{\imath})^2 dl G_{tn_x}(\vec{x};\vec{\xi},t-\tau))\,\sigma(\vec{\xi},\tau) = \vec{n}\cdot\vec{\nabla}\phi(\vec{x},t). \end{aligned} \tag{2.16}$$

A vector expression for the fluid velocity is obtained by operating on equation (2.15) with the operator $\vec{\nabla}_x$. This yields:

$$\int\int_{\bar{S}_b} d\vec{\xi}\vec{\nabla}_x G^{(0)}(\vec{x};\vec{\xi})\,\sigma(\vec{\xi},t) + \int_{t_0}^{t} d\tau \int\int_{\bar{S}_b} d\vec{\xi}\vec{\nabla}_x G_t(\vec{x};\vec{\xi},t-\tau)\,\sigma(\vec{\xi},\tau)$$
$$-\frac{U^2}{g}\int_{t_0}^{t} d\tau \int_{\Gamma}(\vec{n}_{2D}\cdot\hat{\imath})^2 dl\vec{\nabla}_x G_t(\vec{x};\vec{\xi},t-\tau))\,\sigma(\vec{\xi},\tau) = \vec{\nabla}\phi(\vec{x},t). \tag{2.17}$$

To obtain the velocity vector at any field point, equation (2.16) is first solved for the source strength, and then the source strength is used in equation (2.17) to calculate the three components of the velocity. In Appendix B the radiation source strengths and integral equations corresponding to the decomposition discussed in Section 2.8.1 are also developed.

2.6 Uniqueness of Solutions

There are two distinct issues of uniqueness connected with the problem which has been formulated in the preceding: the first concerns existence and uniqueness of solutions to the initial-boundary-value problem, and the second has to do with uniqueness of solutions to the integral equation.

A general proof of the existence and uniqueness of solutions to the linearized initial-boundary-value problem in an unbounded domain is not available. Stoker [50] however, provides a proof of uniqueness for transient motions in a bounded domain, and he writes:

> "... it seems clear that the uniqueness of the solution of the initial value problem is to be expected if the water fills an unbounded region, provided that appropriate assumptions concerning the behavior of the solution at ∞ are made."

For the special case of simple harmonic motion, at zero forward speed, John [19] has shown that trapping modes can exist for special geometries. This does not necessarily

suggest any non-uniqueness in the initial value problem however, and following Stoker we will assume that a unique solution exists.

In the following, a proof is proposed to show that the integral equations developed in Sections 2.4 and 2.5 have unique solutions. On the other hand, discrete numerical solutions are well known to exhibit an irregular behavior which, at zero speed, has a frequency content which is very clearly associated with the irregular frequencies and this is discussed in Section 3.6. In appendix C the motions of a two-dimensional barge of infinite draft are considered as an example of how the initial conditions bar the existence of non-trivial homogeneous solutions to the integral equation. This is expected to be true in general and suggests the that an imperfect satisfaction of the initial conditions may be responsible for introducing an irregular behavior into the discrete solution.

2.6.1 The Transient Integral Equations

Consider Equation (2.14) for the unknown potential $\phi(\vec{x},t)$ due to a prescribed distribution of normal velocity $\phi_n(\vec{x},t)$. This equation can be written

$$
\begin{aligned}
2\pi\phi + \iint_{\bar{S}_b} d\vec{\xi}\,\phi\, G_n^{(0)} - \int_{t_0}^{t} d\tau\, \Bigg\{ \iint_{\bar{S}_b} d\vec{\xi}\,\phi\, G_{\tau n} \qquad & (2.18)\\
+ \frac{U}{g}\int_{\bar{\Gamma}} dl\,(\vec{n}_{2D}\cdot\hat{\imath})\,\Big[-U\,\phi\, G_{\tau\xi} - G_\tau\,\Big(2\phi_\tau - U\phi_l\,(\vec{l}\cdot\hat{\imath}) - U\,\phi_s\,(\vec{s}\cdot\hat{\imath})\Big)\Big]\Bigg\} & \\
= \iint_{\bar{S}_b} d\vec{\xi}\, G^{(0)}\,\phi_n - \int_{t_0}^{t} d\tau\,\left\{ \iint_{\bar{S}_b} d\vec{\xi}\,\phi_n\, G_\tau - \frac{U^2}{g}\int_{\bar{\Gamma}} dl\,(\vec{n}_{2D}\cdot\hat{\imath})(\vec{n}\cdot\hat{\imath})\phi_n\, G_\tau \right\} & \\
\vec{x}\in\bar{S}_b &
\end{aligned}
$$

where the x-derivative of the potential along the waterline has been expressed in coordinates which are tangent and normal to the hull at the waterline (see Section 3.1 and Figure 3-1). Also the term on the waterline involving ϕ and $G_{\tau\tau}$ has been integrated by parts and combined with the term involving ϕ_τ and G_τ. This is a Fredholm second-kind equation in the spatial variables, and appears to be a Volterra second-kind equation in time. Because of the symmetry properties of the kernel and the causality of the solution however, it is more properly described as simply a

Fredholm second kind equation with time as a parameter and a forcing which depends upon the solution over the previous time history. More formally, consider just the surface integral inside the convolution on the left-hand side of Equation (2.18). Since the spatial integral in this expression, which we will call $f(t)$ for the moment, is a continuous function of time we can use the definition of a definite integral to write

$$\int_0^t d\tau \int\int_{\bar{S}_b} d\vec{\xi}\, \phi(\vec{\xi},\tau)\, G_{tn_\xi}(\vec{x},\vec{\xi},t-\tau) = \lim_{\substack{M\to\infty \\ \max \Delta_n t \to 0}} \sum_{n=1}^{M} f(t_n^*)\, \Delta_n t.$$

Here t_n for $n = (0, 1, ..., M)$ is a sequence of times over the interval such that $0 = t_0 < t_1 < ... < t_M = t$, $\Delta_n t = t_n - t_{n-1}$, and the value t_n^* is any time satisfying $t_{n-1} \leq t_n^* \leq t_n$. [For convenience we have taken $t_0 = 0$.] The choice of t_n^* is arbitrary within each interval, but in the limit the last evaluation point in this sum will become the current time $t_M^* \to t$. This makes $f(t_M^*) = 0$, since $G_\tau(\vec{x};\vec{\xi},0) = G_{\tau n_\xi}(\vec{x};\vec{\xi},0) = 0$ (the symmetry property), and consequently the last interval of this summation does not contribute to the integral. Thus the integral over the closed interval $[0,t]$ can be replaced by the integral over the semi-open interval $[0,t)$ in which the current unknown value of the potential $\phi(\vec{x},t)$ does not appear. This argument applies equally well to the waterline integral since $G_{\tau\xi}(\vec{x},\vec{\xi},0) = 0$, and allows Equation (2.18) to be written

$$2\pi\, \phi(\vec{x},t) + \int\int_{\bar{S}_b} d\vec{\xi}\, \phi(\vec{\xi},t)\, G_{n_\xi}^{(0)}(\vec{x},\vec{\xi}) = f_1(\vec{x},t) \tag{2.19}$$

where $f_1(\vec{x},t)$ is known, provided that the solution has been advanced to the present from the initial-conditions. Equation (2.19) is the integral equation representation of the exterior Neumann problem, with ϕ antisymmetric about $z = 0$, and this equation is known to have a unique solution [48][18][21].

Daoud [9] reached a similar conclusion in two dimensions, using the physical argument that between the time $t - \Delta t$ and the time t, gravity has not had time to take effect. He argued that this made the integral over the interval $[0,t]$ approximately equal to the integral over the interval $[0, t - \Delta t]$, and that the integral equation was therefore approximately of the form shown in Equation (2.19). Adachi

and Ohmatsu [2] refer to Daoud's work in support of their claim that the transient potential formulation is free of irregular-frequencies, while the transient source-only integral equation is not. Both formulations, when solved numerically, are known to produce an irregular oscillation in the solution but we argue here that this is not related to any non-uniqueness in the transient integral equation.

Consider the two source-only integral equations for this problem Equations (2.15) and (2.16). The argument outlined above applies equally well to these equations, since $G_{\tau n_x}(\vec{x},\vec{\xi},0) = 0$, and justifies writing them in the following forms:

$$\int\int_{S_b} d\vec{\xi}\, \sigma(\vec{\xi},t)\, G^{(0)}(\vec{x},\vec{\xi}) = f_2(\vec{x},t) \tag{2.20}$$

and,

$$2\pi\sigma(\vec{x},t) + \int\int_{S_b} d\vec{\xi}\, \sigma(\vec{\xi},t)\, G^{(0)}_{n_x}(\vec{x},\vec{\xi}) = f_3(\vec{x},t) \tag{2.21}$$

where again the functions $f_2(\vec{x},t)$ and $f_3(\vec{x},t)$ are known. Equation (2.20) is the difference of the integral equation representations of the interior and the exterior Dirichlet problems, with both ϕ and ϕ' anti-symmetric about $z = 0$. Equation (2.21) is the difference of the gradients of the same two Dirichlet integral equations. All four of these Dirichlet integral equations have unique solutions [48] [18] and therefore Equations (2.20) and (2.21) also have unique solutions.

The same conclusions about uniqueness do not apply to the analogous (zero speed) frequency-domain integral equations, as is briefly reviewed in the following section.

2.6.2 Time-Harmonic Oscillations at Zero Speed

The frequency domain discussion will be limited to zero speed in order to simplify the analysis, and because the Green function and the integral equation representation have been studied extensively in this case. If the unsteady motion of the fluid is assumed to be time harmonic at frequency ω then in the limit as $t \to \infty$ the potential

will become $\Re\{\tilde{\phi}(\vec{x},\omega)\,e^{i\omega t}\}$ where $\tilde{\phi}$ is the solution to:

$$\begin{aligned} \nabla^2\tilde{\phi} &= 0 \quad \text{in } \mathcal{V} \\ -\omega^2\tilde{\phi} + g\tilde{\phi}_z &= 0 \quad \text{on } z = 0 \\ \vec{n}\cdot\nabla\tilde{\phi} &= \tilde{V}_n \quad \text{on } \bar{S}_b. \end{aligned} \tag{2.22}$$

As long as the boundary-value problem of Equation (2.22) is supplemented by a radiation condition to ensure outgoing waves as $R \to \infty$, then this is also a well-posed problem with a unique solution (with the possible exception of certain pathological geometries for which a unique solution has not been proven to exist). In this case $\tilde{\phi}$ and ϕ can be considered to be a Fourier transform pair

$$\tilde{\phi}(\vec{x},\omega) = \int_{-\infty}^{\infty} dt\;\; \phi(\vec{x},t)\,e^{-i\omega t}, \qquad \phi(\vec{x},t) = \Re\int_{-\infty}^{\infty} d\omega\;\; \tilde{\phi}(\vec{x},\omega)\,e^{i\omega t}. \tag{2.23}$$

The appropriate Green function for this problem is

$$\tilde{G}(\vec{x},\vec{\xi},K) = \frac{1}{r} + \frac{1}{r'} + \frac{2\,K}{\pi}\int_0^{\infty} dk\;\; \frac{e^{kZ}}{k-K} J_0(kR), \tag{2.24}$$

where the contour of integration must be indented above the pole in order to satisfy the radiation condition, and $gK = \omega^2$. [The other quantities are identical to those defined in Equation (2.13).] An integral equation representation of the boundary-value problem in frequency space may be derived as a distribution of wave sources and normal dipoles:

$$2\pi\tilde{\phi}(\vec{x},\omega) + \int\int_{\bar{S}_b} d\vec{\xi}\;\tilde{\phi}(\vec{\xi},\omega)\,\tilde{G}_{n_\xi}(\vec{x},\vec{\xi},\omega) = \int\int_{\bar{S}_b} d\vec{\xi}\;\tilde{\phi}_n(\vec{\xi},\omega)\,\tilde{G}(\vec{x},\vec{\xi},\omega), \tag{2.25}$$

or as source-only formulations:

$$\int\int_{\bar{S}_b} d\vec{\xi}\;\tilde{\sigma}(\vec{\xi},\omega)\,\tilde{G}(\vec{x},\vec{\xi},\omega) = \phi(\vec{x},\omega), \tag{2.26}$$

$$2\pi\tilde{\sigma}(\vec{x},\omega) + \int\int_{\bar{S}_b} d\vec{\xi}\;\tilde{\sigma}(\vec{\xi},\omega)\,\tilde{G}_{n_x}(\vec{x},\vec{\xi},\omega) = \vec{n}\cdot\nabla\tilde{\phi}(\vec{x},\omega). \tag{2.27}$$

It can be shown in several ways that these frequency-domain integral equations do not have unique solutions at an infinite discrete set of frequencies, the irregular frequencies (see *e.g.* [2][29] or Appendix C). Away from these frequencies the solutions are unique and coincide with the quantity of interest ($\tilde{\phi}$, or $\tilde{\sigma}$). *At* the irregular frequencies however, the potential formulation has an infinity of solutions, while the source-only equation has no solution at all (in general).

While the solution to the transient initial-boundary-value problem developed in Section 2.3 is uniquely represented in integral equation form (Equation (2.14)), the harmonic solution to the boundary-value problem of Equation (2.22) is not uniquely determined from the solution to its integral equation representation (Equation (2.25)) at the irregular frequencies. The solutions of the respective boundary-value problems are a Fourier transform pair, but a more subtle relationship apparently exists between the solutions of the corresponding integral equations. This is attributed to the lack of initial conditions in the harmonic problem and is discussed further in Appendix C.

2.7 Asymptotic Behavior of the Solution

When a body has a non-zero forward speed the large-time asymptotic behavior of the perturbation problem we have been discussing becomes fundamentally different from the zero-speed case. This is due to the resonance at the critical frequency of oscillation corresponding to $\tau = \frac{\omega_c U}{g} = 1/4$. This resonance is a physically observable phenomenon and has been the subject of many investigations.

Dagan and Miloh [8] have shown that the frequency domain Green function (when $U \neq 0$) has a logarithmic singularity as the critical frequency is approached from below. In the time-domain, this result corresponds to an oscillation at the critical frequency which decays like $\frac{1}{t}$. Newman [42] has shown, through steepest descent analysis, that the transient free-surface Green function (Equation 2.13) has a large time leading asymptotic behavior near the free surface as follows,

$$G_t \sim \Re \frac{-\sqrt{2}\,i\,t}{r'^2}\sqrt{Rr'}\,(|Z| + iR)\,\exp\left(\frac{Zt^2}{4r'^2}\right)\,\exp i\left[\frac{t^2 R}{4r'^2} + \frac{1}{2}\tan^{-1}\left(\frac{R}{|Z|}\right) + \frac{\pi}{4}\right]$$

[The variables are non-dimensionalized by the appropriate combinations of the ship length L and the gravitational acceleration g.] When the body has a steady forward speed U, then as $t \to \infty$ both R and r' will tend to $F_n t$, where the Froude number $F_n = U/\sqrt{gL}$, while $\tan^{-1}\left(\frac{R}{|Z|}\right) \to \frac{\pi}{2}$, which reduces the leading behavior to

$$G_t \sim \frac{\sqrt{2}}{F_n^2 t} \exp\left(\frac{Z}{4F_n^2}\right) \sin(\omega_c\, t)$$

in agreement with the results of Dagan and Miloh.

Wehausen [52] (while extending the work of Havelock [15] and Maruo [37]) showed that the wave resistance felt by an accelerating distribution of singularities (which is confined to the center-plane of a thin ship) has this same behavior as $t \to \infty$. Based upon this work, it has been generally assumed that a distribution of singularities over the ship's surface should exhibit this same sort of asymptotic behavior. Most numerical evidence to date appears to support this contention as well. However, Grue and Palm [13] have presented calculations of the wave forces felt by a submerged circular cylinder in a free-stream which approach a finite value as $\tau \to 1/4$. And, subsequently, Liu & Yue [35], analyzed a source-distribution boundary-integral equation solution to the frequency-domain sea-keeping problem in both two and three-dimensions. They find that the solution is finite as $\tau \to 1/4$, as long as the geometry and speed dependent parameter $\Gamma \neq 0$, where

$$\Gamma = \int_{S_b} d\vec{x}(-i\, n_1 + n_3) e^{2\kappa z},$$

and $\kappa = \frac{4\omega_c^2}{g}$. The same condition applies for both submerged and surface-piercing bodies. An analogous analysis for the transient problem of a body which is accelerated to a constant forward speed [36] leads to a leading asymptotic behavior of the transient solution which is dominated by a decaying oscillation about a constant mean value. The decay of the oscillatory behavior is found to be

$$\phi \sim \Re\left\{C_1 \frac{e^{-\alpha t}}{t} e^{i\omega_c t} + C_2 \frac{1}{t^2} e^{i\omega_c t}\right\}$$

where C_1 and C_2 are complex constants, and the time constant α will be non-zero as long as $\Gamma \neq 0$. The parameter α is difficult to put into explicit form but, like Γ, it depends upon both the Froude number and the geometry of the ship.

In Section 3.4 a numerical experiment is carried out to investigate the asymptotic behavior of the numerical solution.

2.8 The Radiation Problem

The steady perturbation potential, when solved as the limit of a transient problem, and the radiation potentials are all solutions to similar (and in some cases identical) forced motion problems. The only difference is that in the steady problem it is the steady-state limit which is of interest, while in the radiation problem we seek a transient response.

For each radiation problem, the steadily translating ship is moved impulsively in mode k, and the force on the ship in mode j (*i.e.* the corresponding radiation impulse-response function) is calculated. Define a general radiation potential, due to an arbitrary motion of the ship in mode k to be $\Phi_k(\vec{x},t)$. This potential can be calculated from any derivative (or integral) of the ship's motion, as long as the response of the ship to an impulse in that quantity is known. Define the set of canonical potentials, $\phi_k^{(n)}$, to be the potential due to an impulse in the n^{th} derivative of the ship's motion in mode k. The general radiation potential can now be expressed in terms of the canonical potentials through convolution,

$$\Phi_k = \int_{-\infty}^{\infty} d\tau \; \phi_k^{(n)}(t-\tau) \, \frac{d^n x_k(\tau)}{d\tau^n} \, . \tag{2.28}$$

The force on the ship in mode j due to this arbitrary motion in mode k is found by integrating the consequent linearized pressure over the body surface

$$F_{jk} = -\rho \int\int_{\bar{S}_b} dS \, \left(\frac{\partial \Phi_k}{\partial t} - U \frac{\partial \Phi_k}{\partial x} \right) n_j . \tag{2.29}$$

The canonical radiation potentials $\phi_k^{(n)}$ are related to each other through time

derivatives by the expression

$$\frac{\partial \phi_k^{(n)}}{\partial t} = \phi_k^{(n-1)}. \tag{2.30}$$

This follows directly from Equation (2.28). The canonical potential $\phi^{(n-1)}$ can be written,

$$\phi^{(n-1)}(t) = \int_{-\infty}^{\infty} d\tau \; \phi^{(n-1)}(t-\tau) \frac{d^{(n-1)}x(\tau)}{d\tau^{(n)}} = \int_{-\infty}^{\infty} d\tau \; \phi^{(n-1)}(t-\tau)\,\delta(\tau)$$

where $\delta(t)$ is the Dirac delta function, but also

$$\phi^{(n-1)}(t) = \int_{-\infty}^{\infty} d\tau \; \phi^{(n)}(t-\tau) \frac{d^{(n)}x(\tau)}{d\tau^{(n)}} = \int_{-\infty}^{\infty} d\tau \; \phi^{(n)}(t-\tau)\,\delta'(\tau) = \frac{\partial \phi_k^{(n)}}{\partial t}$$

where $\delta'(t)$ is the derivative of the delta function. This relationship is also clear from the body boundary condition. As an example, the body boundary condition corresponding to an impulsive acceleration of the ship is

$$\vec{n} \cdot \nabla \phi_k^{(2)} = n_k\, h(t) + m_k\, r(t), \tag{2.31}$$

where $h(t)$ is the Heaviside step function and $r(t)$ is the ramp function $r(t) = t\,h(t)$. The body boundary condition produced by an impulse in the ship's velocity is the time derivative of equation (2.31)

$$\vec{n} \cdot \nabla \phi_k^{(1)} = n_k\, \delta(t) + m_k\, h(t) \tag{2.32}$$

and because this is a linear system, the two solutions are related in the same way.

It is worth noting that the radiation problem can also be solved using a non-impulsive motion of the body, as long as a convenient Fourier transform of the motion exists with which to reconstruct the impulse response from the non-impulse response [23].

In practice, calculating the impulse-response function directly from Equation (2.29) is inconvenient, since it involves a spatial derivative of the potential, and this calcula-

tion may be simplified by using a variant of Stokes' theorem attributed to Tuck [45]:

$$\int\int_{\bar{S}_b} dS \left[m_j \Phi_k - n_j (\nabla \bar{\Phi} \cdot \nabla \Phi_k) \right] = - \int_{\Gamma} dl \; n_j \; \Phi_k (\vec{l} \times \vec{n}) \cdot \nabla \bar{\Phi}, \qquad (2.33)$$

where $\vec{l}$ is the unit vector tangent to the mean waterline. For a wall sided ship, the line integral is identically zero and we may write

$$F_{jk} = -\rho \int\int_{\bar{S}_b} dS \left(\frac{\partial \Phi_k}{\partial t} n_j - \Phi_k \, m_j \right). \qquad (2.34)$$

2.8.1 Impulse-Response Functions

Since the canonical radiation problems do not (in general) provide a continuous velocity which can be used in the integral equation, it is usually necessary to decompose each radiation potential into solvable pieces. The following development is a generalization of the theory of impulse-response functions as applied to linearized ship motions which appears in Cummins [7], and Ogilvie [44].

The body boundary condition for the canonical radiation potential can be written

$$\vec{n} \cdot \nabla \phi_k^{(n)}(\vec{x}, t) = n_k(\vec{x}) \, \dot{x}(t) + m_k(\vec{x}) \, x(t)$$

where $x(t)$ and $\dot{x}(t)$ represent the generalized functions which are appropriate to an impulse in the n^{th} derivative of the body's motion. It is natural then to consider an analogous decomposition of each radiation potential:

$$\phi_k^{(n)}(\vec{x}, t) = \mathcal{N}_k(\vec{x}) \, \dot{x}(t) + \mathcal{M}_k(\vec{x}) \, x(t) + \psi_k^{(n)}(\vec{x}, t) \, h(t) \qquad (2.35)$$

The time constant potentials $\mathcal{N}_k(\vec{x})$ and $\mathcal{M}_k(\vec{x})$, are solutions to *pressure release* type problems, and they solve the following pair of boundary value problems:

$$\begin{aligned} \nabla^2 \mathcal{N}_k &= 0, & \nabla^2 \mathcal{M}_k &= 0 \qquad (2.36) \\ \mathcal{N}_k &= 0, & \mathcal{M}_k &= 0, \quad \text{on } z = 0 \\ \vec{n} \cdot \nabla \mathcal{N}_k &= n_k, & \vec{n} \cdot \nabla \mathcal{M}_k &= m_k, \quad \text{on } \bar{S}_b, \end{aligned}$$

These are waveless problems for which the Green function is simply $G^{(0)}$, as defined in Equation (2.13). Applying Green's theorem results in the following pair of integral equations.

$$\begin{aligned} 2\pi\mathcal{N}_k + & \int\int_{\bar{S}_b} d\vec{\xi} \left(\mathcal{N}_k G_n^{(0)} - n_k G^{(0)}\right) = 0 \\ 2\pi\mathcal{M}_k + & \int\int_{\bar{S}_b} d\vec{\xi} \left(\mathcal{M}_k G_n^{(0)} - m_k G^{(0)}\right) = 0. \end{aligned} \tag{2.37}$$

The transient or *memory* potential, $\psi_k^{(n)}$, solves an initial-boundary-value problem which depends upon the choice of n. All of the memory potentials are harmonic, and satisfy a homogeneous boundary condition on the body:

$$\begin{aligned} \nabla^2\psi_k^{(n)} = & \quad 0 \quad \text{in } \mathcal{V} \\ \vec{n}\cdot\nabla\psi^{(n)} = & \quad 0 \quad \text{on } \bar{S}_b. \end{aligned} \tag{2.38}$$

The free-surface boundary condition and the initial conditions satisfied by the memory potential are inhomogeneous in general.

In the following we will discuss three particular values of n, $(n = 0, 1, 2)$ corresponding to an impulsive displacement, velocity, and acceleration of the ship in mode k respectively. The same analysis can be applied at any n if desired. The free-surface boundary conditions satisfied by the memory potentials follow from substituting the decomposition of each potential into Equation (2.5), while the initial conditions may be derived by integrating $\phi_{tt} + g\phi_z = 0$ across $t = 0$. Let $\mathcal{L}$ represent the linearized free-surface boundary condition operator (Equation 2.10) then

$$\begin{aligned} \mathcal{L}\left(\psi_k^{(0)}\right) = & \quad 0 \\ \mathcal{L}\left(\psi_k^{(1)}\right) = & \quad -g\frac{\partial\mathcal{M}_k}{\partial z} \\ \mathcal{L}\left(\psi_k^{(2)}\right) = & \quad -g\left(\frac{\partial\mathcal{N}_k}{\partial z} + \frac{\partial\mathcal{M}_k}{\partial z}\,t\right) \qquad \text{on z} = 0,\ \text{t} > 0, \end{aligned} \tag{2.39}$$

and the initial conditions are

$$\begin{aligned}
\psi_k^{(0)} &= -g\frac{\partial \mathcal{N}_k}{\partial z} & \frac{\partial \psi_k^{(0)}}{\partial t} &= -g\frac{\partial \mathcal{M}_k}{\partial z} \\
\psi_k^{(1)} &= 0 & \frac{\partial \psi^{(1)}}{\partial t} &= -g\frac{\partial \mathcal{N}_k}{\partial z}. \\
\psi_k^{(2)} &= 0 & \frac{\partial \psi_k^{(2)}}{\partial t} &= 0 \qquad \text{on } z = 0,\ t = 0.
\end{aligned} \tag{2.40}$$

Integral equations for the memory potentials may be derived by repeating the derivation of Equation (2.14) (in Appendix A) and using the appropriate free-surface and initial conditions. The same results can also be obtained by simply substituting the appropriate decomposition of both the potential and the body boundary condition into integral Equation (2.14) and using the conditions (and integral equations) satisfied by the pressure release potentials. The results of these manipulations are the following three integral equations.

Impulsive displacement:

$$\begin{aligned}
&2\pi\psi^{(0)} + \int\int_{\bar{S}_b} d\vec{\xi}\, \psi^{(0)} G_n^{(0)} - \int_0^t d\tau \int\int_{\bar{S}_b} d\vec{\xi}\, \psi^{(0)} G_{\tau n} \\
&\qquad -\frac{U}{g}\int_0^t d\tau \int_{\bar{\Gamma}} dl\, (\vec{n}_{2D}\cdot\hat{\imath})\, \left[\psi^{(0)}\left(G_{\tau\tau} - U\, G_{\tau\xi}\right) - G_\tau\left(\psi_\tau^{(0)} - U\,\psi_\xi^{(0)}\right)\right] \\
&= \int\int_{\bar{S}_b} d\vec{\xi}\, \left[\left(n_k\, G_{\tau\tau}(t) - G_{\tau\tau n}(t)\,\mathcal{N}_k\right) - \left(m_k\, G_\tau(t) - G_{\tau n}(t)\,\mathcal{M}_k\right)\right] \\
&\qquad\qquad -\frac{U}{g}\int_{\bar{\Gamma}} dl\, (\vec{n}_{2D}\cdot\hat{\imath})\, G_\tau(t)\psi^{(0)}(0)
\end{aligned}$$

Impulsive velocity:

$$\begin{aligned}
&2\pi\psi^{(1)} + \int\int_{\bar{S}_b} d\vec{\xi}\, \psi^{(1)} G_n^{(0)} - \int_0^t d\tau \int\int_{\bar{S}_b} d\vec{\xi}\, \psi^{(1)} G_{\tau n} \\
&\qquad -\frac{U}{g}\int_0^t d\tau \int_{\bar{\Gamma}} dl\, (\vec{n}_{2D}\cdot\hat{\imath})\, \left[\psi^{(1)}\left(G_{\tau\tau} - U\, G_{\tau\xi}\right) - G_\tau\left(\psi_\tau^{(1)} - U\,\psi_\xi^{(1)}\right)\right] \\
&= -\int\int_{\bar{S}_b} d\vec{\xi}\, \left[\left(n_k\, G_\tau(t) - G_{\tau n}(t)\,\mathcal{N}_k\right) - \left(m_k\, H(t) - H_n(t)\,\mathcal{M}_k\right)\right]
\end{aligned}$$

Impulsive acceleration:

$$2\pi\psi^{(2)} + \int\int_{\bar{S}_b} d\vec{\xi}\, \psi^{(2)} G_n^{(0)} - \int_0^t d\tau \int\int_{\bar{S}_b} d\vec{\xi}\, \psi^{(2)} G_{\tau n}$$
$$- \frac{U}{g} \int_0^t d\tau \int_\Gamma dl\, (\vec{n}_{2D} \cdot \hat{\imath}) \left[\psi^{(2)} (G_{\tau\tau} - U\, G_{\tau\xi}) - G_\tau \left(\psi_\tau^{(2)} - U\, \psi_\xi^{(2)} \right) \right]$$
$$= \int\int_{\bar{S}_b} d\vec{\xi}\, (n_k\, H(t) - H_n(t)\, \mathcal{N}_k) - \int_0^t d\tau \int\int_{\bar{S}_b} d\vec{\xi}\, (m_k\, H - H_n\, \mathcal{M}_k)$$

It is clear from the initial conditions that the impulsive displacement memory potential $\psi^{(0)}(\vec{x}, 0)$ is non-zero at $t = 0$, in contrast to the memory potentials at any other n. As with any other $t = 0$ problem this function may be calculated using a Rankine Green function given the relation

$$G_{\tau\tau}(\vec{x}, \vec{\xi}, 0) = 2g \frac{\partial}{\partial \zeta} \left(\frac{1}{r'} \right)$$

which follows directly from the definition of G. The integral equation for $\psi^{(0)}(\vec{x}, 0)$ may be written

$$2\pi\psi^{(0)}(\vec{x}, 0) + \int\int_{\bar{S}_b} d\vec{\xi}\, \psi^{(0)}(\vec{\xi}, 0) G_n^{(0)} = 2g \int\int_{\bar{S}_b} d\vec{\xi} \left[n_k \frac{\partial}{\partial \zeta} \left(\frac{1}{r'} \right) - \mathcal{N}_k \frac{\partial^2}{\partial \zeta \partial n} \left(\frac{1}{r'} \right) \right] \tag{2.41}$$

The numerical solution to these integral equations is discussed in Chapter 3.

Note that for $n \geq 2$ the ship's velocity is a continuous function of time and there is no need to decompose the radiation potential at all. In this case Equation (2.14) may be used directly to solve for the potential. For $n < 2$, however, the body's velocity is discontinuous and the above decomposition is always necessary.

The six-by-six matrix of impulse-response functions which appears on the left hand side of the equations of motion (2.1) is calculated from the combination of (2.28) and (2.34), using the six canonical radiation potentials at any n. By inserting the decomposition of the potential into Equation (2.28), a general radiation potential can be written as

$$\Phi_k = \mathcal{N}_k \dot{x}(t) + \mathcal{M}_k x(t) + \int_{-\infty}^t d\tau\, \psi_k^{(n)}(t - \tau) \frac{d^n x_k(\tau)}{d\tau^n}$$

and the time derivative of this potential as

$$\frac{\partial \Phi_k}{\partial t} = \mathcal{N}_k \ddot{x}(t) + \mathcal{M}_k \dot{x}(t) + \psi_k^{(n)}(0) \frac{d^n x_k(t)}{d t^n} + \int_{-\infty}^{t} d\tau \, \frac{\partial \psi_k^{(n)}}{\partial t}(t-\tau) \frac{d^n x_k(\tau)}{d \tau^n}.$$

When these two expressions are inserted into Equation (2.34) the complete radiation impulse-response function can be expressed in terms of the canonical radiation potentials as follows:

$$\begin{aligned}
a_{jk}(\vec{x}) &= \rho \int\int_{\bar{S}_b} dS \, \mathcal{N}_k n_j \\
b_{jk}(\vec{x}) &= \rho \int\int_{\bar{S}_b} dS \, (\mathcal{M}_k n_j - \mathcal{N}_k m_j) \\
c_{jk}^{(0)}(\vec{x}) &= \rho \int\int_{\bar{S}_b} dS \, \psi_k^{(0)}(0) \, n_j \\
c_{jk}(\vec{x}) &= -\rho \int\int_{\bar{S}_b} dS \, \mathcal{M}_k m_j \\
K_{jk}^{(n)}(t) &= \rho \int\int_{\bar{S}_b} dS \left(\frac{\partial}{\partial t} \psi_k^{(n)}(t) \, n_j - \psi_k^{(n)}(t) \, m_j \right)
\end{aligned} \tag{2.42}$$

For $n \geq 0$

The new coefficient, $c_{jk}^{(0)}$, is present only when $n = 0$ and should be included with c_{jk} in this case. This term appears because $\psi_k^{(0)}(\vec{x}, 0) \neq 0$, while the corresponding terms for $n > 0$ do not appear because $\psi_k^{(n)}(\vec{x}, 0) = 0$ for all $n > 0$.

It has been pointed out in the past that the coefficient a_{jk} is a genuine added-mass coefficient which is independent of both time (or frequency) and forward speed. The coefficients b_{jk} and c_{jk} are, on the other hand, functions of the forward speed. The constants b_{jk} satisfy the following relations,

$$\begin{aligned}
b_{jk} &= 0 \qquad \text{for } j = k \\
b_{jk} + b_{kj} &= 0 \qquad \text{for } j \neq k.
\end{aligned} \tag{2.43}$$

This result follows from an application of Green's theorem to $\mathcal{N}_k$ and $\mathcal{M}_j$, combined

with the same operation using $\mathcal{N}_j$ and $\mathcal{M}_k$.

$$\int\int_S dS \left(\mathcal{M}_j \frac{\partial}{\partial n} \mathcal{N}_k - \mathcal{N}_k \frac{\partial}{\partial n} \mathcal{M}_j \right) = 0$$

Both $\mathcal{N}$ and $\mathcal{M}$ vanish at infinity and are zero on the free-surface so the integrals over those surfaces vanish leaving only an integral over the body,

$$\int\int_{\bar{S}_b} dS \left(\mathcal{M}_j \frac{\partial}{\partial n} \mathcal{N}_k - \mathcal{N}_k \frac{\partial}{\partial n} \mathcal{M}_j \right) = 0.$$

Similarly,

$$\int\int_{\bar{S}_b} dS \left(\mathcal{M}_k \frac{\partial}{\partial n} \mathcal{N}_j - \mathcal{N}_j \frac{\partial}{\partial n} \mathcal{M}_k \right) = 0.$$

Adding these equations and using the body-boundary conditions satisfied by the pressure-release potentials gives the desired result.

2.8.2 Frequency-Response Functions

If the motion of the ship is considered to be time harmonic at frequency ω, (*i.e.* $x_k \propto e^{i\omega t}$) then the force on the ship may be written in complex form as

$$F_{jk} = \Re\, x_k \left(-\omega^2 A_{jk}(\omega) + i\omega B_{jk}(\omega) + C_{jk} \right)$$

and the time-dependent impulse-response functions may be related to the analogous frequency-dependent coefficients as follows

$$-\omega^2 A_{jk}(\omega) + i\omega B_{jk}(\omega) + C_{jk} = \qquad (2.44)$$
$$-\omega^2 a_{jk} + i\omega\, b_{jk} + c_{jk} + (i\omega)^n \int_0^\infty K_{jk}^{(n)}(t) e^{-i\omega t}\, dt$$
$$\text{for } n \geq 0,$$

where $c_{jk}^{(0)}$ must be included with c_{jk} when $n = 0$.

In this section we have posed a general radiation problem, based on a series of canonical problems, which can be used to calculate the impulse-response functions

appearing in the transient equations of motion. These impulse-response functions can in turn be used to obtain the equivalent frequency-response functions. The details of calculating the canonical radiation potentials are worked out for three particular cases corresponding to impulses in the ship's acceleration, velocity, or position. Any two of the canonical potentials can be related through time derivatives, and the corresponding impulse response functions are related in the same way (as long as the non-zero value of $K^{(0)}(\vec{x},0)$ is not neglected). In principle, given $K^{(n)}$ for $n = N$, the impulse-response function at any $n < N$ can be calculated by taking the appropriate number of time derivatives. In practice, a balance must be struck between the errors introduced by rendering the function well behaved at $t \to \infty$, and the errors introduced into the initial-conditions by the discontinuity of the motion at $t = 0$. (See Sections 3.5 and 3.6.) The results which appear in this thesis have all been made using calculations of $\phi^{(2)}$ to obtain $K^{(2)}$, which is then numerically differentiated up to two times to obtain a memory function which goes to zero at large time. This choice has the advantage that the steady potential can be obtained directly from the mean value of the large time surge potential (as is discussed in the following section).

2.9 The Steady Problem

2.9.1 Impulsive Acceleration

The steady perturbation potential, $\bar{\phi}(\vec{x})$, can be calculated as the steady-state limit of a particular radiation problem: that of an impulsive acceleration of the ship to a forward speed U. This problem is defined by the boundary conditions

$$\left(\frac{\partial}{\partial t} - U\frac{\partial}{\partial x}\right)^2 \phi_1^{(2)} + g\frac{\partial}{\partial z}\phi_1^{(2)} = 0 \qquad \text{on z} = 0$$

$$\phi_n^{(2)} = U\, n_1\, h(t) \qquad \text{on } \bar{S}_b,$$

which in the limit as $t \to \infty$ will become the steady-state Neumann-Kelvin conditions

$$U^2\bar{\phi}_{xx} + g\bar{\phi}_z = 0 \qquad \text{on z} = 0$$

$$\bar{\phi}_n = U\, n_1 \quad \text{on } \bar{S}_b.$$

Solving a transient problem for a steady-state quantity may appear to be somewhat inefficient, especially since the steady-state Green function for this problem is known [53]. The most direct way of calculating the steady potential would be to apply Green's theorem, with the steady Green function, and to solve the resulting integral equation directly for $\bar{\phi}$. However, efforts to calculate the steady Green function in a robust and efficient way have not yet been entirely successful [6], and a transient approach, while somewhat computationally expensive, has been found to produce reliable results (See Chapter 4).

The wave forces on the body due to its steady translation may be calculated by integrating the consequent pressures over the body surface.

$$F_j = -\rho \int\int_{\bar{S}_b} dS \left(\frac{\partial \phi_1^{(2)}}{\partial t} - U \frac{\partial \phi_1^{(2)}}{\partial x} \right) n_j. \tag{2.45}$$

In the steady-state limit this will provide a value for the steady forces $\bar{F}_j$,

$$\bar{F}_j = \rho\, U \int\int_{\bar{S}_b} dS \, \frac{\partial \phi_1^{(2)}(\vec{x}, t \to \infty)}{\partial x} n_j. \tag{2.46}$$

Notice that force expressed by Equation (2.46) is a quantity which has been neglected in the calculation of the surge radiation impulse-response function. [When the convective term in the total pressure is replaced by a combination of the potential and the m-terms using Tuck's theorem, and then the Neumann-Kelvin m-terms are used, this term is identically zero for surge.] In the steady problem we are looking for a steady-state force which is smaller than the preceding transient response, and we should expect this calculation to be more sensitive than the corresponding radiation problem. This can be especially true for the wave resistance calculation where large pressures at the bow and stern are being combined to produce a relatively small total force.

2.9.2 Non-Impulsive Acceleration

If it is desired to consider something other that an impulsive acceleration of the body to a forward speed U, then it is necessary to work in a frame of reference which is fixed in space (the $\vec{x}_0$ coordinates). An integral equation for the potential in this frame of reference appears in Appendix A and the corresponding source formulation is derived in Appendix B. This equation may be used with an arbitrary velocity of the ship along the x-axis. In Section 3.7.1 a smooth acceleration of the ship defined by the velocity

$$U(t) = U_0 \, e^{\frac{-t_0^2}{t^2}}$$

is used in Equation (B.4) to investigate the influence of the initial acceleration on the calculation of the steady wave forces. [t_0 is a constant.] The ship's position along the x-axis due to this acceleration is related to the complimentary error function

$$x(t) = U_0 t_0 \left[\frac{t}{t_0} \, e^{-\frac{t_0^2}{t^2}} - \sqrt{\pi} \, erfc\left(\frac{t_0}{t}\right) \right].$$

2.10 The Diffraction Problem

In principle the solution of the diffraction problem is identical to the solution of the forced motion problems discussed in Sections (2.8) and (2.9). There are however subtle points concerning the definition of the impulsive incident wave, as well as its use in following seas; these topics will not be discussed in this thesis. A more complete discussion of the diffraction problem can be found in Bingham *et al* [5] or King [23]. When the diffraction problem is forced by an impulsive wave elevation, the computed transient forces are the impulse-response functions. These impulse-response functions are the kernels of convolutions which can be used to compute the exciting forces and moments which appear on the right-hand side of the equations of motion (2.1) given an arbitrary, known, incident wave elevation.

For the results presented here Equation (2.14) has been solved using the body

boundary condition:

$$\frac{\partial \phi_S}{\partial n} = -\frac{\partial \phi_I}{\partial n}, \tag{2.47}$$

and the force in mode j, $K_{jD}(t)$, is computed as indicated in (2.34) with $\Phi_k = \phi_I + \phi_S$, namely the complete diffraction potential. The definition of the impulsive incident wave is entirely in the moving frame of reference [22].

$$\phi_I(\vec{x}, t) = \Re \frac{g}{\pi} \int_{-\infty}^{\infty} d\omega_e \, \frac{i}{\omega} \exp\left[kz - ik\left[x\cos\beta + y\sin\beta\right] + i\omega_e t\right], \tag{2.48}$$

where the wavenumber k is related to the absolute frequency ω by $k = \frac{\omega^2}{g}$, $\omega_e = \omega - Uk\cos\beta$ is the encounter frequency, and β is the angle of wave propagation measured from the positive x-axis.

This incident velocity potential, is a uni-directional wave system which contains all frequencies and describes a wave elevation which is the Dirac function in time, $\delta(t)$, when viewed from the origin of the ship-fixed reference frame. Once the impulse-response function has been calculated, the exciting forces on the ship due to an incident wave elevation measured at a fixed point in the ship-fixed reference frame, $\zeta(t)$, may be computed by

$$X_j(t) = \int_{-\infty}^{\infty} d\tau \; K_{jD}(t-\tau)\zeta(\tau). \tag{2.49}$$

The wave elevation in the ship fixed frame, $\zeta(t)$, can always be computed from a given wave elevation in an earth-fixed reference frame by transforming to Fourier space (see King [22]).

There is no particular significance in choosing to have this temporal impulse occur along a line through the origin. Any convenient location is acceptable as long as it is accounted for in the interpretation of the impulse-response function or its Fourier transform. In Korsmeyer [26] it is shown that such a shift in the location is equivalent to a phase shift in the frequency domain.

The frequency domain exciting force coefficients are related to $K_{jD}(t)$ by

$$X_j(\omega_e) = \frac{1}{\pi}\int_{-\infty}^{\infty} dt\, K_{jD}(t)e^{-i\omega_e t}. \tag{2.50}$$

2.11 Other Approximations of the m-terms

The Neumann-Kelvin linearization performs quite well for slender bodies, such as the Wigley hull, but we must expect this linearization to fare somewhat worse when faced with a ship of fuller form. Clearly the Neumann-Kelvin m-terms will become a worse approximation to the real coupling between the steady and the unsteady flows as the ship becomes more full-formed (at a given Froude number). Thus we have some motivation for attempting to improve the satisfaction of the body boundary condition through a better approximation of the m-terms, even though there is no way of obtaining a similar improvement in the free-surface boundary condition (without discarding the free-surface Green function). It could be argued that there are situations where the combination of a more exact body boundary condition and the Neumann-Kelvin linearized free-surface condition is appropriate. A submerged bulbous bow is one example.

Perhaps the most obvious way of improving the satisfaction of the body boundary condition is to satisfy this condition exactly by using the body-exact formulation of the problem, in combination with a solution to the equations of motion and a repanelization of the body at every time step. Computationally, this is an expensive method however, and care must be taken to integrate the equations of motion very accurately. An alternative is to improve the satisfaction of the body boundary condition in the moving frame of reference.

When the body boundary condition for the unsteady radiation potentials are linearized about an arbitrary steady basis flow $\bar{\Phi}(\vec{x})$, the resultant definition of the m-terms is [41]

$$(m_1, m_2, m_3) = -(\vec{n}\cdot\vec{\nabla})\vec{\nabla}\bar{\Phi}$$

$$(m_4, m_5, m_6) = -(\vec{n}\cdot\vec{\nabla})(\vec{r}\times\vec{\nabla}\bar{\Phi}).$$

[If $\bar{\Phi} = -Ux$ then the Neumann-Kelvin m-terms are recovered.] Consider the integrals appearing in Equation (2.14) (or (2.37)) which involve the m-terms. These are all of the form,

$$\int\int_{\bar{S}_b} d\vec{\xi}\, m_k(\vec{\xi})\, F(\vec{x};\vec{\xi},t). \tag{2.51}$$

The m-terms themselves require the calculation of second gradients of $\bar{\Phi}$ on the body surface, a task which a constant strength panel method may have difficulty performing in a robust way. To avoid this we employ Stokes' theorem to exchange a gradient from the m-terms to the function F. It can be shown (Nakos [40]) that an integral in the form of Equation (2.51) can be written

$$\int\int_{\bar{S}_b} d\vec{\xi}\, m_k(\vec{\xi})\, F(\vec{x};\vec{\xi},t) = -\int\int_{\bar{S}_b} d\vec{\xi}\, n_k(\vec{\xi})\, \vec{\nabla}\bar{\Phi}(\vec{\xi}) \cdot \vec{\nabla}_{\xi} F(\vec{x};\vec{\xi},t) \tag{2.52}$$

as long as the function $F(\vec{\xi})$ is differentiable on the body surface $\bar{S}_b$, and the potential $\bar{\Phi}$ satisfies the condition $\vec{n} \cdot \vec{\nabla}\bar{\Phi} = 0$ on $\bar{S}_b$. Having used this manipulation, we still require the gradient of $\bar{\Phi}$ and experience with low-order panel methods suggests that a source formulation will be preferred for this purpose.

Once an approximation of $\vec{\nabla}\bar{\Phi}$ has been obtained, Equation (2.52) may be used in Equation (2.14) to improve the calculation of the radiation potentials. Notice however, that the m-terms also appear in the expressions used to calculate the impulse response functions from the potentials. These integrals (see Eq. (2.34)) are of the same form as Equation (2.51) except that in this case the function F is an unsteady perturbation potential ϕ, rather than a Green function. The perturbation potentials satisfy the properties required of F so relation (2.52) applies to these integrals as well, but, in order to use this method to calculate the impulse response functions, gradients of the potentials are needed along with the potentials themselves. A fairly elaborate procedure has been developed in order to continue to avoid taking numerical derivatives. Having solved for the potential on each panel (using the improved m-terms) we now solve a first kind integral equation for the corresponding source

strengths using Equation (2.15),

$$\phi(\vec{x},t) = \int\int_{\bar{S}_b} d\vec{\xi}\, G^{(0)}\,\sigma(t) + \int_0^t d\tau \int\int_{\bar{S}_b} d\vec{\xi}\, G_t(t-\tau)\,\sigma(\tau)$$
$$-\frac{U_0^2}{g}\int_0^t d\tau \int_{\bar{\Gamma}} n_1^2 dl\, G_t(t-\tau)\,\sigma(\tau)$$

With the source strengths known, the gradients of the potentials may be calculated using Equation (2.17), and finally, with both the potentials and their gradients known, the manipulation discussed above is used in Equation (2.34) to calculate the impulse response functions. This procedure essentially triples the computational effort (not including the effort of calculating $\vec{\nabla}\bar{\Phi}$), but is a robust way of improving the satisfaction of the body boundary condition.

Two ready alternatives exist to the free-stream alone which can be used to improve the approximation of $\vec{\nabla}\bar{\Phi}$ in the definition of the m-terms. The most obvious choice is to combine the free-stream velocities with mean value of $\vec{\nabla}\phi_1^{(2)}$, as discussed in Section 2.9. A less obvious but computationally simpler option is to use the double-body velocities $\vec{\nabla}\Phi^{db}$.

2.11.1 The Double-Body Flow

The double-body flow is the result of the body, along with its reflection about the $z = 0$ plane, traveling with constant speed U in an infinite fluid. The potential due to this flow satisfies the following boundary-value problem

$$\begin{aligned}
\nabla^2\Phi^{db} &= 0 \\
\frac{\partial\Phi^{db}}{\partial z} &= 0 \quad \text{on } z = 0 \\
\vec{n}\cdot\nabla\Phi^{db} &= 0 \quad \text{on } \bar{S}_b. \\
\vec{\nabla}\Phi^{db} &\to -U\hat{\imath} \quad \text{as } \vec{x} \to \infty
\end{aligned} \tag{2.53}$$

To solve this problem we consider $\Phi^{db} = -Ux + \phi^{db}$ where $\phi^{db} \to 0$ at spatial infinity and $\vec{n} \cdot \nabla \phi^{db} = U n_1$ on $\bar{S}_b$. A Green function for this problem is

$$G^{(\infty)} = \frac{1}{r} + \frac{1}{r'} \tag{2.54}$$

and by applying Green's theorem to ϕ^{db} and $G^{(\infty)}$ an integral equation for this potential can be written

$$2\pi\phi^{db}(\vec{x}) + \int\int_{\bar{S}_b} d\vec{\xi}\, \phi^{db}(\vec{\xi})\, G_n^{(\infty)}(\vec{x},\vec{\xi}) = \int\int_{\bar{S}_b} d\vec{\xi}\, \phi_n^{db}(\vec{\xi})\, G^{(\infty)}(\vec{x},\vec{\xi}). \tag{2.55}$$

Source-only formulations for the double-body flow may be derived in the usual way:

$$\phi^{db}(\vec{x}) = \int\int_{\bar{S}_b} d\vec{\xi}\, \sigma(\vec{\xi})\, G^{(\infty)}(\vec{x};\vec{\xi}) \tag{2.56}$$

$$2\pi\sigma(\vec{x},t) + \int\int_{\bar{S}_b} d\vec{\xi}\, \sigma(\vec{\xi})\, (\vec{n}_x \cdot \vec{\nabla}_x) G^{(\infty)}(\vec{x};\vec{\xi}) = \vec{n} \cdot \vec{\nabla} \phi^{db}(\vec{x}) \tag{2.57}$$

and these can be used to obtain $\vec{\nabla}\phi^{db}$.

Results using this technique are preliminary and are not presented.

Chapter 3

Numerical Solution

The work involved in implementing a numerical solution to the transient ship motions problem described in Chapter 2 has been eased by the achievements of more than a decade of *panel-method* development at the Computational Hydrodynamics Facility of the Department of Ocean Engineering at MIT. The panel-method, originally developed by Hess and Smith [16], is a technique for solving boundary integral equations where the body surface is described by a finite number of panels, and the integral equation is enforced at a similar number of *collocation* points in the domain of integration. This method relies on the fast and accurate evaluation of the Green function along with its spatial and temporal derivatives.

Ours is a *low-order* panel-method where each panel is defined by four co-planar vertices, and each of the perturbation velocity potentials is assumed to be constant over a panel. The *Rankine* part of the Green function ($G^{(0)}$ in Equation 2.13), and its normal derivative are integrated analytically over a planar panel for a particular source point using the subroutine RPAN, while the *wave* part (H in Equation 2.13), and its derivatives are evaluated between any pair of points in the fluid using TGREEN. These two calculations are made to an absolute accuracy of six to seven digits. (See Newman [42]) TGREEN is fully vectorized and takes approximately 1.5 microseconds per evaluation on the CRAY Y/MP. The integration of the wave part over a panel is done using a one point quadrature (multiplication by the panel area). Higher order quadrature rules will require more Green function evaluations, and our experience

indicates that better overall accuracy (and efficiency) is achieved by simply increasing the number of panels used to discretize the body. The convolution integrals are computed by the trapezoid rule which introduces an error on the order of Δt^3 into the computations (where Δt is the discrete time step size).

The solution of the radiation problem, using Equation (3.2), when the body has zero forward speed is described in detail by Korsmeyer [24], and results are presented for various bodies in [27]. Liapis [31] describes his solution technique for the radiation problem (which is practically identical to that discussed here) at both zero and non-zero forward speed. King [22] discusses the solution of the diffraction problem. This technique has also been used to solve the *body-exact* problem, where the computations are made in an earth-fixed frame of reference with the body-boundary condition applied on the instantaneous position of the hull. (*e.g.* [33], [3]) This formulation is used in Section 4.2 to investigate the effects of the initial acceleration of the ship on the steady forces. (See Appendices A and B for the body-exact integral equations.)

The computer code T$\bar{\text{I}}$MIT , originally developed by Korsmeyer [24], has been extended to include the effects of steady forward speed (and to solve for the steady perturbation potential) as part of this thesis. Since the solution at zero forward speed has been fully documented in the above mentioned reference, only the treatment of the waterline integrals will be discussed further.

3.1 Evaluating the Waterline Integral

Because of the accuracy in calculating the Green function, it is convenient to use integration by parts to exchange a time and a spatial derivative between the potential and the Green function and avoid any numerical differentiation of the solution. [These manipulations essentially follow Liapis [31].] In its continuous form the waterline integral is

$$I_w = \frac{U}{g}\int_{t_0}^{t} d\tau \int_{\Gamma} dl\,(\vec{n}_{2D}\cdot\hat{\imath}) \quad (\phi(\tau)\,[G_{\tau\tau}(t-\tau) - UG_{\tau\xi}(t-\tau)] \\ -G_{\tau}(t-\tau)\,[\phi_{\tau}(\tau) - U\phi_{\xi}(\tau)])$$

where the spatial arguments have been removed for brevity. If the term involving G_τ and ϕ_τ is integrated by parts it may be combined with the first term.

$$I_w = \frac{U}{g}\int_{t_0}^{t} d\tau \int_{\bar{\Gamma}} dl\,(\vec{n}_{2D}\cdot\hat{\imath})\;(\phi(\tau)\,[2\,G_{\tau\tau}(t-\tau) - U\,G_{\tau\xi}(t-\tau)] + U\,G_\tau(t-\tau)\,\phi_\xi(\tau))$$

[There are no boundary contributions because of the initial conditions satisfied by the two functions.] A similar manipulation can be made with the term involving the x-derivative of the potential. First express the x-component of velocity in an orthogonal coordinate system which is tangent to the hull at the waterline as shown in figure 3-1

$$\int_{\bar{\Gamma}} dl\,(\vec{n}_{2D}\cdot\hat{\imath})\;\phi_\xi G_\tau = \int_{\bar{\Gamma}} dl\,(\vec{n}_{2D}\cdot\hat{\imath})\;\left[(\vec{n}\cdot\hat{\imath})\phi_n + (\vec{l}\cdot\hat{\imath})\phi_l + (\vec{s}\cdot\hat{\imath})\phi_s\right]\,G_\tau.$$

We will assume that the ship is wall sided at the waterline (recall that this has also been assumed in the development of the impulse-response function) in which case $(\vec{s}\cdot\hat{\imath}) = 0$. [This assumption also means that $\vec{n}_{2D} = \vec{n}$.] The term involving ϕ_l can be integrated by parts and the boundary terms, as they are taken at the same point in space, cancel:

$$\int_{\bar{\Gamma}} dl\,(\vec{n}\cdot\hat{\imath})(\vec{l}\cdot\hat{\imath})\,\phi_l\,G_\tau = -\int_{\bar{\Gamma}} dl\,\phi\,\frac{\partial}{\partial l}\left(G_\tau\,(\vec{n}\cdot\hat{\imath})(\vec{l}\cdot\hat{\imath})\right)$$

$$= -\int_{\Gamma} dl\,\phi\,\left[G_\tau\,\frac{\partial}{\partial l}(n_1\,n_2) + G_{\tau l}\,(n_1\,n_2)\right].$$

T n_1, n_2 has been introduced to represent the x and y components of the vector normal to a waterline segment and we have used the fact that $(\vec{l}\cdot\hat{\imath}) = (\vec{n}\cdot\hat{\jmath})$. This allows the waterline integral to be calculated from

$$\begin{aligned} I_w = \;& \frac{U}{g}\int_{t_0}^{t} d\tau \int_{\bar{\Gamma}} dl\,\phi(\tau)\,\{[2\,G_{\tau\tau}(t-\tau) - UG_{\tau\xi}(t-\tau)]\;n_1 \\ & -U\,\left[\tfrac{\partial}{\partial l}(n_1\,n_2)\,G_\tau(t-\tau) + (n_1\,n_2)\,G_{\tau l}(t-\tau)\right] + U\,\phi_n(\tau)(n_1^2)\,G_\tau(t-\tau)\Big\}. \end{aligned} \tag{3.1}$$

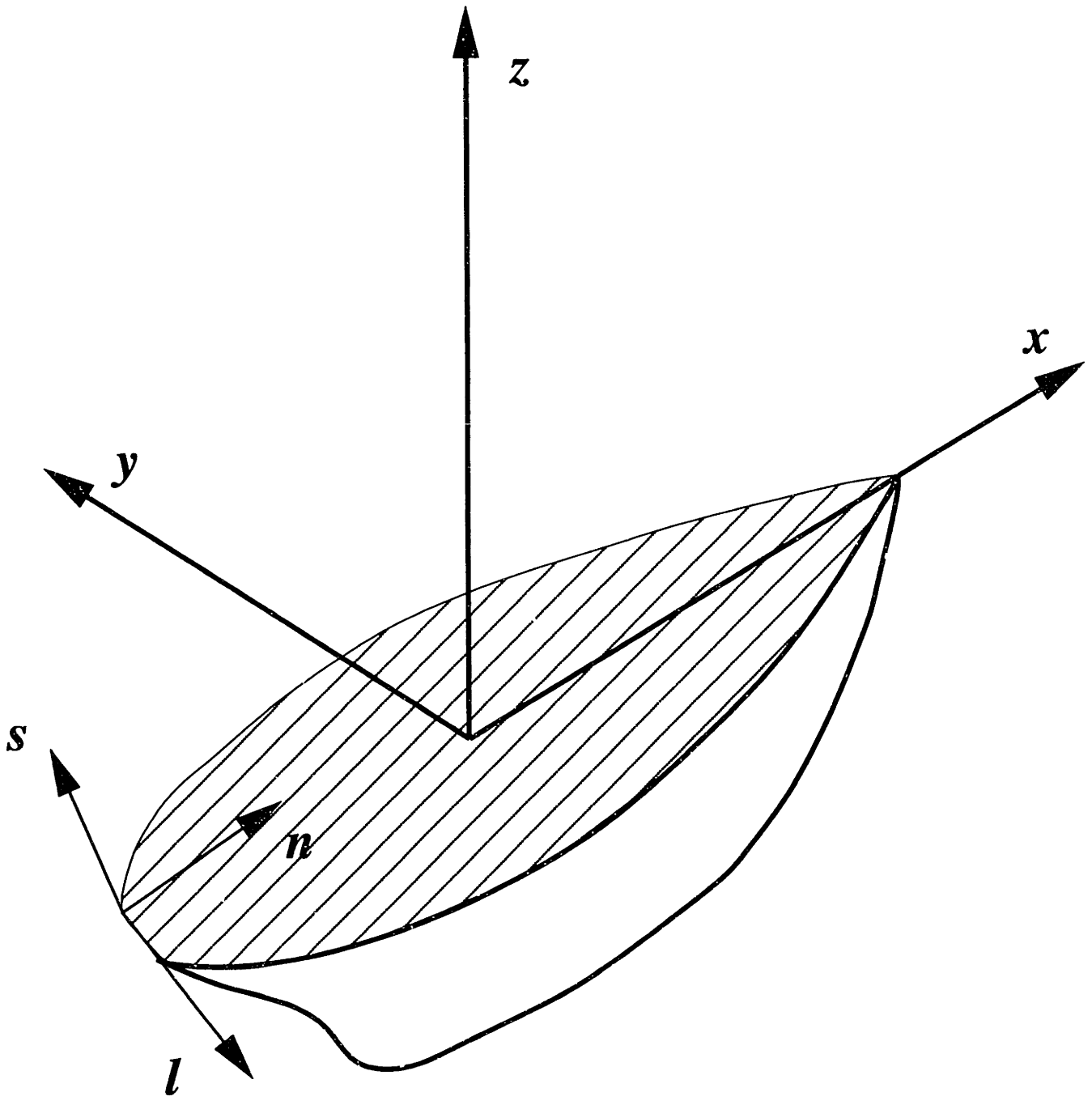

Figure 3-1: The coordinate system tangent and normal to the hull surface.

The tangential derivative of the Green function is calculated by resolving the x and y velocity components into the tangential direction, $G_{\tau l} = (G_{\tau\xi}\, n_2 - G_{\tau\eta}\, n_1)$.

3.2 A Discrete Integral Equation

The discretization scheme described above leads to a discrete form of the continuous integral equation (2.14). This equation is a linear system of N_p equations for N_p unknowns, which must be factored twice (once at $t = 0$ and once for $t > 0$), and solved at each of $N_t + 1$ time steps with a new right-hand side. [N_p is the number of panels used to discretized the body.]

$$
\begin{aligned}
2\pi\phi_{iM} + \sum_{j=1}^{N_p} \phi_{jM} \int\int_{S_j} d\vec{\xi}\, \frac{\partial G^{(0)}(\vec{x};\vec{\xi})}{\partial n_\xi} - U\,\Delta t \sum_{k=1}^{N_w} \phi_{kM}\, n_1 \int_{\Gamma_k} dl \frac{\partial}{\partial \zeta}\left(\frac{1}{r'}\right) \\
= \sum_{j=1}^{N_p} \left(\frac{\partial \phi}{\partial n_\xi}\right)_{jM} \int\int_{S_j} d\vec{\xi}\, G^{(0)}(\vec{x};\vec{\xi}) \\
+ \sum_{m=0}^{M-1}{}' \Delta t \left\{ \sum_{j=1}^{N_p} \left[\left(\frac{\partial \phi}{\partial n_\xi}\right)_{jm} \int\int_{S_j} d\vec{\xi} \left(\frac{\partial G(\vec{x};\vec{\xi})}{\partial t}\right)_{M-m} \right.\right. \\
\left. - \phi_{jm} \int\int_{S_j} d\vec{\xi} \left(\frac{\partial^2 G(\vec{x};\vec{\xi})}{\partial n_\xi\, \partial t}\right)_{M-m} \right] \\
+ \frac{U}{g} \sum_{k=1}^{N_w} \phi_{km} \left[\int_{\Gamma_k} dl \left(2\frac{\partial^2 G(\vec{x},\vec{\xi})}{\partial t^2} + U \frac{\partial^2 G(\vec{x},\vec{\xi})}{\partial t\, \partial \xi} \right) n_1 \right. \\
+ U \left(\frac{\partial}{\partial l}(n_1\, n_2) \frac{\partial G(\vec{x},\vec{\xi})}{\partial t} + (n_1\, n_2) \frac{\partial^2 G(\vec{x},\vec{\xi})}{\partial t\, \partial l_\xi} \right) \Big]_{M-m} \\
\left. \left. - \left(\frac{\partial \phi}{\partial n_\xi}\right)_{km} \int_{\Gamma_k} dl\, n_1^2 \left(\frac{\partial G(\vec{x},\vec{\xi})}{\partial t}\right)_{M-m} \right\}
\end{aligned}
$$

$$
\text{for } i = 1, N_p,\ M = 0, N_t \qquad (3.2)
$$

where S_j is the surface of the j^{th} panel on the hull, and Γ_k is the k^{th} line segment along the ship's waterline. The prime on the summation in time indicates that a weight of one-half is applied when $m = 0$ in accordance with the trapezoid rule, and the collocation points $\vec{x}_i$ are located at the panel centroids. The relations, $G_t = -G_\tau$

and $G_{\tau\tau}(0) = 2g\frac{\partial}{\partial\zeta}(\frac{1}{r'})$ have also been used. Notice that there is one contribution from the convolution integrals when $\tau = t$ because $G_{\tau\tau}(\vec{x},\vec{\xi},0) \neq 0$, and that this term has been included on the left hand side of the equation.

As mentioned above, the spatial integrations involving Rankine terms are done analytically, (at least to machine precision) and this includes the waterline integral which appears on the left hand side of Equation (3.2). For a line segment which is parallel to the plane of the free-surface, this integral may be written in a local coordinate system with its origin at the reflection of the end point about the free surface, and the x_l-axis running parallel to the segment. These coordinates are defined by

$$\begin{aligned} x_l &= (x-\xi)\cos\theta + (y-\eta)\sin\theta \\ y_l &= -(x-\xi)\sin\theta + (y-\eta)\cos\theta \\ z_l &= (z+\zeta) \end{aligned}$$

where θ is the angle that the segment makes with the global x-axis. In this local coordinate system the integral becomes

$$\int_{\Gamma_k} dl \frac{-(z+\zeta)}{r'^3(\vec{x},\vec{\xi})} = \int_0^{l_k} d\xi_l \frac{-z_l}{((x_l-\xi_l)^2+y_l^2+z_l^2)^{3/2}}$$

where l_k is the total length of the waterline segment of the kth waterline panel. This integral is straightforward to evaluate, and the result is

$$= \frac{z_l}{y_l^2+z_l^2}\left[\frac{x_l-l_j}{\sqrt{(x_l-l_j)^2+y_l^2+z_l^2}} - \frac{l_j}{\sqrt{x_l^2+y_l^2+z_l^2}}\right].$$

If the body geometry has symmetry planes, then this information can be exploited to make the hydrodynamic calculations more efficient by reducing the number of unknowns and the number of Green function calculations. In general, any of the perturbation potentials, and the incident potential, can be decomposed into components which are either symmetric or anti-symmetric with respect to a given plane

of symmetry. At zero forward speed, TIMIT has been written to accept as input a discretization of one half of the body when it is symmetric about either the $x = 0$ or the $y = 0$ plane. If the body is symmetric about both the $x = 0$ and the $y = 0$ planes, then only one quarter of the hull needs to be discretized. At non-zero forward speed, only $y = 0$ plane symmetry is exploited. At forward speed the flow is no longer symmetric fore and aft, even when the geometry is, which means that each radiation potential must be decomposed which reduces the benefit by a factor of two. Since most ships are not symmetric fore and aft anyway, exploiting this symmetry is not felt to be worth the effort of implementation.

3.3 Computational Cost and Storage Requirements

The bulk of the computational burden of the solution is in calculating (or fetching from storage) the transient Green function coefficients which appear in the convolution integrals. The number of coefficients needed at each time step is

$$2(N_p + N_w) \times N \times M$$

where $N = N_p, 2N_p, 4N_p$ corresponds to $0, 1$, or 2 planes of geometric symmetry having been exploited respectively (N is the total number of panels on the entire body), N_p is the number of unknowns in the linear system and N_w is the number of segments used to discretize the waterline; M is the number of the current time step. At any given time step M all but N^2 of these coefficients have already been calculated at previous time steps. If there is sufficient physical memory available, the most efficient strategy is to store the coefficients in memory. If there is not, then they must either all be recalculated at each step, or fetched from storage on disk. On a typical work-station (or the CRAY) storing the coefficients on disk is from three to six times faster than recalculating. In the diffraction problem, the incident potential must be calculated at each time step as well, but only N_p evaluations are required and this is not a significant contribution to the overall computational effort.

If the transient coefficients are stored, the number of machine words required, whether in RAM or on disk is

$$2(N_p + N_w) \times N \times N_t$$

where N_t is the total number of time steps used. (Typical words are 4 bytes on a work-station and 8 bytes on the CRAY.) The total cost of the computation, regardless of whether the coefficients are recalculated or stored, scales like

$$\text{Cost} \propto N_p^2 \times N_t^2. \tag{3.3}$$

There is an N_p^3 term in the cost equation, reflecting the factorization of the left-hand side, but this term is dominated by the N_p^2 term for any typical computation.

Clearly it is important to use the spatial and temporal discretizations which are as coarse as possible, within the desired limits of accuracy. Symmetries should always be exploited when possible as this both reduces the size of the linear system and reduces the number of coefficients which must be computed. Minimizing the total time range of the calculation is also important and is discussed in Section 3.4.

3.4 Asymptotic Continuation at Forward Speed

In this section we analyze the large time behavior of the radiation potentials calculated using TIMIT . In practice we would like to make calculations over the shortest possible interval of time, and use our knowledge of the asymptotic behavior of the solution to continue the calculation to large time. All of the results presented in the thesis have been calculated assuming that the decay rate of the solution is proportional to $1/t$. As discussed in Section 2.7 however, recent work by Liu and Yue [36] predicts that the asymptotic behavior of the transient solution at non-zero forward speed is really

$$\phi(\vec{x}, t) \sim \Re\{\frac{C_1 e^{-\alpha t}}{t} e^{i\omega_e t} + \frac{C_2}{t^2} e^{i\omega_e t}\}, \tag{3.4}$$

where C_1 and C_2 are complex constants.

From a practical point of view, to obtain frequency-domain results from time-domain calculations for example, it makes little difference whether the solution is continued to infinity using a t^{-1} or a t^{-2} decay. Figures 3-2 through 3-5 show the Fourier transform of a calculation made using a heaving Wigley hull at $F_n = 0.3$. A comparison is made between extending the calculation using a t^{-1} and a t^{-2} rate of decay and it is clear that only a very narrow band of frequencies near the critical frequency is affected. [It will become apparent that we expect the true solution to lie somewhere in between these two calculations.] The true asymptotics are of theoretical importance however, and it is interesting to analyze the asymptotics of the numerical solution in an attempt to observe the predicted behavior.

Figure 3-6 shows a long calculation of the impulsive surge velocity potential on one panel of a coarsely discretized Wigley hull (64 panels on half of the hull) at a Froude number of 0.3. The non-dimensional time step size is 0.1 and this is a converged result for this spatial discretization (*i.e.* halving the time step does not graphically change the solution). Using a finer discretization of the hull has been found not to affect the asymptotic behavior of the solution, and while this discretization would not be suitable for making realistic calculations of the forces, it is apparently adequate for this particular experiment.

Figure 3-7 shows a comparison between the calculated potential and a $1/t$ and a $1/t^2$ decay rate. [The two matching curves are a least squares fit to all of the data points from $t = 20$ to $t = 100$.] The asymptotics appear to be indistinguishable from a $1/t$ rate of decay in this figure, however, assuming that $\alpha \neq 0$ then it should be possible to make an estimate of its value. In order to estimate α, the peak values of the potential shown in Figure 3-6 are determined, call this $f(t)$, and we plot $log(t \cdot f(t))$ in figure 3-8 along with a least squares fit of the data to a straight line. The slope of this line provides an estimate of the rate of exponential decay, $\alpha \approx 8.7 \times 10^{-4}$. This estimate of α means that the $e^{-\alpha t}/t$ term and the $1/t^2$ term will become of comparable magnitude after a non-dimensional time on the order of several thousand. Given the uncertain size of the accumulated numerical error in a calculation of this duration,

Froude number	α
0.3	8.7×10^{-4}
0.25	5.9×10^{-3}
0.2	3.0×10^{-2}
0.15	3.6×10^{-1}
0.1	1.6×10^{-1}

Table 3.1: Estimates of the exponential decay rate α at various Froude numbers.

this is not very convincing. However, we expect α to be a function of the Froude number, and in Figures 3-9 through 3-12 the same potential is shown as the Froude number is reduced from 0.3 to 0.1. It seems clear from this series that there is an exponentially decaying region in the solution which becomes shorter as the Froude number decreases. Using the technique described above the value of α has been estimated from these calculations and is tabulated in table 3.1. The magnitude of α estimated for $F_n = 0.1$ predicts the exponentially decaying term to be an order of magnitude smaller than the next term at a non-dimensional time of $t \approx 30$. After this time the asymptotics should be dominated by a $1/t^2$ decay. Figure 3-13 shows a fit of the data starting from $t = 30$ to decay rates of $1/t$ and $1/t^2$. The asymptotics of the solution have apparently become dominated by a $1/t^2$ decay as predicted by the theory.

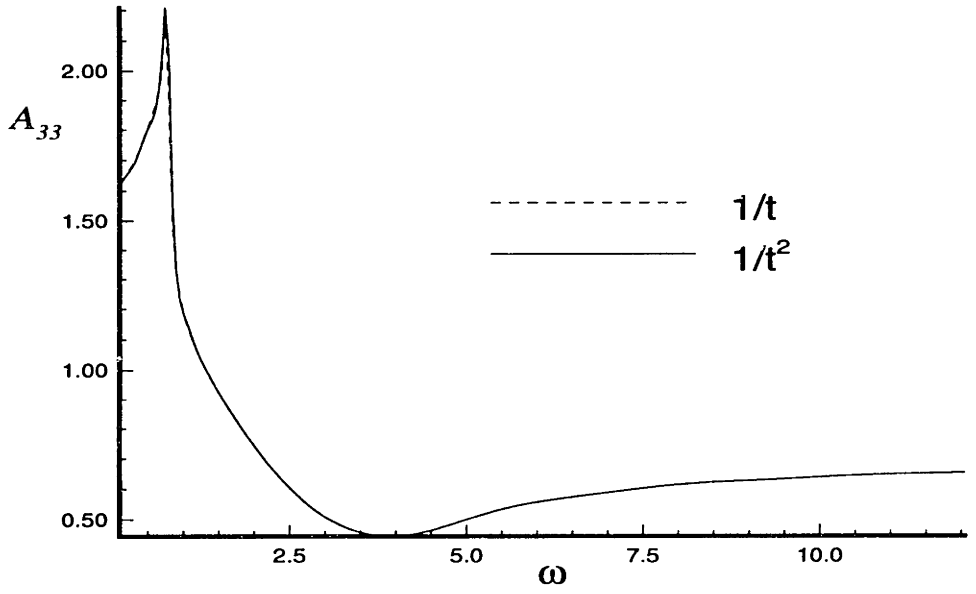

Figure 3-2: Wigley hull at $F_n = 0.3$, added-mass coefficients calculated using both a $1/t$ and a $1/t^2$ continuation of the impulse-response function.

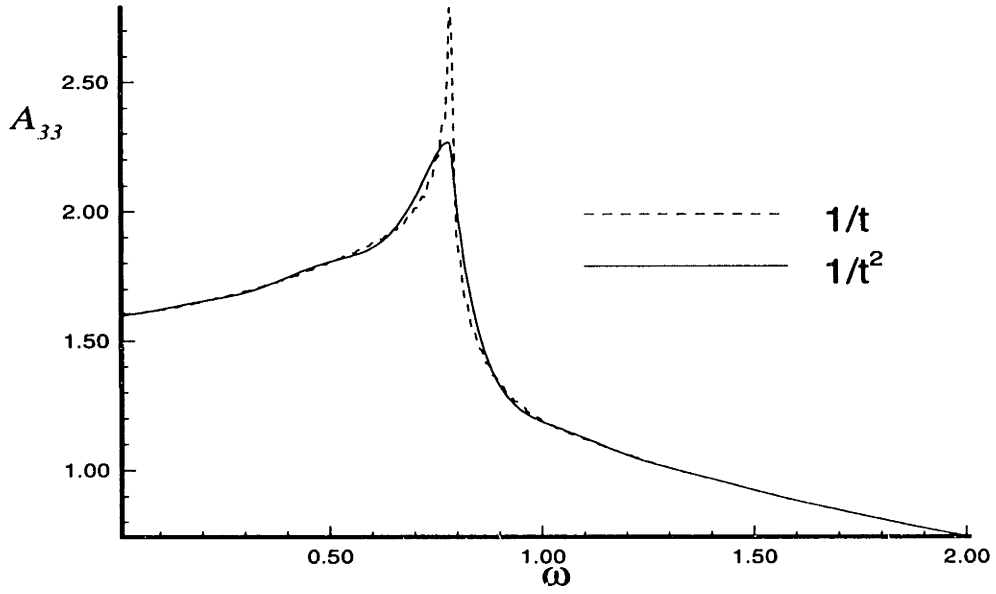

Figure 3-3: Expanded view near $\tau = 1/4$

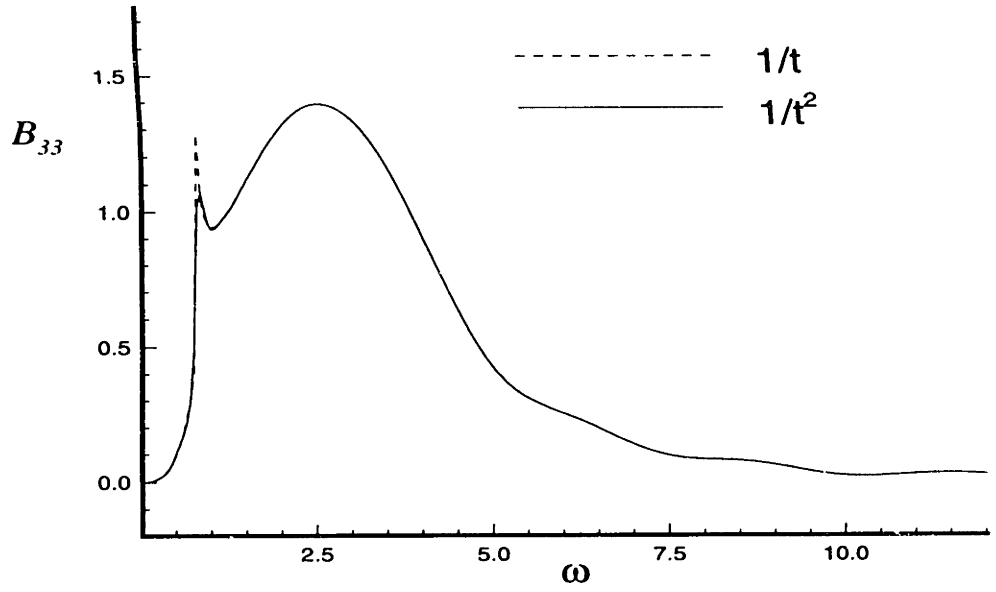

Figure 3-4: Wigley hull at $F_n = 0.3$, damping coefficients calculated using both a $1/t$ and a $1/t^2$ continuation of the impulse-response function.

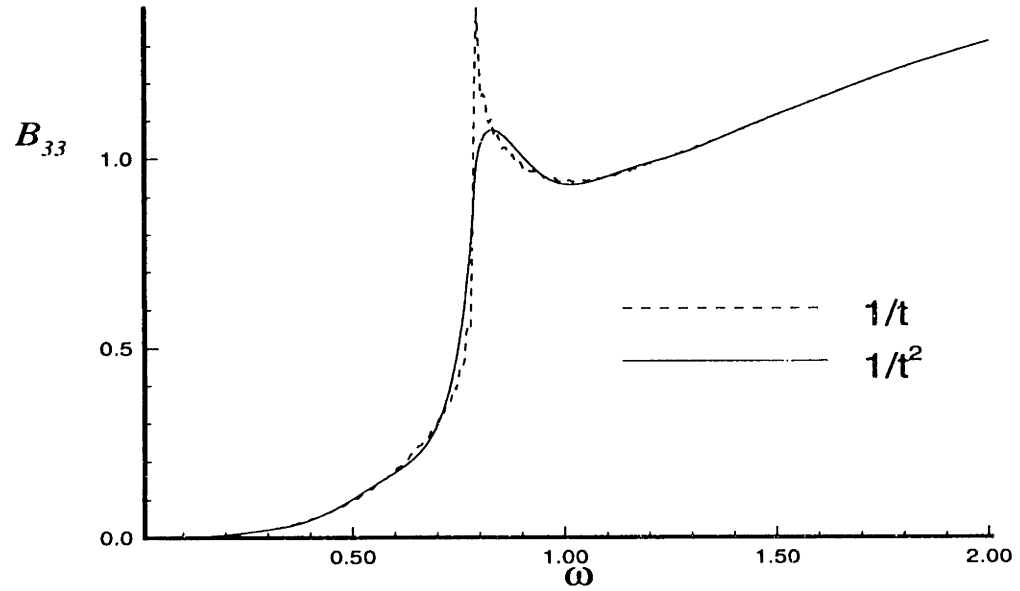

Figure 3-5: Expanded view near $\tau = 1/4$

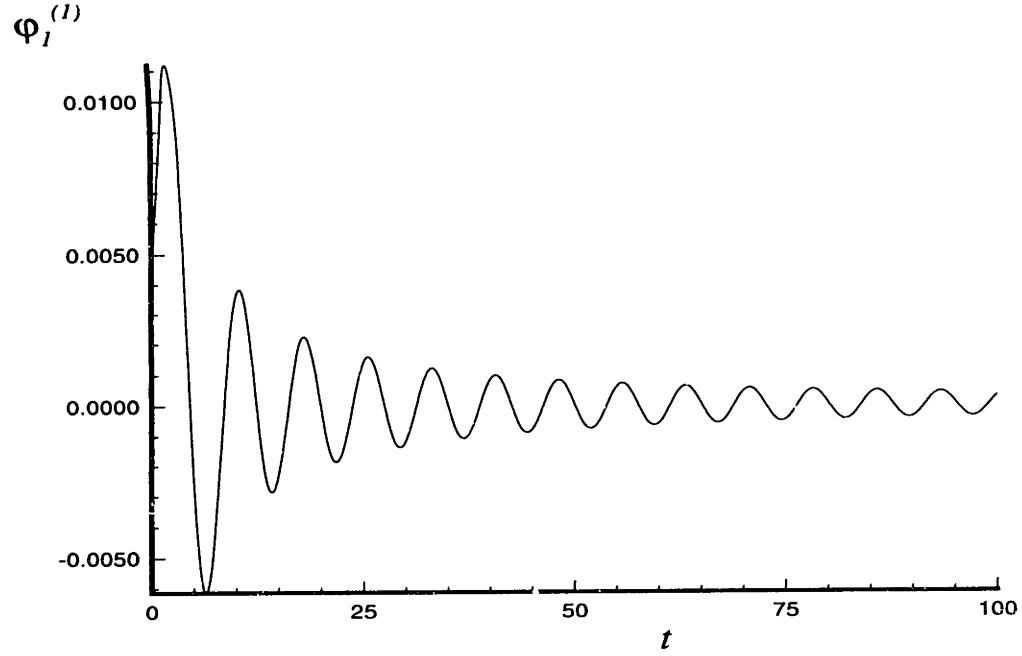

Figure 3-6: Wigley hull at $F_n = 0.3$, impulsive surge velocity potential on a bow-waterline panel.

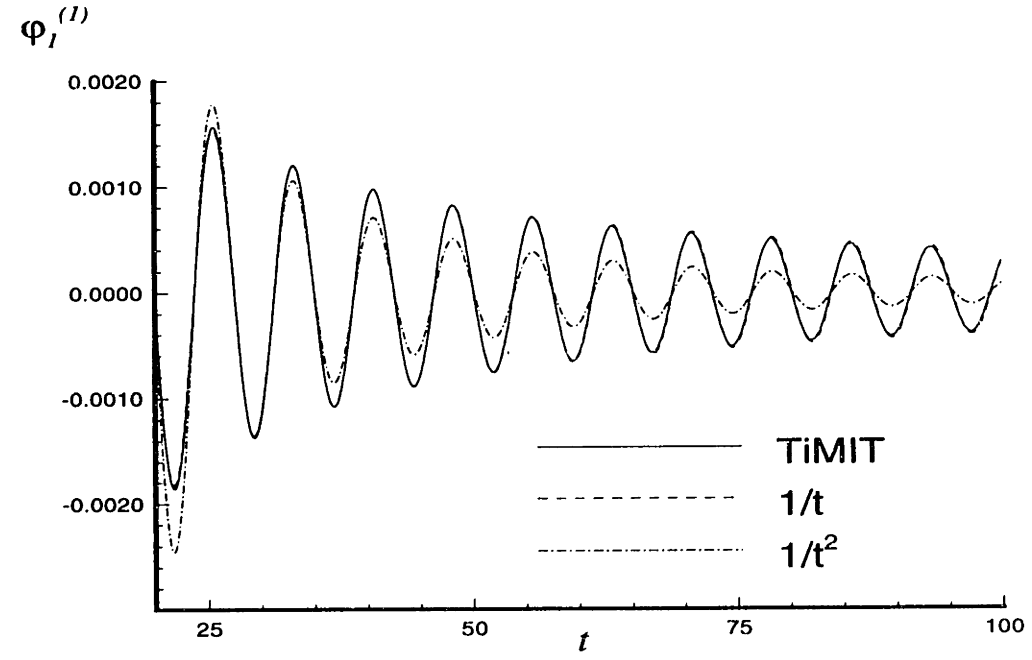

Figure 3-7: Wigley hull at $F_n = 0.3$, potential on a panel and a least squares fitting of the data to two rates of decay.

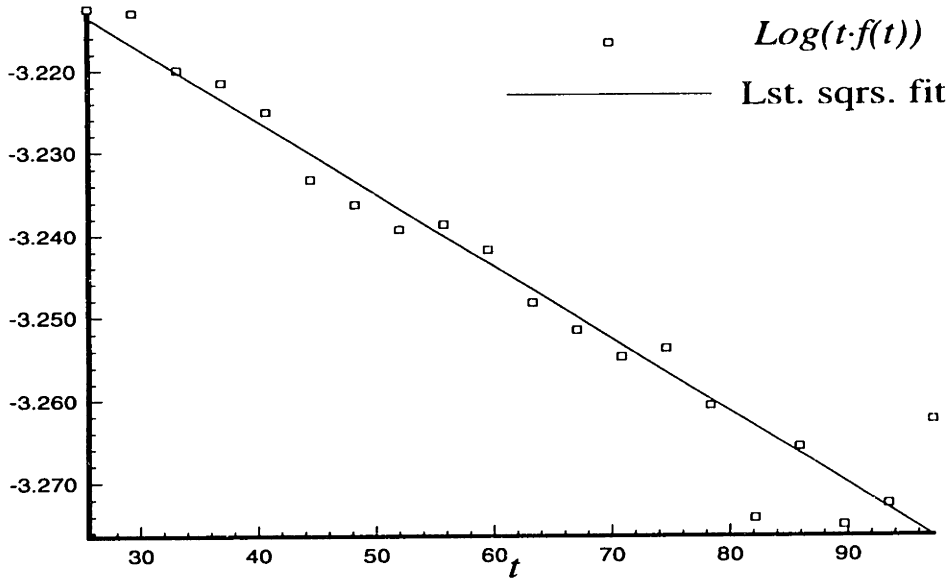

Figure 3-8: Wigley hull at $F_n = 0.3$, a straight line least squares fit to the function $log(t \cdot f(t))$ where $f(t) =$ the values at the extrema of the potential.

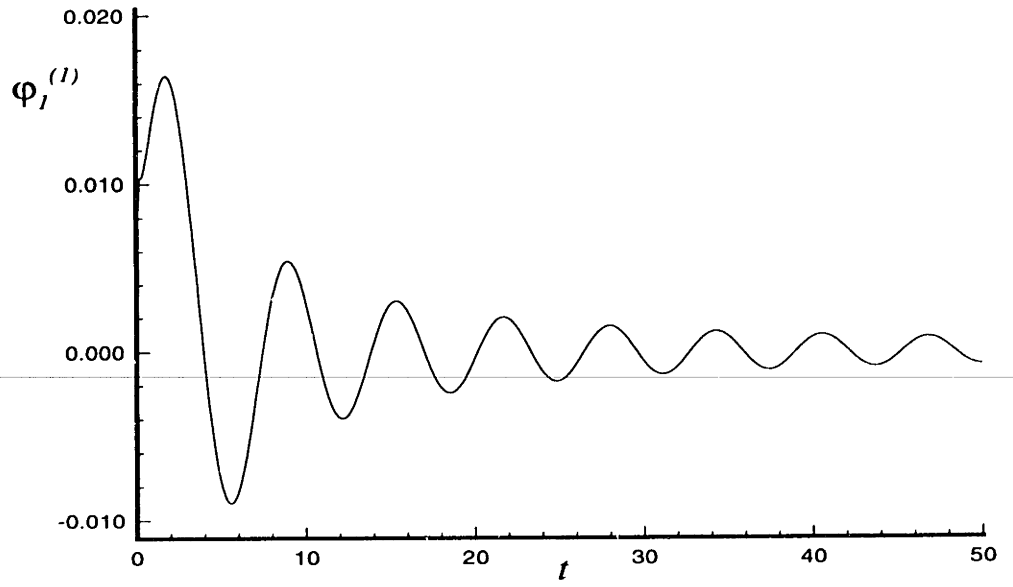

Figure 3-9: Wigley hull at $F_n = 0.25$, impulsive surge velocity potential on a bow-waterline panel.

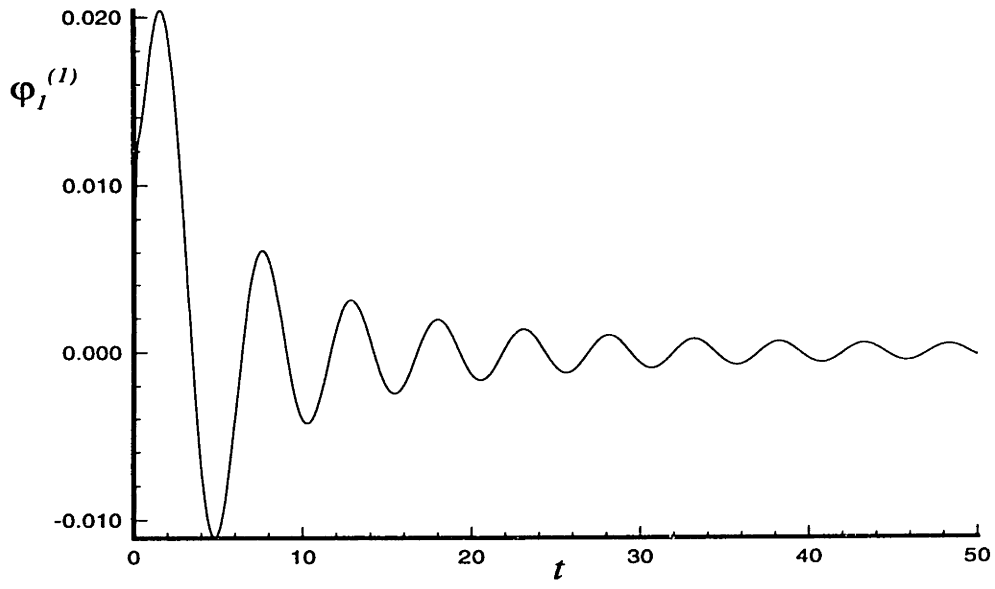

Figure 3-10: Wigley hull at $F_n = 0.2$, impulsive surge velocity potential on a bow-waterline panel.

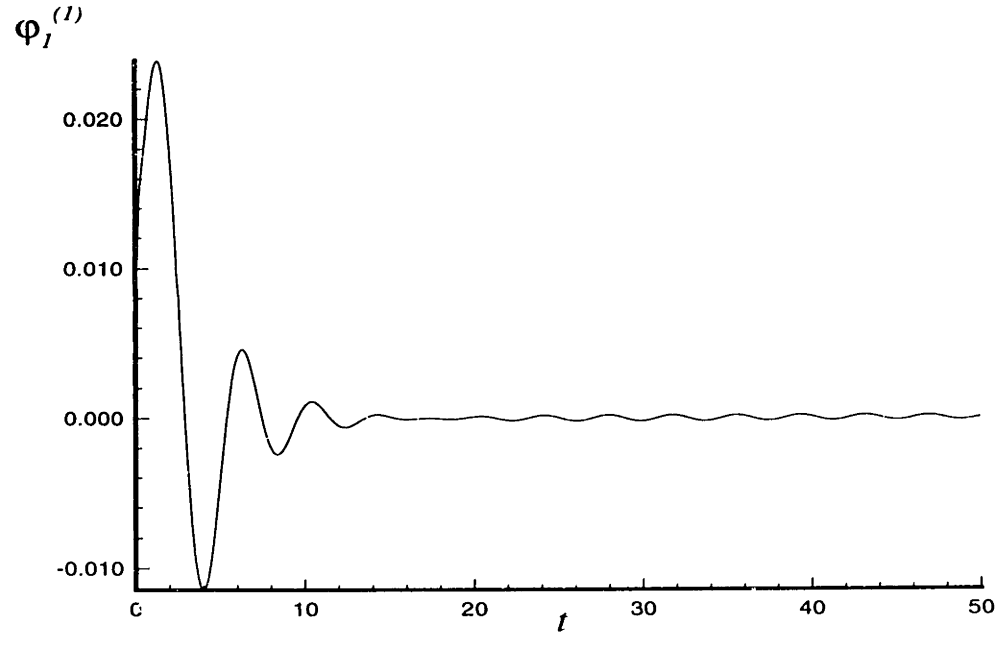

Figure 3-11: Wigley hull at $F_n = 0.15$, impulsive surge velocity potential on a bow-waterline panel.

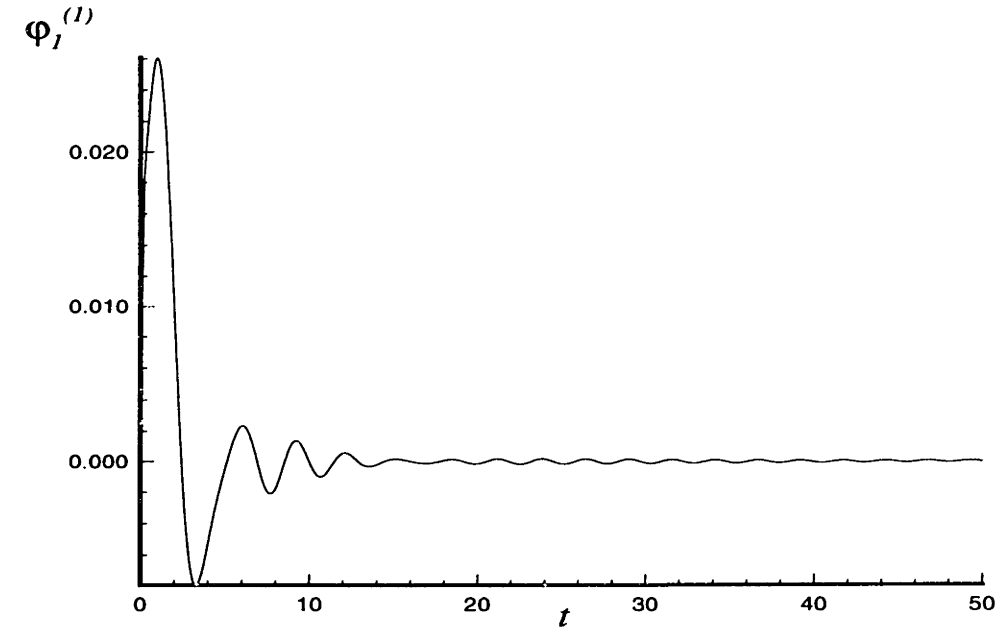

Figure 3-12: Wigley hull at $F_n = 0.1$, impulsive surge velocity potential on a bow-waterline panel.

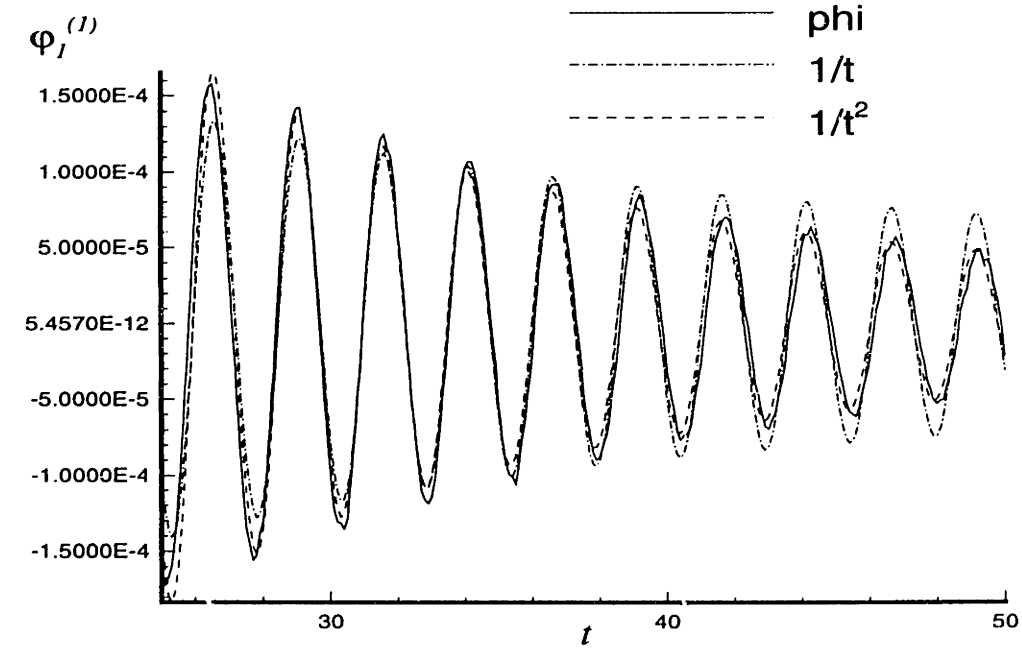

Figure 3-13: Wigley hull at $F_n = 0.1$, expanded view of the large-time asymptotics of the potential and a least squares fit of the data to two rates of decay.

3.5 Numerical Fourier Transform

When the body has zero forward speed, the impulse-response function will decay rapidly to zero (excepting the numerical irregular frequency effects). It is a *good* function, in the sense used by Lighthill [32], which can be readily transformed into the frequency-domain using Filon integration, or some other Fourier transform technique. At non-zero forward speed, however, the situation is more complicated.

The impulsive displacement memory function, $K_{jk}^{(0)}$, is always a good function and needs only to be continued asymptotically to infinite time, as discussed above. The memory function at $n > 0$ will in general tend to some non-zero steady-state limit which must be dealt with appropriately before a transform can be taken. The most straightforward way of making $K_{jk}^{(n)}$ a good function is to take n time derivatives and thereby transform it into $K_{jk}^{(0)}$, as discussed in Section 2.8. [In practice, however, taking a large number of numerical time derivatives can be troublesome.] An alternative is to subtract the steady-state limits from the memory function, (having found them through some sort of data-fitting technique) and add them to the appropriate constant coefficients. For example, it can be shown that,

$$\begin{aligned} K_{jk}^{(2)}(t) = &\quad \bar{K}_{jk}^{(2)}(t) + b_{jk}^{(2)} h(t) + c_{jk}^{(2)} r(t) \\ K_{jk}^{(1)}(t) = &\quad \bar{K}_{jk}^{(1)}(t) + c_{jk}^{(2)} k(t) \end{aligned}$$

where, $\bar{K}_{jk}^{(n)}$ are always good functions, and the new coefficients (which may be zero) will combine with the constant damping and hydrodynamic restoring force coefficients already defined in Section 2.8. Having obtained a good memory function, it can be continued to infinite time and transformed into the frequency-domain.

3.5.1 Analytic Transform of the Asymptotics

The Fourier transform of an impulse response function which has been continued to infinite time using a $1/t$ rate of decay can be done in a semi-analytic way. The integral over the asymptotic portion of the impulse response function can be related to

a combination of sine and cosine integrals and integrated analytically. This function of frequency can be combined with a numerical integration over the calculated portion of the impulse-response function to obtain the complete Fourier transform.

Recall the relationship between the impulse-response and the frequency-response functions, Equation (2.44). The frequency dependent parts of the added mass and damping coefficients can be expressed as

$$\begin{aligned} A_{jk}(\omega) = &\ \Re \frac{-(i\omega)^n}{\omega^2} \int_0^\infty \bar{K}_{jk}^{(n)}(t) \left[\cos(\omega t) - i \sin(\omega t)\right] \, dt \\ B_{jk}(\omega) = &\ \Im \frac{(i\omega)^n}{\omega} \int_0^\infty \bar{K}_{jk}^{(n)}(t) \left[\cos(\omega t) - i \sin(\omega t)\right] \, dt. \end{aligned} \tag{3.5}$$

The function $\bar{K}_{jk}^{(n)}(t)$ has been calculated from $t = 0$ to some point t_m and the last portion of this time history has been fit to the function

$$\frac{1}{t}[a_1 \sin(\omega_c t) + a_2 \cos(\omega_c t)]$$

so that the two coefficients a_1 and a_2 are known. [The results in this thesis have all been fit in a least squares sense to all of the calculated points in the last 1/4 of a $\tau = 1/4$ period.] We now take the integral from $t = 0$ to $t = t_m$ numerically, and consider the two quantities

$$I_1 = \int_{t_m}^\infty \frac{1}{t} \left[a_1 \sin(\omega_c t) + a_2 \cos(\omega_c t)\right] \sin(\omega t) \, dt$$

and,

$$I_2 = \int_{t_m}^\infty \frac{1}{t} \left[a_1 \sin(\omega_c t) + a_2 \cos(\omega_c t)\right] \cos(\omega t) \, dt.$$

I_1 can be written in two ways:

$$\begin{aligned} I_1 = &\ a_1 \int_{t_m}^\infty \frac{1}{t} \left\{\cos(\omega_c t) \cos(\omega t) - \cos[(\omega + \omega_c) t]\right\} \, dt \\ &+ a_2 \int_{t_m}^\infty \frac{1}{t} \left\{\sin[(\omega + \omega_c) t] - \sin(\omega_c t) \cos(\omega t)\right\} \, dt \end{aligned}$$

but also,

$$I_1 = a_1 \int_{t_m}^{\infty} \frac{1}{t} \{\cos(|\omega - \omega_c|\, t) - \cos(\omega\, t)\cos(\omega_c\, t)\}\, dt$$
$$+a_2 \int_{t_m}^{\infty} \frac{1}{t} \{\sin(\omega_c\, t)\cos(\omega\, t) \pm \sin(|\omega - \omega_c|\, t)\}\, dt$$
$$\omega \gtrless \omega_c. \qquad (3.6)$$

Add these two equations to get

$$2I_1 = a_1 \int_{t_m}^{\infty} \frac{1}{t} \{\cos(|\omega - \omega_c|\, t) - \cos[(\omega + \omega_c)\, t]\}\, dt$$
$$+a_2 \int_{t_m}^{\infty} \frac{1}{t} \{\sin[(\omega + \omega_c)\, t] \pm \sin(|\omega - \omega_c|\, t)\}\, dt$$
$$\omega \gtrless \omega_c \qquad (3.7)$$

and using the definitions of the sine and cosine integrals (*e.g.* Abramowitz and Stegun [1]) we find that

$$I_1 = \frac{1}{2} \{a_1 [\mathrm{Ci}[(\omega + \omega_c)\, t_m] - \mathrm{Ci}(|\omega - \omega_c|\, t_m)]$$
$$- a_2 [\mathrm{si}[(\omega + \omega_c)\, t_m] \pm \mathrm{si}(|\omega - \omega_c|\, t_m)]\}$$
$$\omega \gtrless \omega_c. \qquad (3.8)$$

A similar manipulation shows that

$$I_2 = -\frac{1}{2} \{a_2 [\mathrm{Ci}[(\omega + \omega_c)\, t_m] + \mathrm{Ci}(|\omega - \omega_c|\, t_m)]$$
$$- a_1 [-\mathrm{si}[(\omega + \omega_c)\, t_m] \pm \mathrm{si}(|\omega - \omega_c|\, t_m)]\}$$
$$\omega \gtrless \omega_c. \qquad (3.9)$$

3.6 Irregular Behavior of Solutions

Discrete numerical solutions of the transient integral equations generally contain a non-physical oscillation in the solution. At zero forward speed the oscillation persists

indefinitely in time and, when Fourier transformed, produces an irregular behavior in the vicinity of the irregular frequencies which is nearly identical to what is observed in solutions to the corresponding frequency domain equations. At non-zero forward speed, the oscillation becomes of finite duration and becomes less clearly associated with the zero speed irregular frequencies as the speed is increased. This section provides a demonstration of these effects in both the time and the frequency domain, and at both zero and non-zero forward speed. Refinement of the discretizations in both space and time is shown to remove the errors associated with this oscillation. It is suggested that discretization introduces this behavior into the transient solution by relaxing the satisfaction of the initial conditions, and this conjecture is supported by the analysis which appears in Appendix C.

The above mentioned non-physical oscillation of the solution is visible in Figure 3-14, and more clearly in the expanded view of Figure 3-15. These plots show a calculation of the heave-heave impulse response function for a Wigley hull at zero forward speed with 144 panels used to describe half of the hull. Notice that the oscillation persists indefinitely. Figures 3-16 and 3-17 are the Fourier transform of this calculation and show the irregular behavior in the frequency domain. The same quantities calculated directly in the frequency domain using the computer program WAMIT [10] (and with the same input) are also shown in these plots. WAMIT is a numerical solution of Equation (2.25), the zero-speed time-harmonic analog to the equation which is solved by T$\bar{\text{I}}$MIT . The expanded views of these two figures show that the behavior of the two solutions is nearly identical, even in the vicinity of the irregular frequencies. [At least it is close enough that the differences can be attributed to the combination of truncating and taking a numerical Fourier transform of the transient solution.]

At non-zero forward speed the irregular oscillations in the solution become of finite duration. A time t_1 can always be found after which these oscillations are entirely absent from the solution, and t_1 is very close to the time needed for the ship to travel one ship length after the initial impulse. If the variables are non-dimensionalized by the ship length then t_1 is approximately the inverse of the Froude number. The series

of Figures 3-20 through 3-26 demonstrates this behavior in the surge-surge impulse-response function as the speed is increased from $F_n = 0.0$ to $F_n = 0.4$. The irregular behavior is relatively strong in the surge response (presumably because the absolute magnitude is so small) and the change due to the increasing speed is therefore more apparent, although this effect can be seen in all modes. The value of t_1 is indicated on each plot and can be identified as approximately the point of transition between the irregular frequency contaminated region of the calculation and the asymptotics which are dominated by the critical frequency (see Section 2.7).

This compression in time of the irregular frequency effects leads to an expansion in the frequency content of the contaminated region surrounding each irregular-frequency. Figures 3-27 through 3-31 are a demonstration. These figures show the pitch-pitch damping coefficients with increasing speed. Experimental results are also shown in Figure 3-30 providing a further indication that this oscillation in Fourier space is not related to any physical phenomenon. As in the zero speed case, the irregular behavior is reduced by refining the discretization. Figures 3-32 and 3-33 show the effect of increasing the numbers of panels in both the time and the frequency domain. The error introduced into the solution by the numerical irregular frequencies appears to be sensitive to the shape of the vessel, especially near the stern, and is magnified in the case of the Series 60 hull.

The foregoing has been a demonstration of the irregular behavior of numerical solutions to the discrete form of the transient integral equation. This behavior is clearly associated with the irregular frequencies at zero forward speed, but becomes less so as the speed is increased. Both at zero and at non-zero forward speed, the errors associated with this behavior are removed from the solution by refinement of the discretizations in both space and time. We attribute the introduction of this behavior into the the discrete solution to an imperfect satisfaction of the initial conditions. [By "initial conditions", it is understood that these appear in the transient problem at all times in the sense that the "initial" time is arbitrary and has initial conditions which depend upon the solution at all previous times.] This theory is motivated by considering a simplified problem and the details appear in Appendix C.

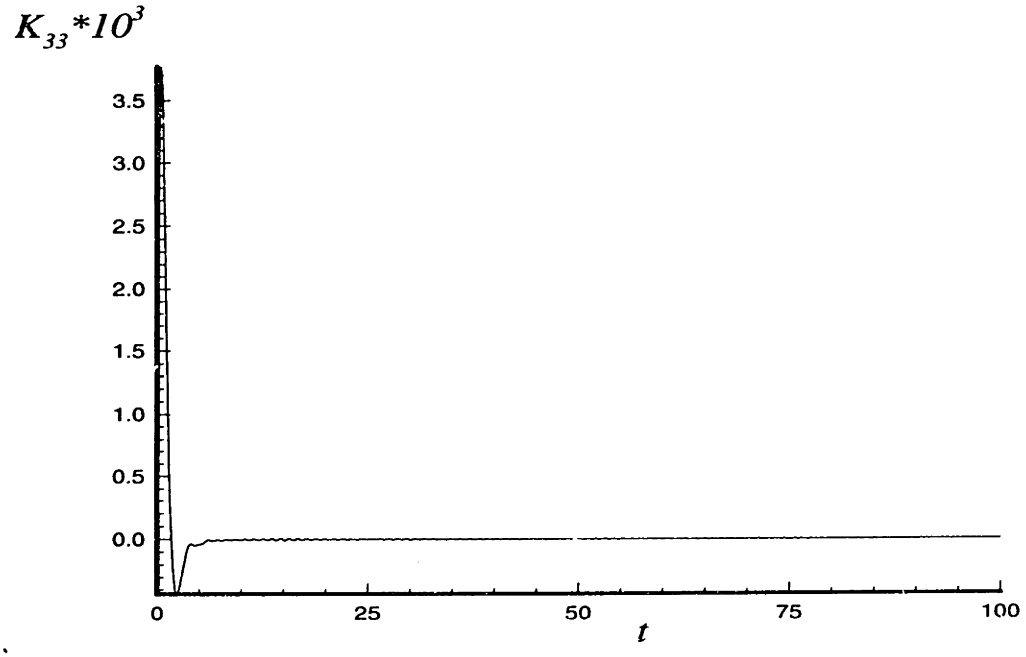

Figure 3-14: Impulsive acceleration heave-heave memory function for a Wigley hull at $F_n = 0.0$

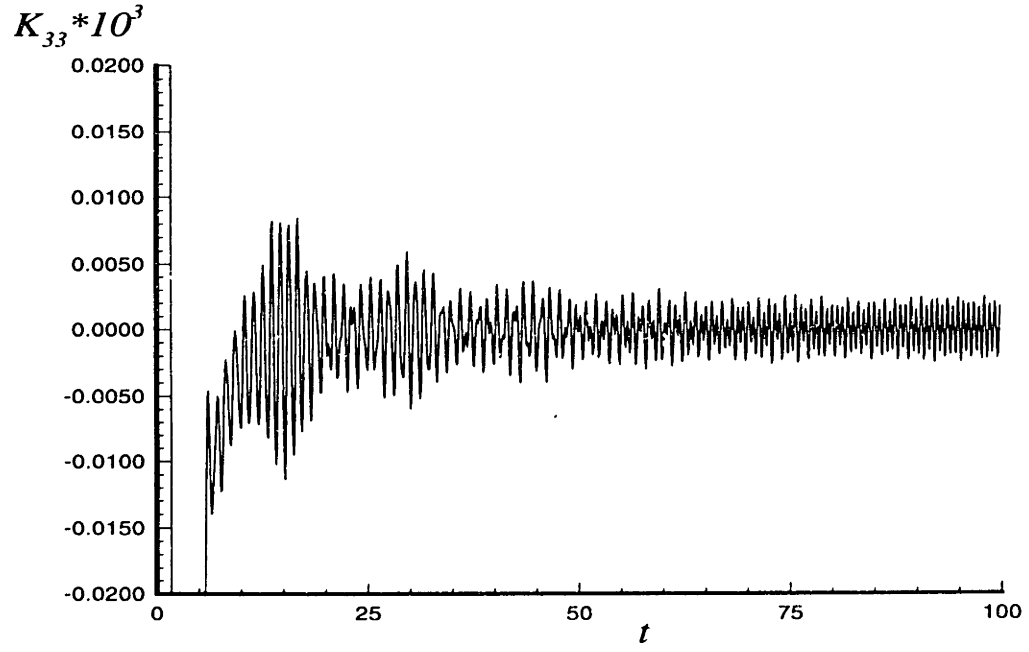

Figure 3-15: Expanded view of the effect of the irregular-frequencies, $F_n = 0.0$

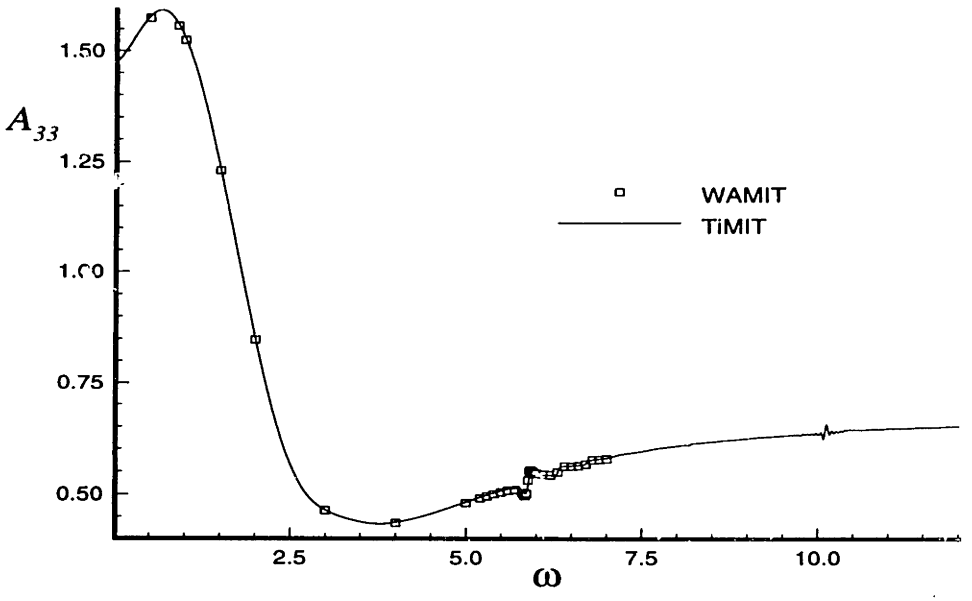

Figure 3-16: Heave-heave added-mass coefficients for a Wigley hull at $F_n = 0.0$

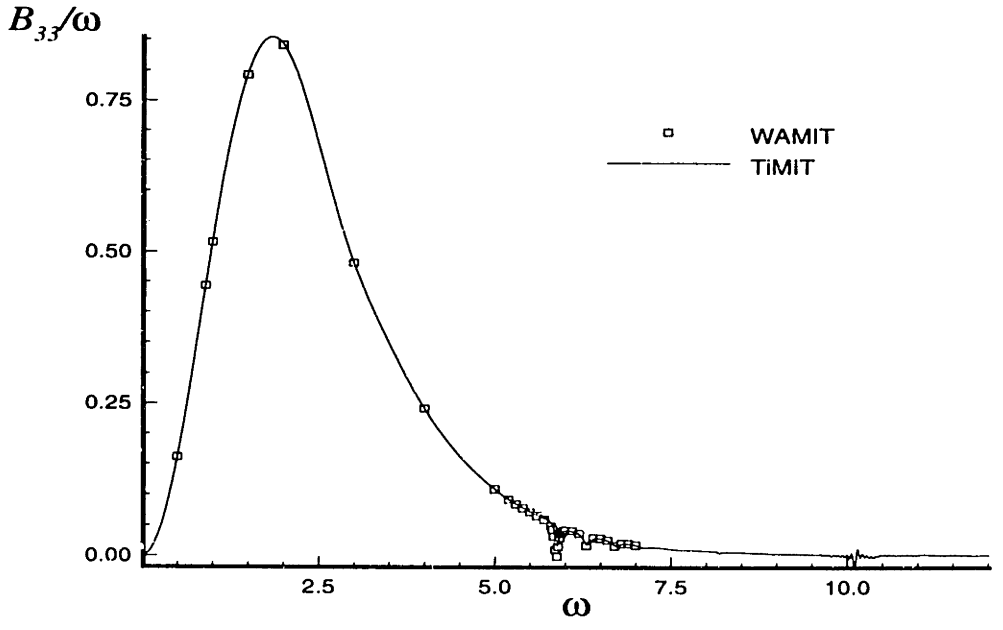

Figure 3-17: Heave-heave damping coefficients for a Wigley hull at $F_n = 0.0$

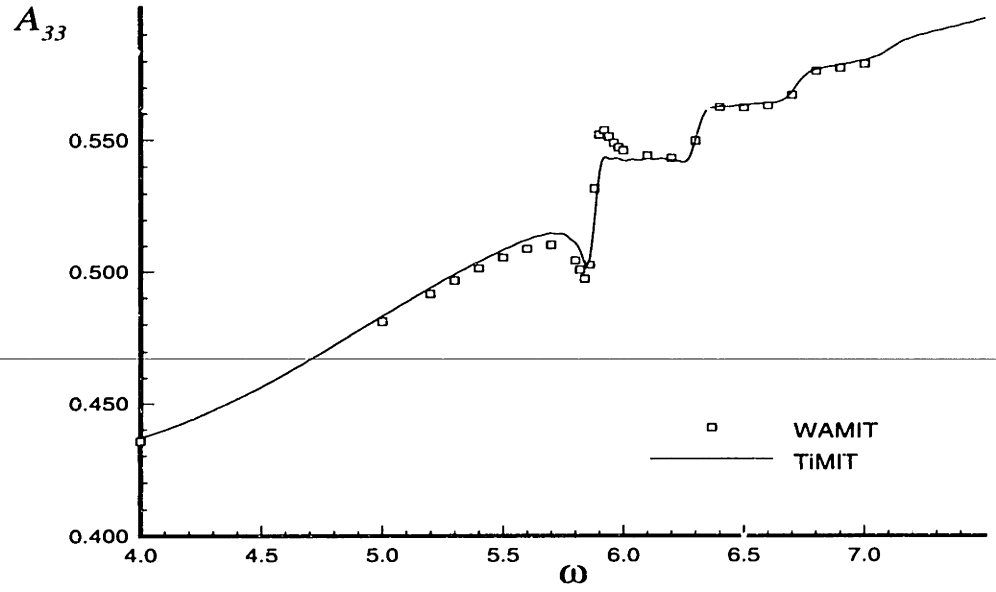

Figure 3-18: Expanded view of the heave-heave added-mass coefficients for a Wigley hull at $F_n = 0.0$

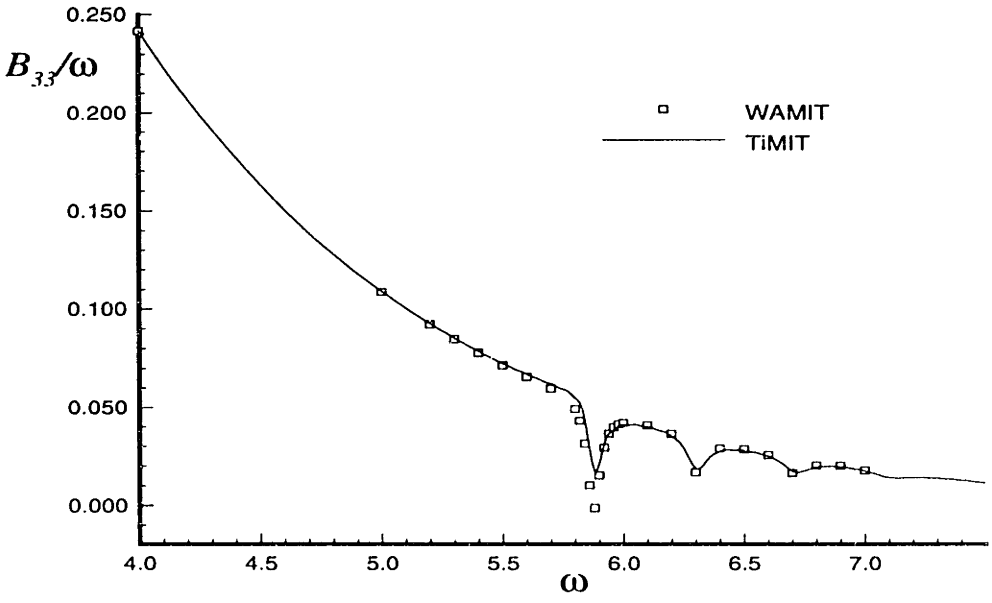

Figure 3-19: Expanded view of the heave-heave damping coefficients for a Wigley hull at $F_n = 0.0$

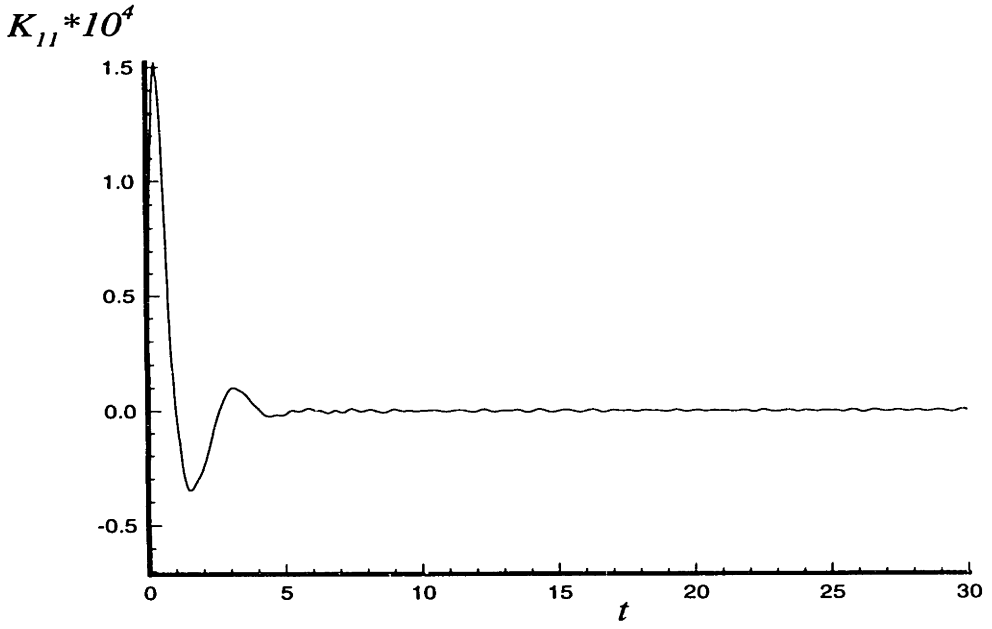

Figure 3-20: Surge-surge memory function for a Wigley hull at $F_n = 0.0$

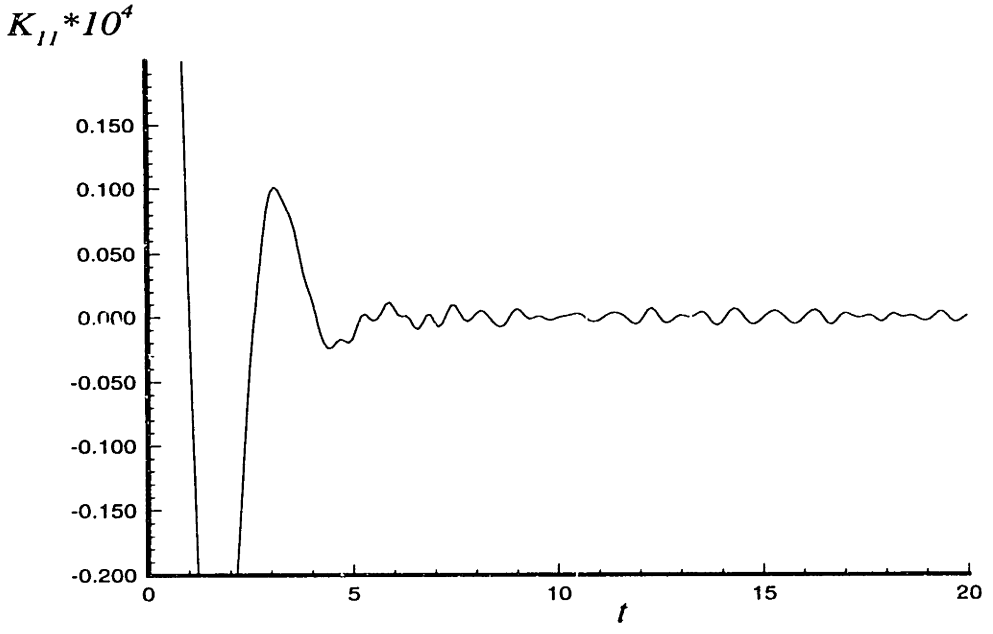

Figure 3-21: Expanded view, $F_n = 0.0$

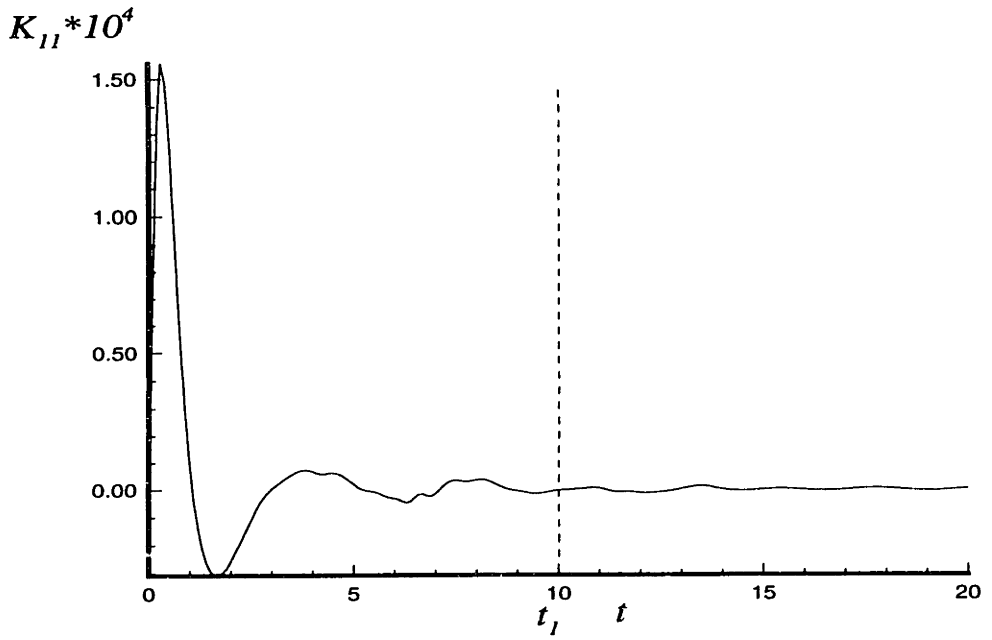

Figure 3-22: Impulsive acceleration surge-surge memory function for a Wigley hull at $F_n = 0.1$

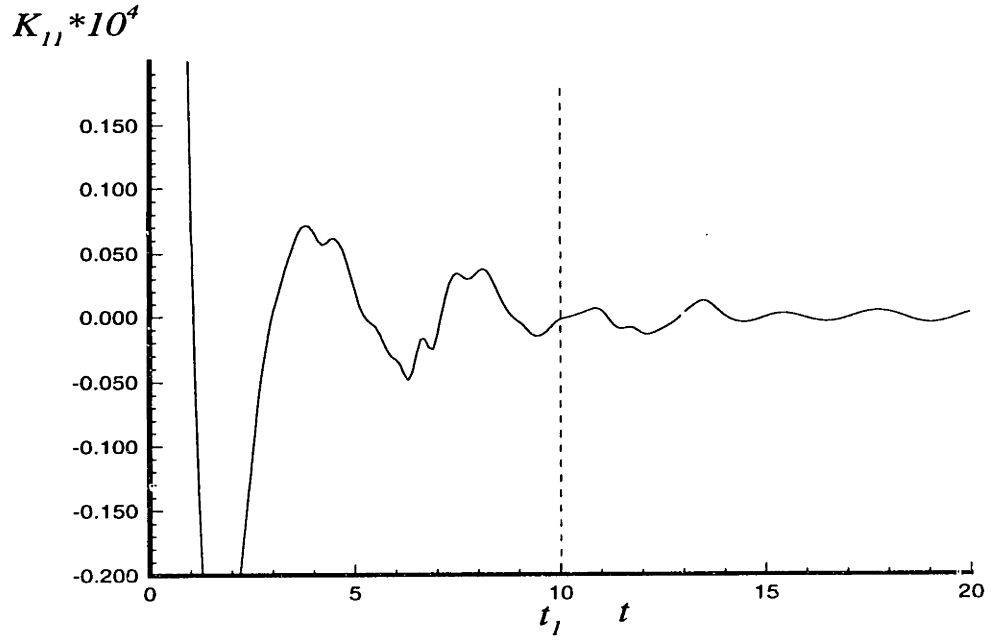

Figure 3-23: Expanded view, $F_n = 0.1$

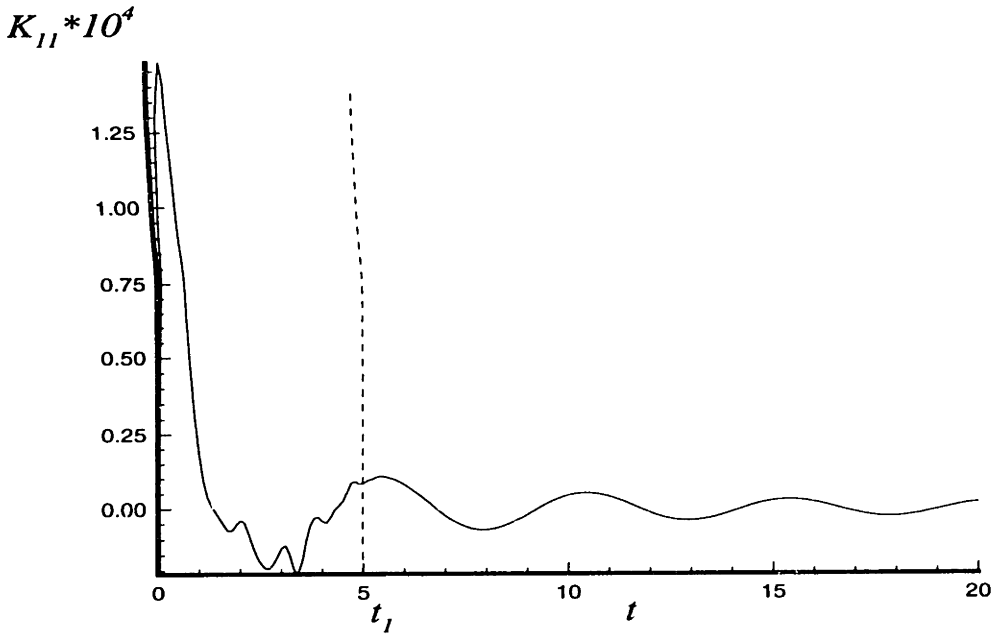

Figure 3-24: Impulsive acceleration surge-surge memory function for a Wigley hull at $F_n = 0.2$

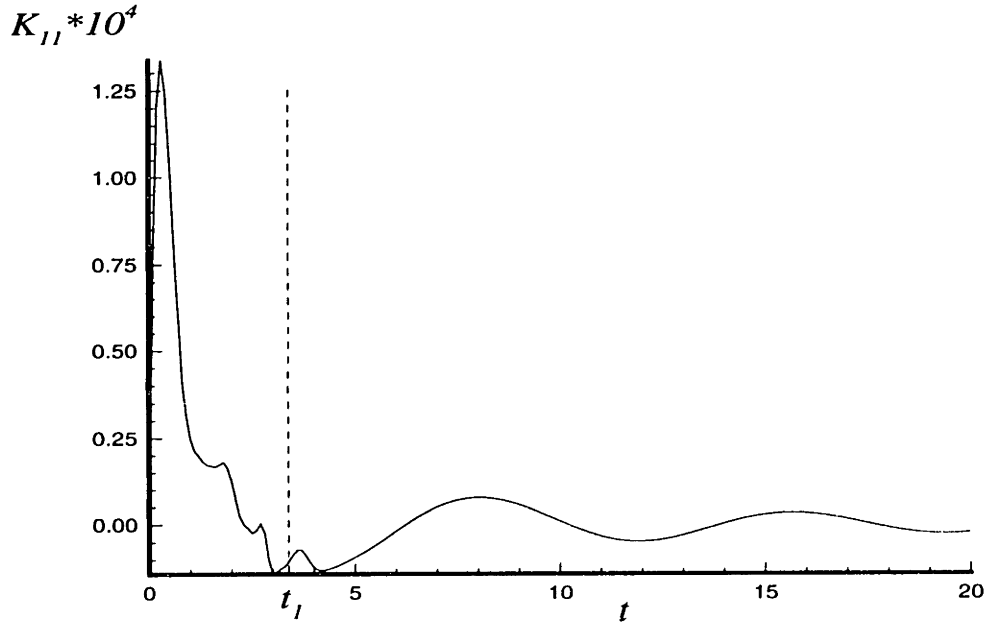

Figure 3-25: Impulsive acceleration surge-surge memory function for a Wigley hull at $F_n = 0.3$

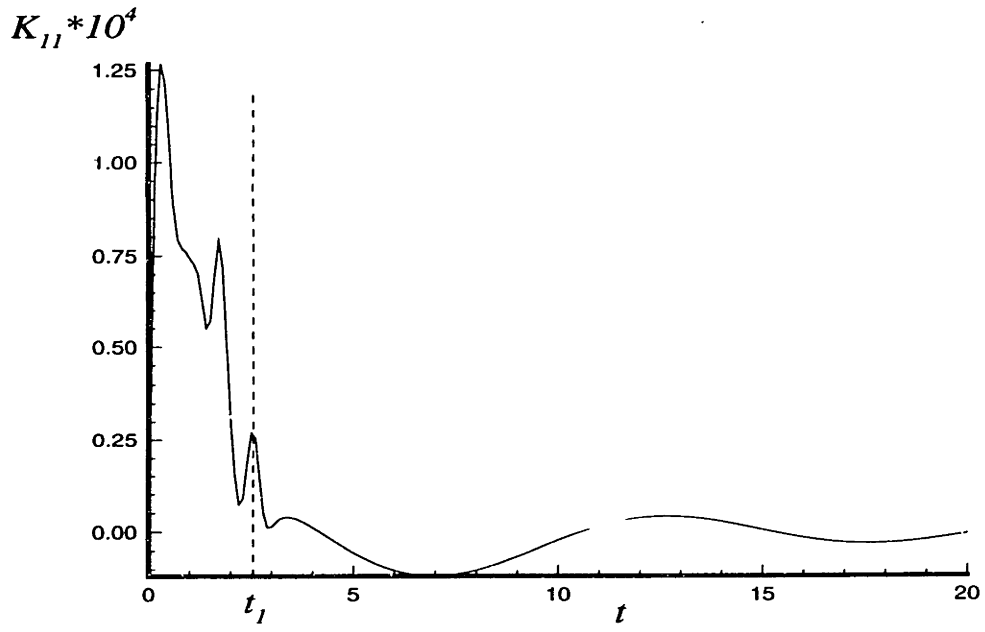

Figure 3-26: Impulsive acceleration surge-surge memory function for a Wigley hull at $F_n = 0.4$

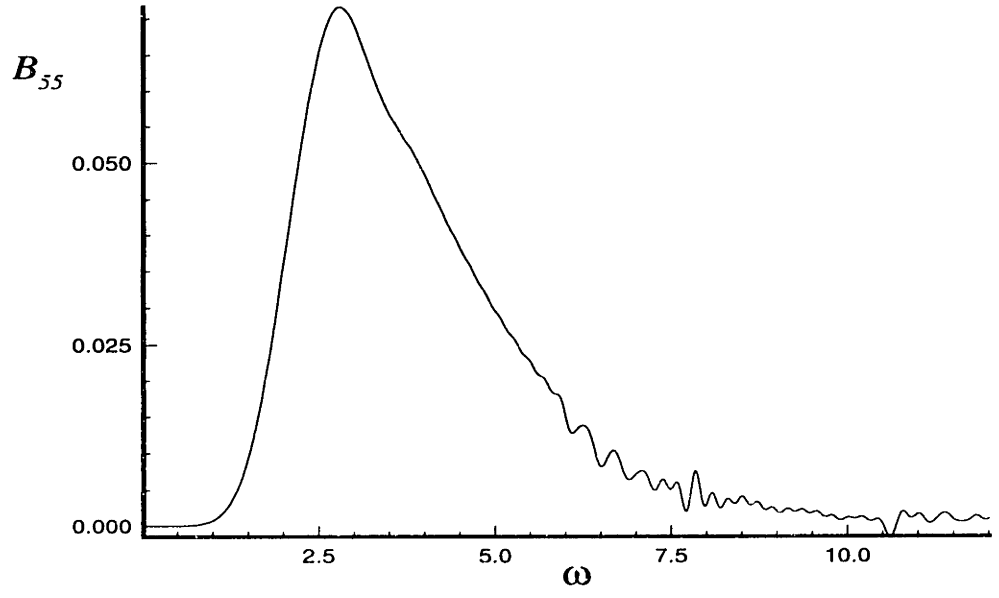

Figure 3-27: Pitch-pitch damping coefficients for a Wigley hull at $F_n = 0.0$

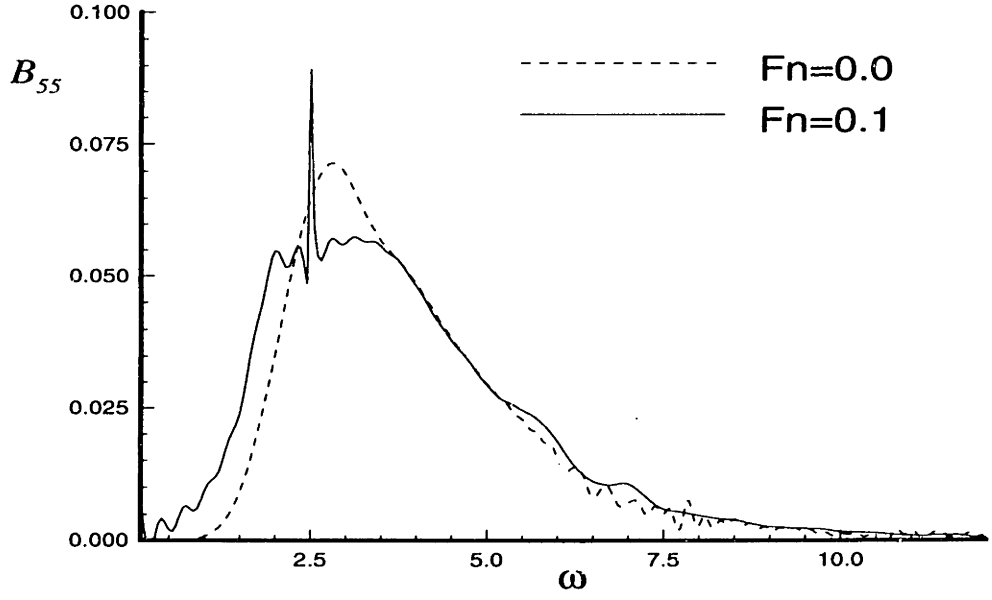

Figure 3-28: Pitch-pitch damping coefficients for a Wigley hull at Fn=0.1

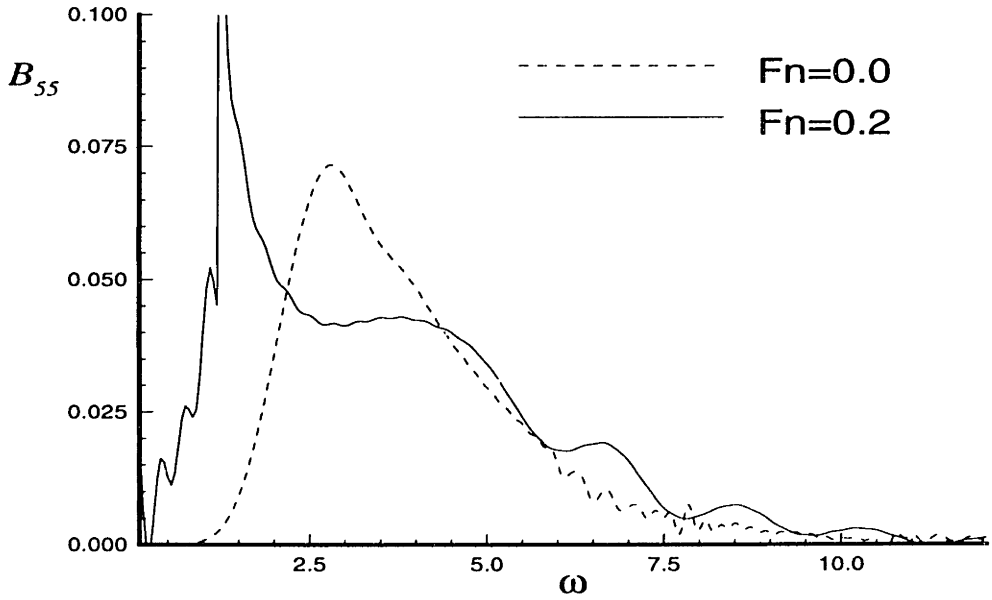

Figure 3-29: Pitch-pitch damping coefficients for a Wigley hull at $F_n = 0.2$

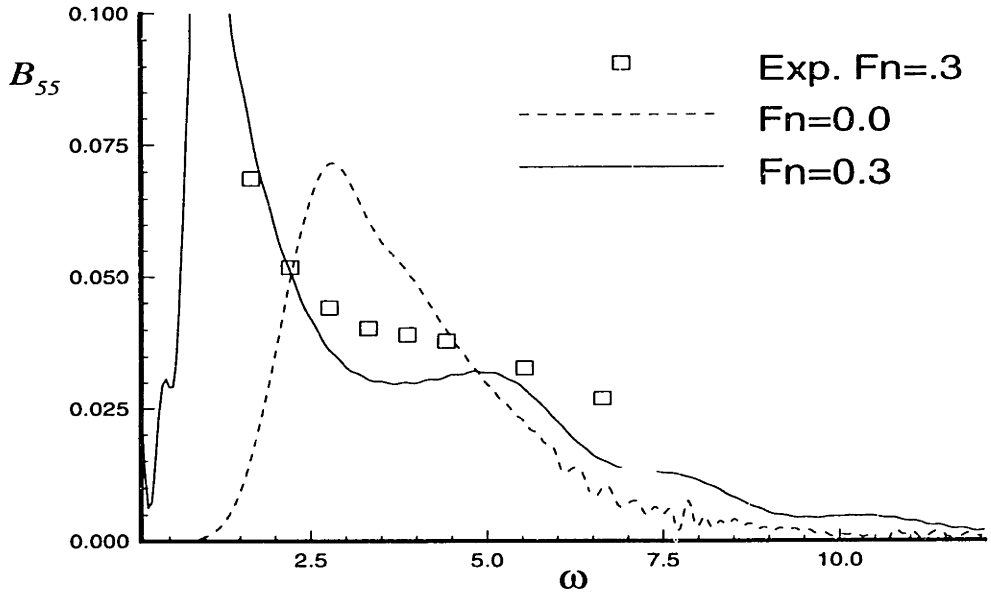

Figure 3-30: Pitch-pitch damping coefficients for a Wigley hull at $F_n = 0.3$

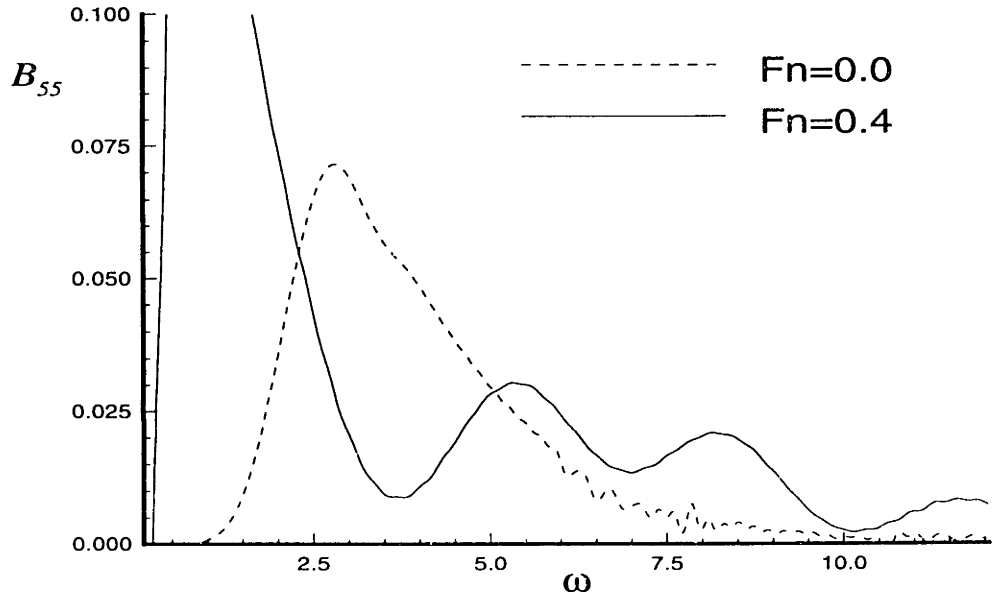

Figure 3-31: Pitch-pitch damping coefficients for a Wigley hull at $F_n = 0.4$

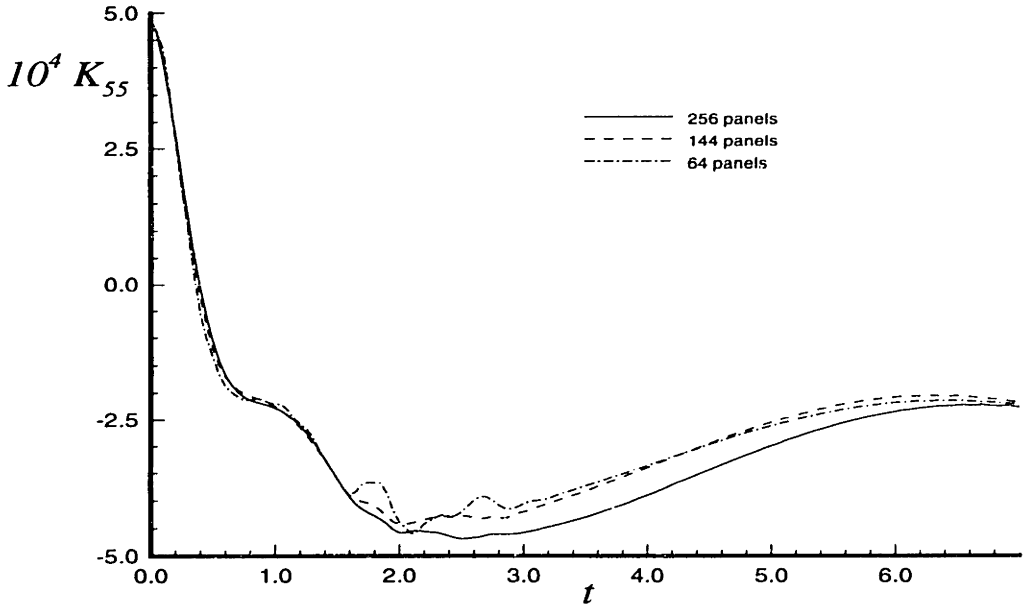

Figure 3-32: Pitch-pitch response of a Wigley hull at $F_n = 0.3$, showing how the the irregular behavior in the time domain is reduced with refinement of the discretization.

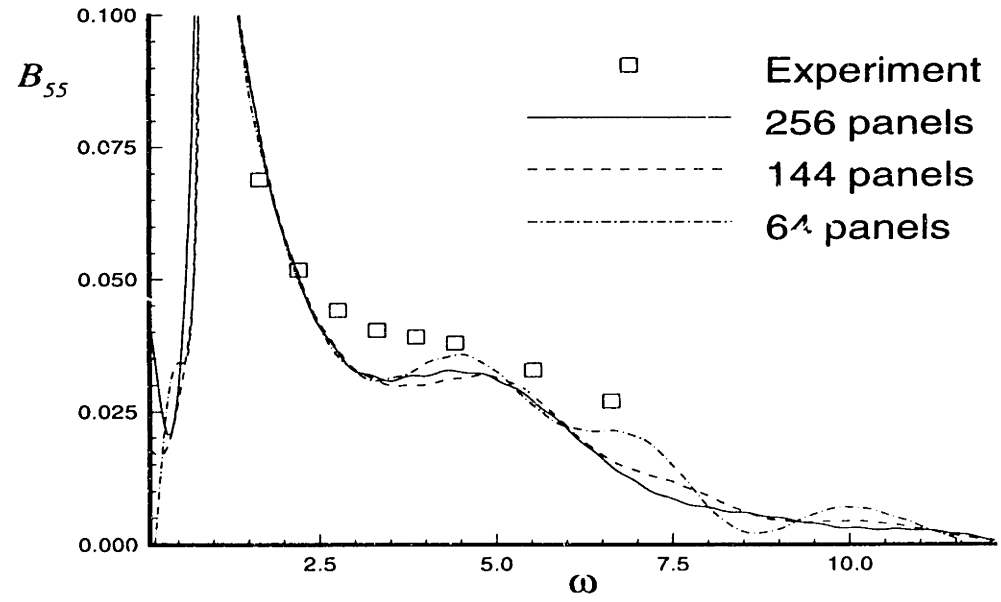

Figure 3-33: Pitch-pitch damping coefficients of a Wigley hull at $F_n = 0.3$, showing the corresponding reduction of the irregular behavior in the frequency domain.

3.7 Convergence of the Calculations

As shown in Section 2.9 the steady perturbation potential can be thought of as the large time limit of the radiation potential due to an impulsive acceleration in surge. The integrated quantities in the steady problem (wave resistance, sinkage force and trim moment) are in general more difficult to calculate than the impulse-response functions, (since they are relatively smaller) so this section will provide a demonstration of convergence for the steady calculations.

3.7.1 Wigley Hull

Figure 3-34 is a plot of the steady wave resistance of a Wigley hull at a Froude number of 0.3. The hull has been discretized using 64 panels (on half of the hull) and the curves show convergence as the time step size is refined. The next two plots show the same thing using spatial discretizations of 144 and 256 panels respectively. Figure 3-37 plots the converged (with respect to time discretization) results from the previous three figures to show convergence with spatial and temporal discretization. This sequence is repeated for the steady sinkage force and trim moment in the following eight plots.

The last three plots for the steady forces on the Wigley hull, Figures 3-46 through 3-48, are a comparison of the steady forces calculated by accelerating the ship impulsively with the same quantities calculated using the gradual acceleration which was discussed in Section 2.9.2. The comparison is made using the 64 panel discretization of the ship at a non-dimensional time step size of 0.5. The mean values of each calculation are included in these figures as well, and they appear as one since they differ from each other by less than 0.2%. Note that when the ship's velocity is allowed to vary, a fixed relationship between the ship's position and time no longer exists which means that previously calculated Green function coefficients can no longer be re-used. This increases the effort of the calculation by approximately a factor of six on a typical work-station (or the CRAY).

3.7.2 Series 60 Block 70 Hull

It is more difficult to show convergence of the calculations for the Series 60 hull. Convergence with time step size is achieved at approximately 1/2 the step size necessary with the Wigley hull. Although the convergence with refinement of the time-step is not shown, each of the curves appearing in Figures 3-49 through 3-51 is a converged result for that spatial discretization.

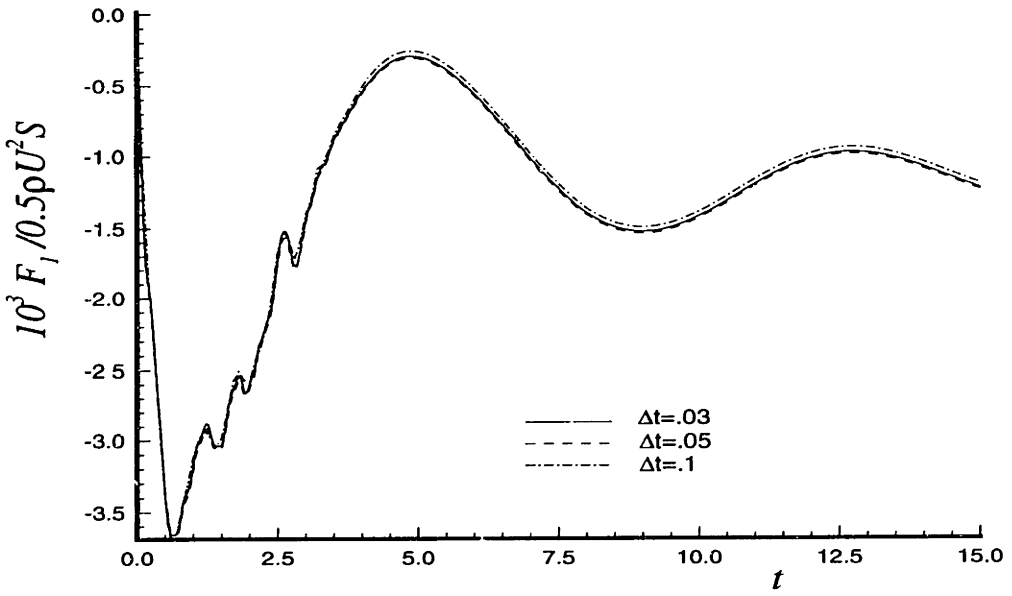

Figure 3-34: Convergence with time step size of the steady wave resistance on a Wigley hull at $F_n = 0.3$, 64 panels.

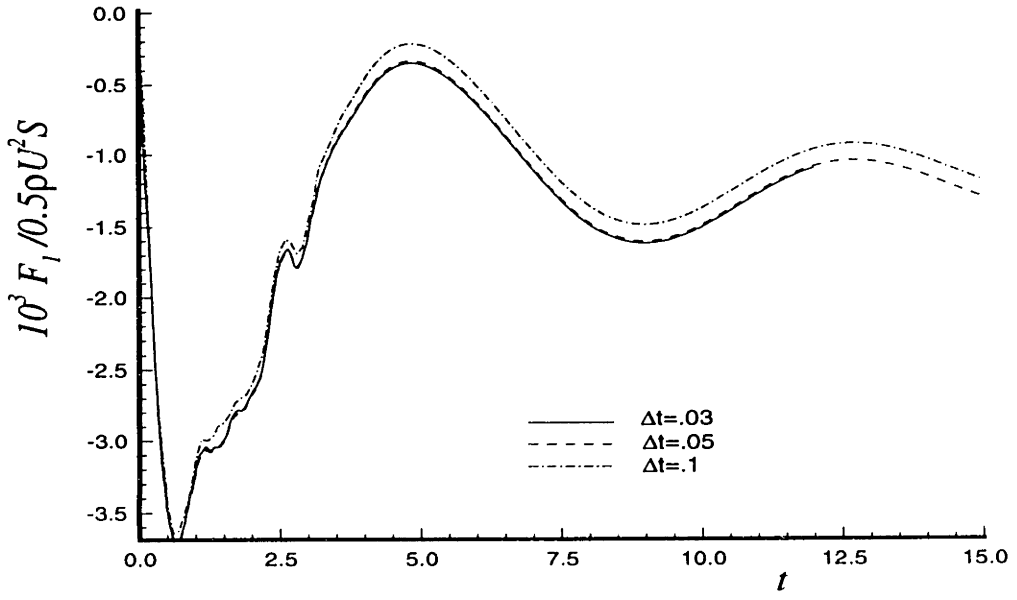

Figure 3-35: Convergence with time step size of the steady wave resistance on a Wigley hull at $F_n = 0.3$, 144 panels.

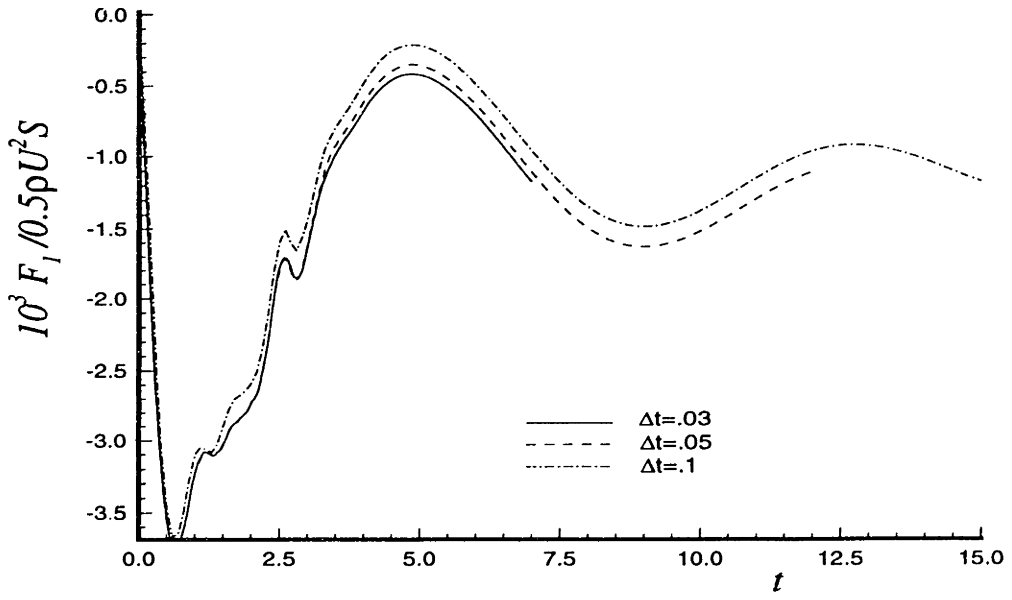

Figure 3-36: Convergence with time step size of the steady wave resistance on a Wigley hull at $F_n = 0.3$, 256 panels.

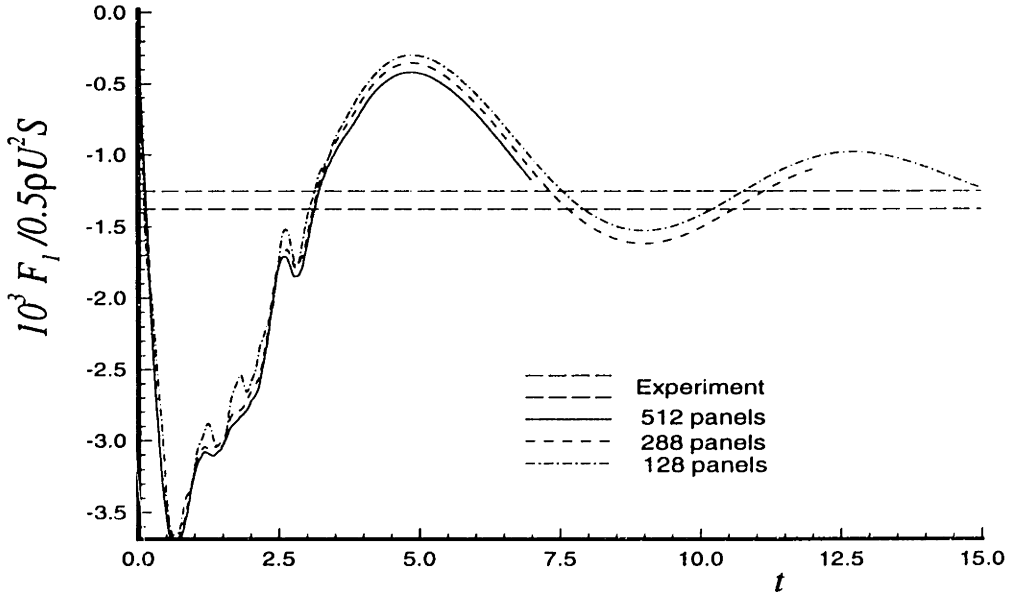

Figure 3-37: Convergence of the steady wave resistance on a Wigley hull at $F_n = 0.3$.

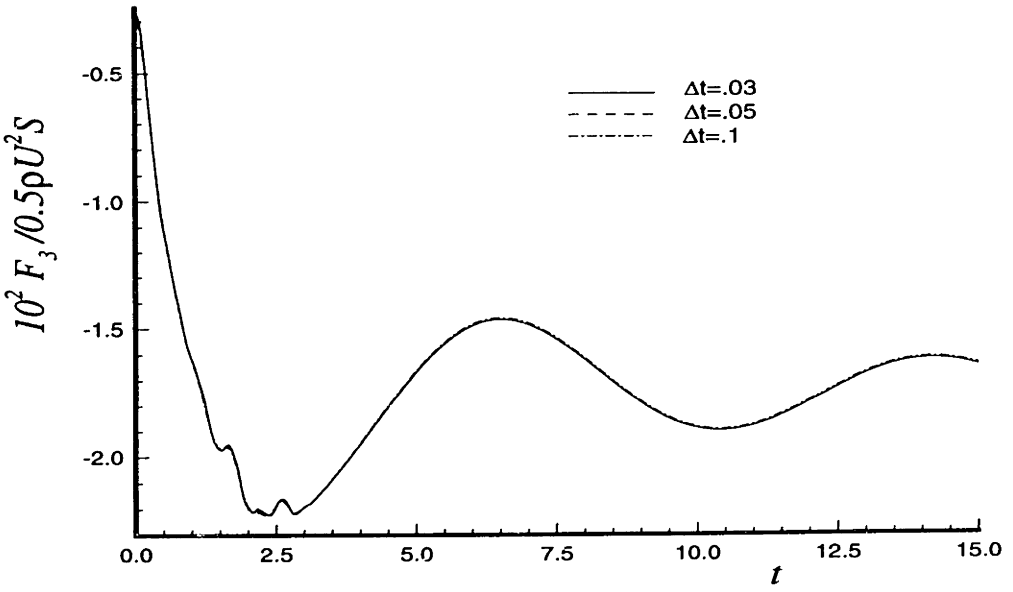

Figure 3-38: Convergence with time step size of the steady sinkage force on a Wigley hull at $F_n = 0.3$, 64 panels.

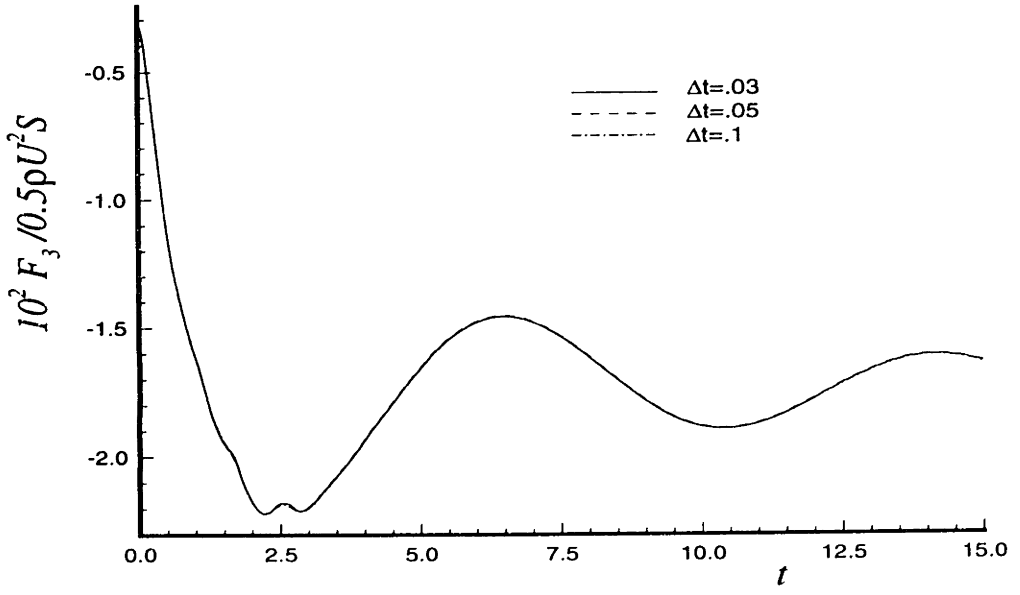

Figure 3-39: Convergence with time step size of the steady sinkage force on a Wigley hull at $F_n = 0.3$, 144 panels.

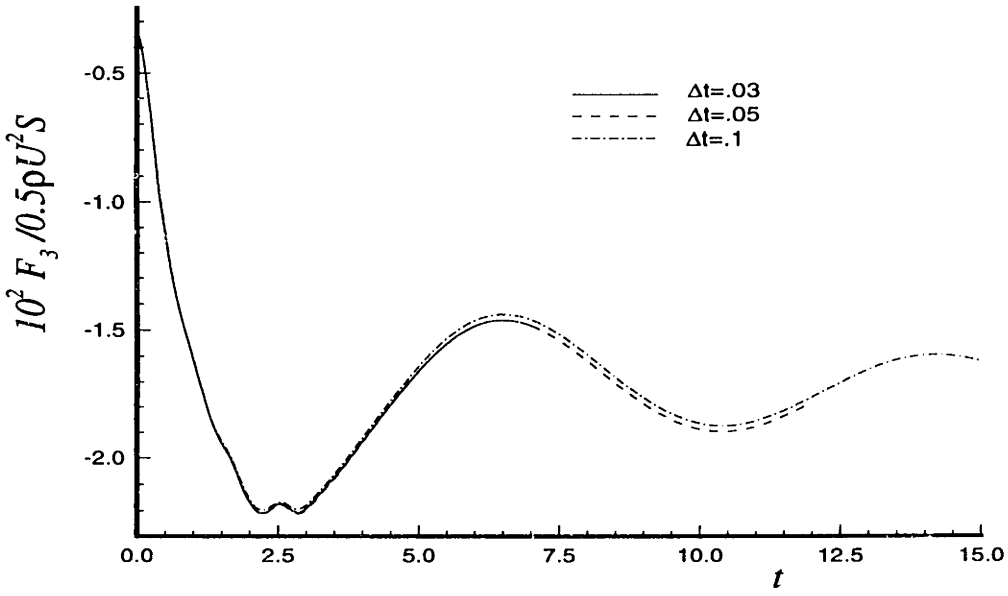

Figure 3-40: Convergence with time step size of the steady sinkage force on a Wigley hull at $F_n = 0.3$, 256 panels.

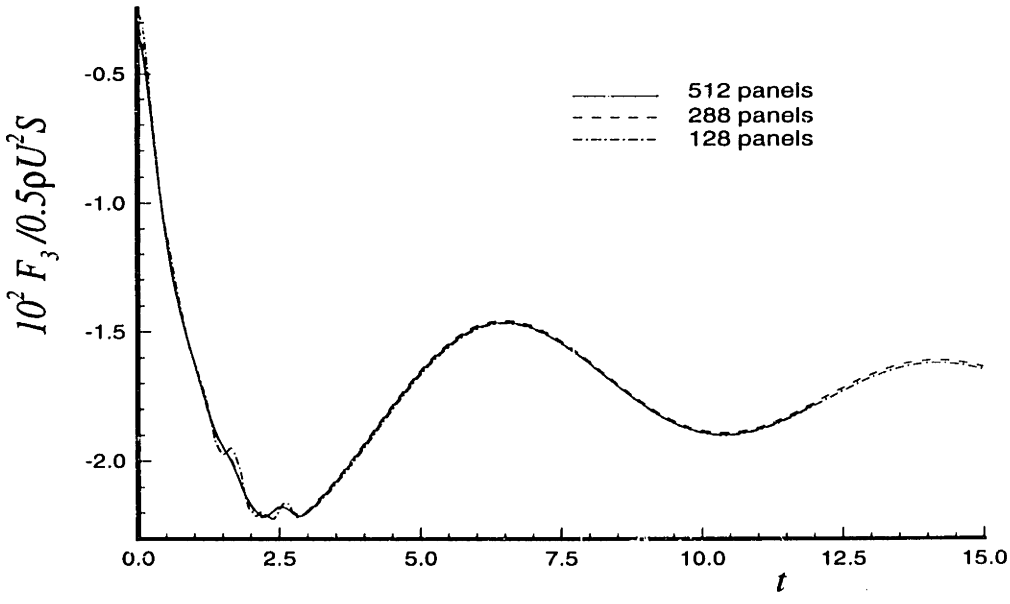

Figure 3-41: Convergence of the steady sinkage force on a Wigley hull at $F_n = 0.3$.

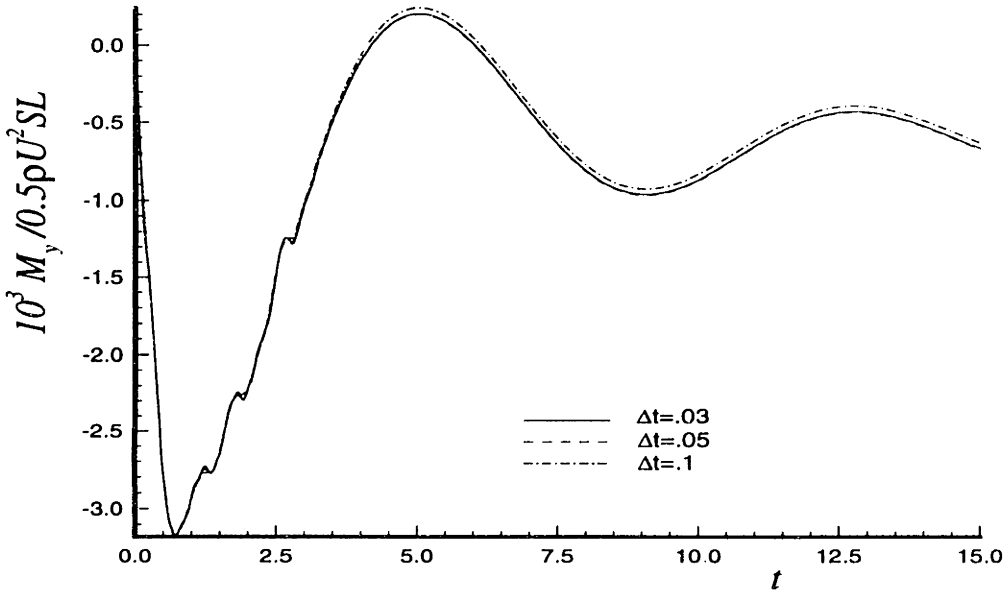

Figure 3-42: Convergence with time step size of the steady trim moment on a Wigley hull at $F_n = 0.3$, 64 panels.

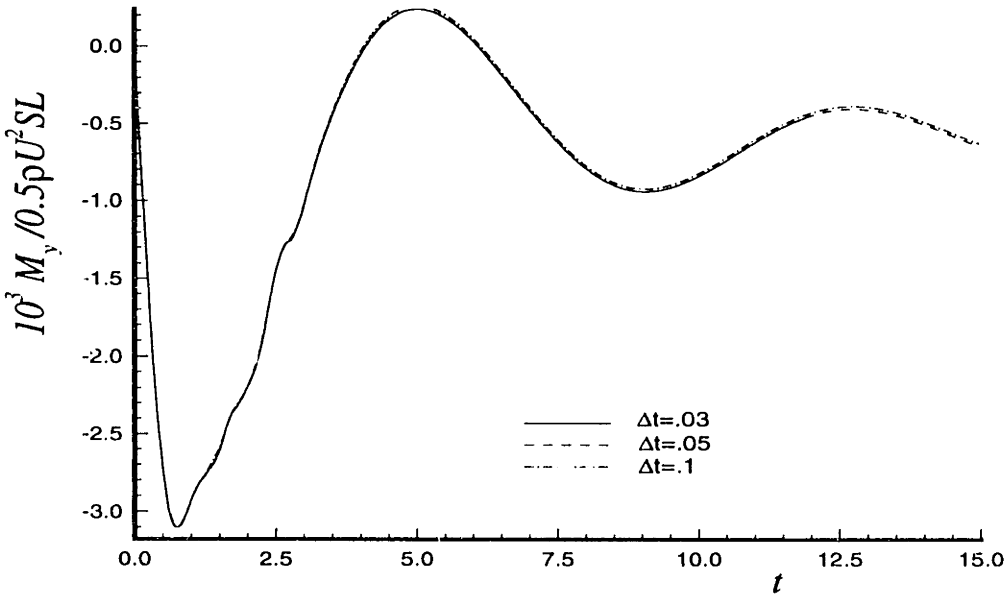

Figure 3-43: Convergence with time step size of the steady trim moment on a Wigley hull at $F_n = 0.3$, 144 panels.

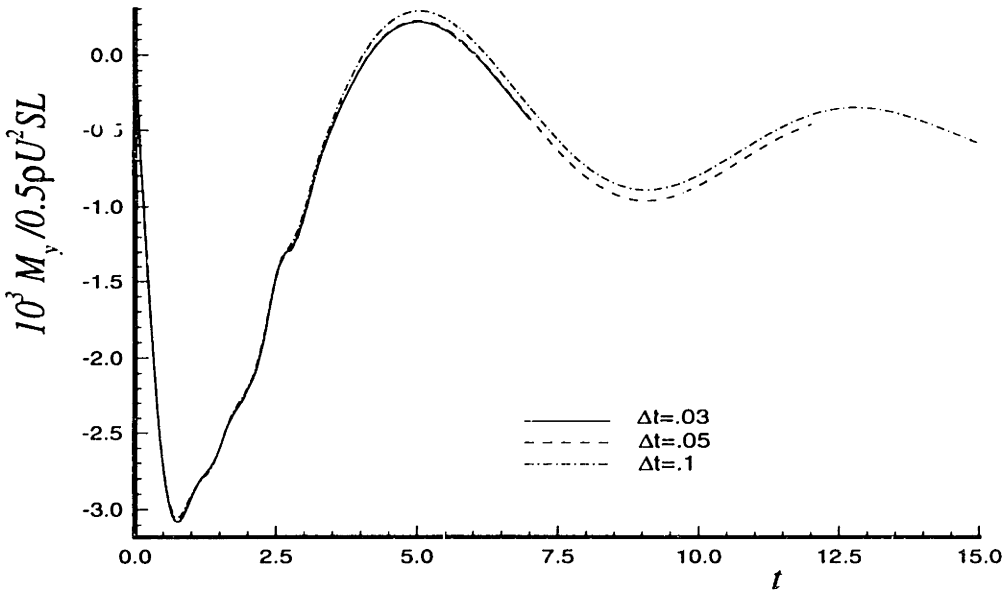

Figure 3-44: Convergence with time step size of the steady trim moment on a Wigley hull at $F_n = 0.3$, 256 panels.

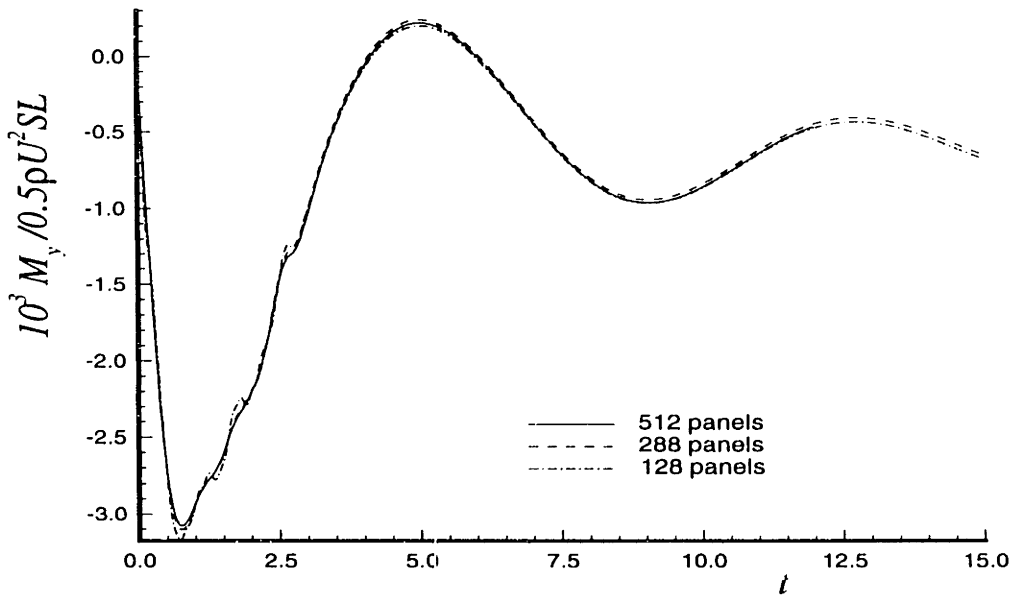

Figure 3-45: Convergence of the steady trim moment on a Wigley hull at $F_n = 0.3$.

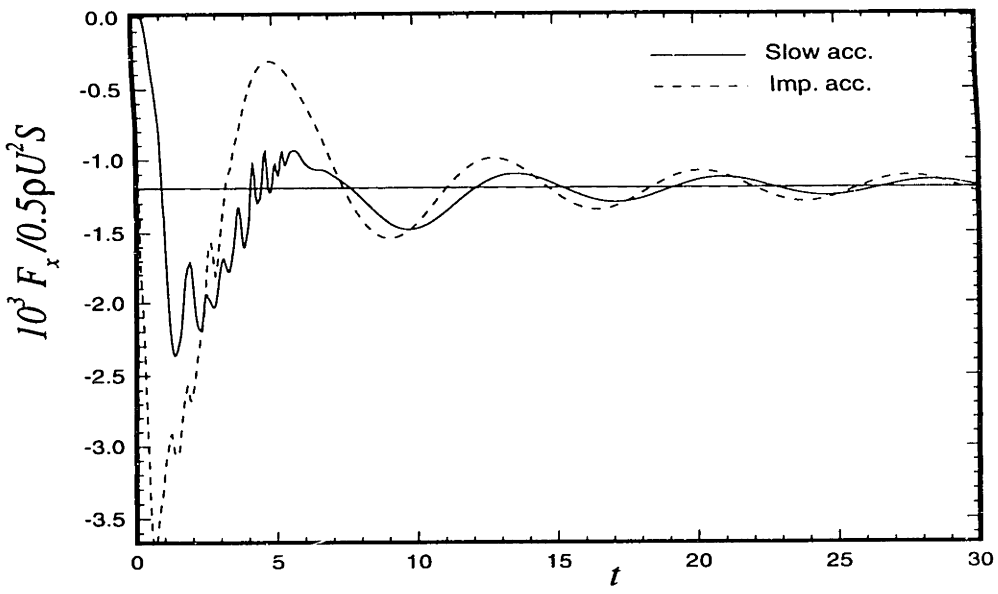

Figure 3-46: Comparison of the steady wave resistance calculated using an impulsive and a gradual acceleration of the ship, Wigley hull at $F_n = 0.3$.

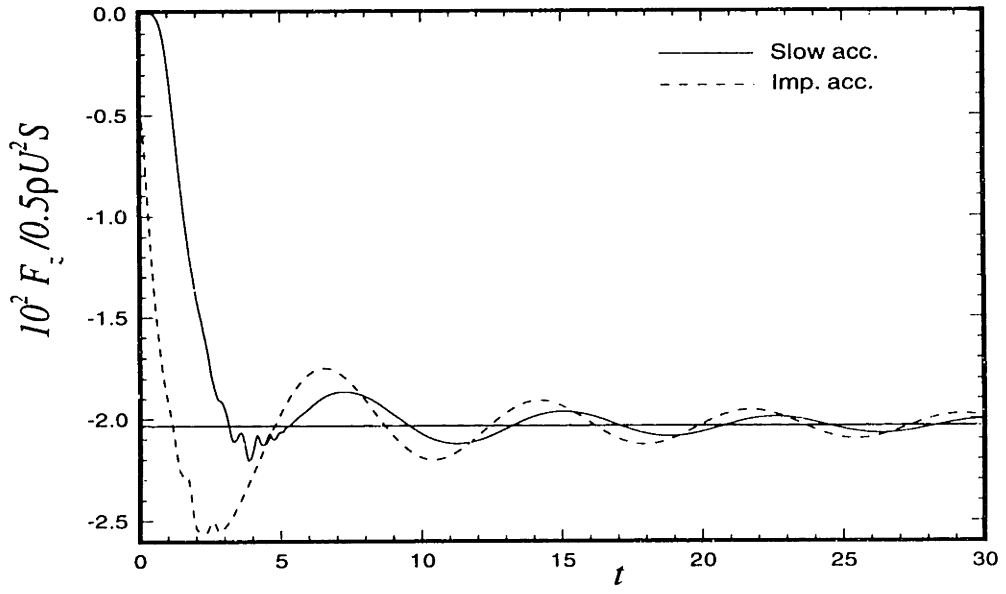

Figure 3-47: Comparison of the steady sinkage force calculated using an impulsive and a gradual acceleration of the ship, Wigley hull at $F_n = 0.3$.

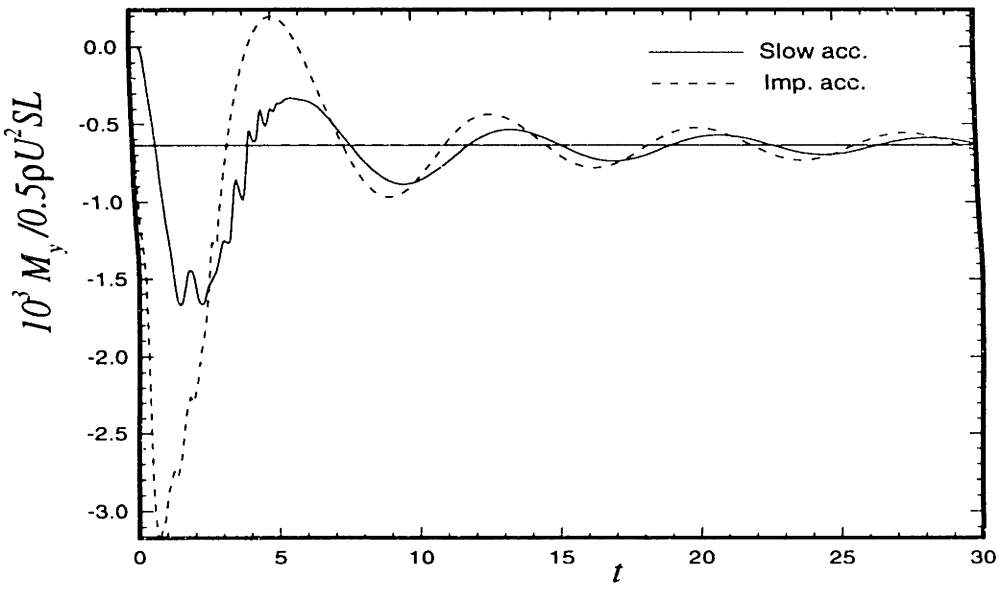

Figure 3-48: Comparison of the steady trim moment calculated using an impulsive and a gradual acceleration of the ship, Wigley hull at $F_n = 0.3$.

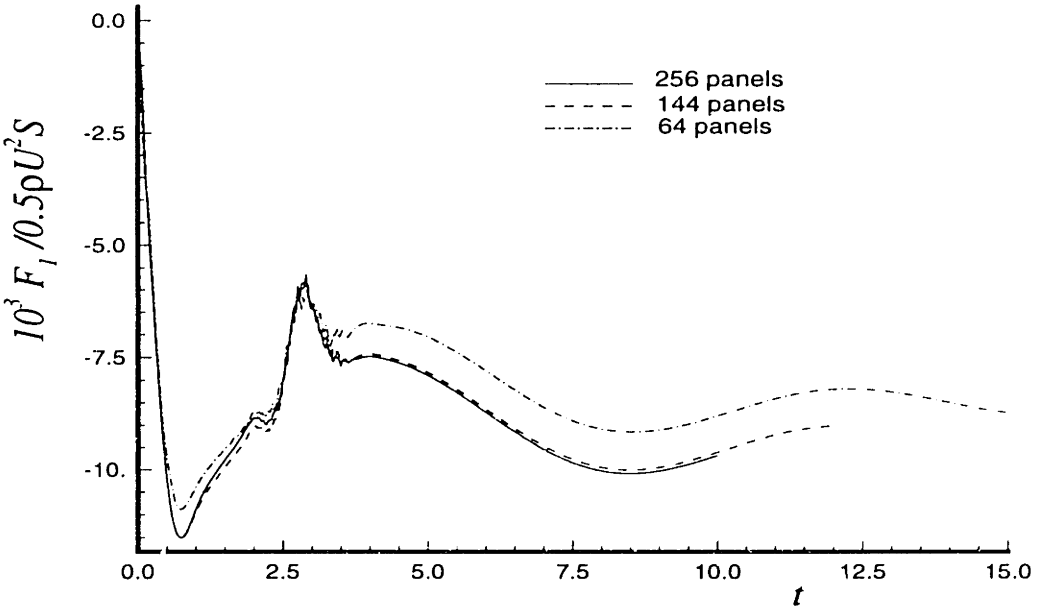

Figure 3-49: Convergence of the steady wave resistance on a Series 60 block 70 hull at $F_n = 0.3$.

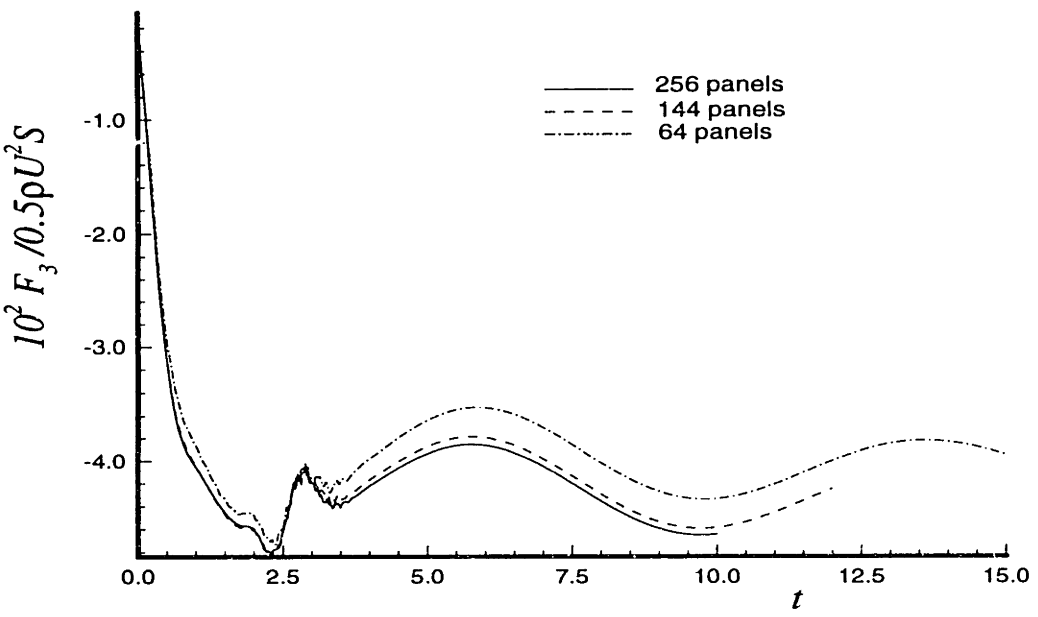

Figure 3-50: Convergence of the steady sinkage force on a Series 60 block 70 hull at $F_n = 0.3$.

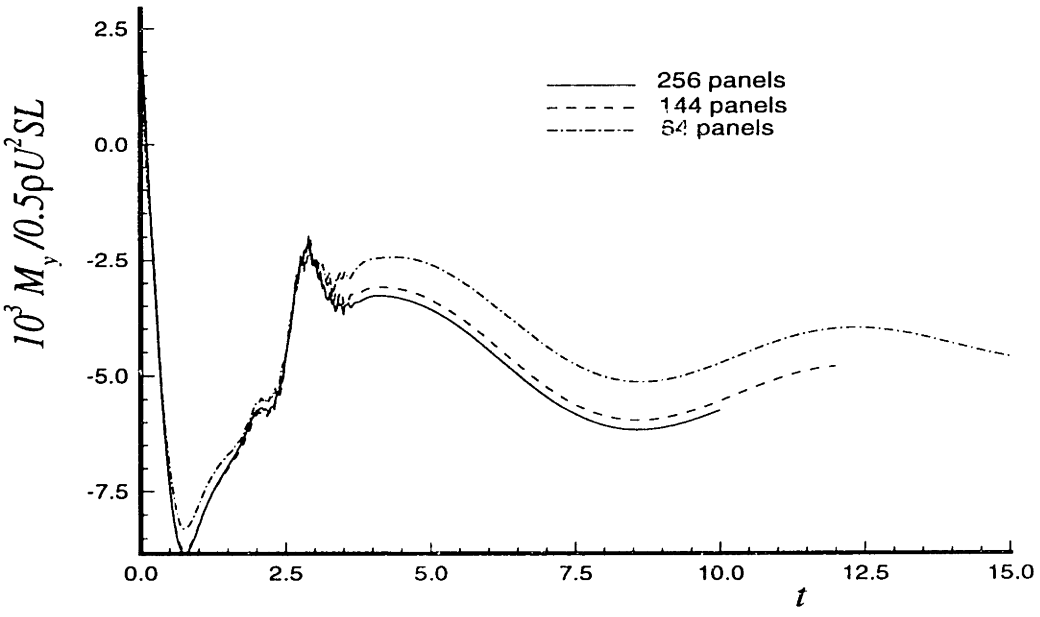

Figure 3-51: Convergence of the steady trim moment on a Series 60 block 70 hull at $F_n = 0.3$.

Chapter 4

Results

4.1 Hull Geometries for the Calculations

4.1.1 Wigley Hull

The Wigley hull is a mathematically defined ship hull which has been model-tested extensively and provides a convenient body to use for comparison, both with experiment and with the results of other calculations. The results which follow (and precede) have been calculated using the modified hull for which the surface geometry is defined by the equation:

$$\eta = (1-\zeta^2)(1-\xi^2)(1+0.2\,\xi^2) + \zeta^2(1-\zeta^8)(1-\xi^2)^4$$

where the non-dimensional variables are defined by

$$\xi = \frac{2x}{L}, \qquad \eta = \frac{2y}{B}, \qquad \zeta = \frac{z}{T}$$

with L the ship's length, B the beam, and T the draft. The standard hull used here has

$$\frac{L}{B} = 10, \qquad \frac{L}{T} = 16,$$

and a block coefficient of

$$C_b = \frac{\nabla}{LBT} = 0.5606$$

where ∇ is the submerged volume. The four discretizations shown in Figures 4-1 through 4-4 were used for the calculations and employ twice as many panels in the longitudinal direction as in the girth-wise direction, along with cosine spacing towards the ends.

4.1.2 Series 60 Hull

The Series 60 hull with block coefficient $C_b = 0.7$ was chosen as a second test case for the hydrodynamic calculations. This hull has the design characteristics:

$$L = 400', \quad B = 57.14', \quad T = 22.86', \Delta = 10441\,\text{tons}, \quad SA = 31777\,\text{ft}^2.$$

Figures 4-5 through 4-8 show the discretizations used for the calculations.

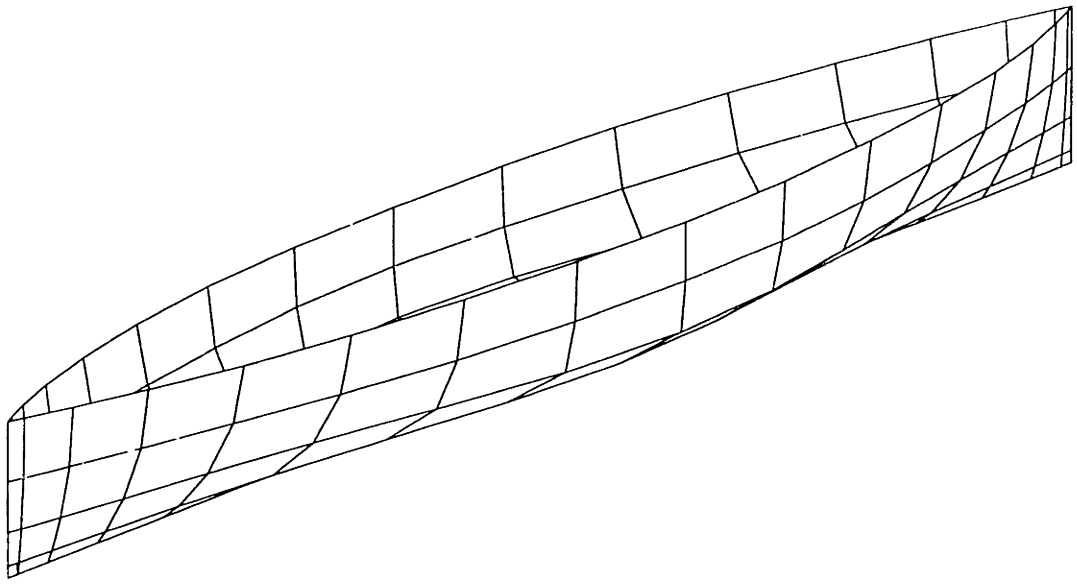

Figure 4-1: 64 panel discretization of the Wigley hull.

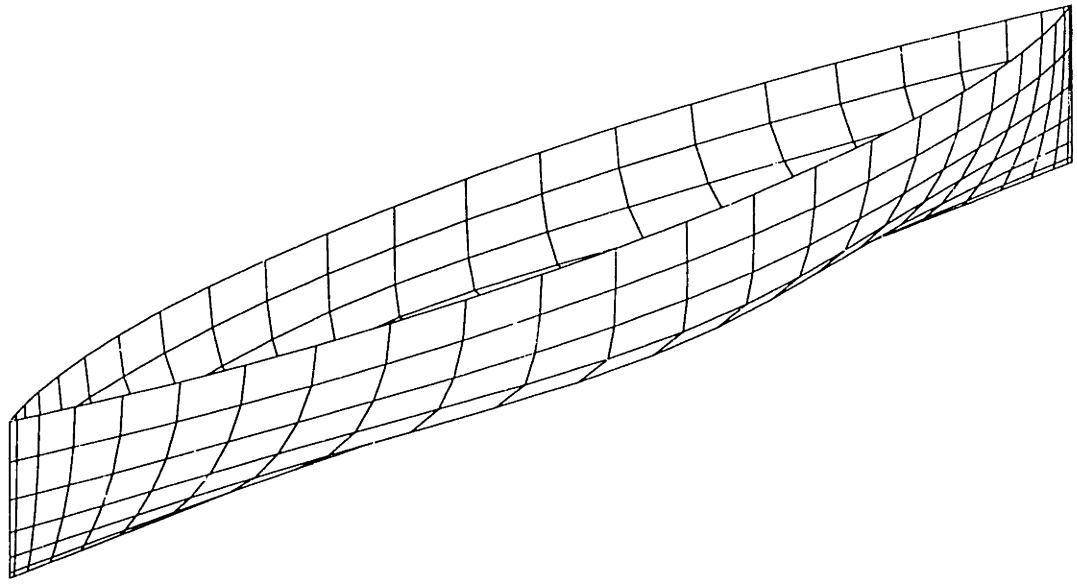

Figure 4-2: 144 panel discretization of the Wigley hull.

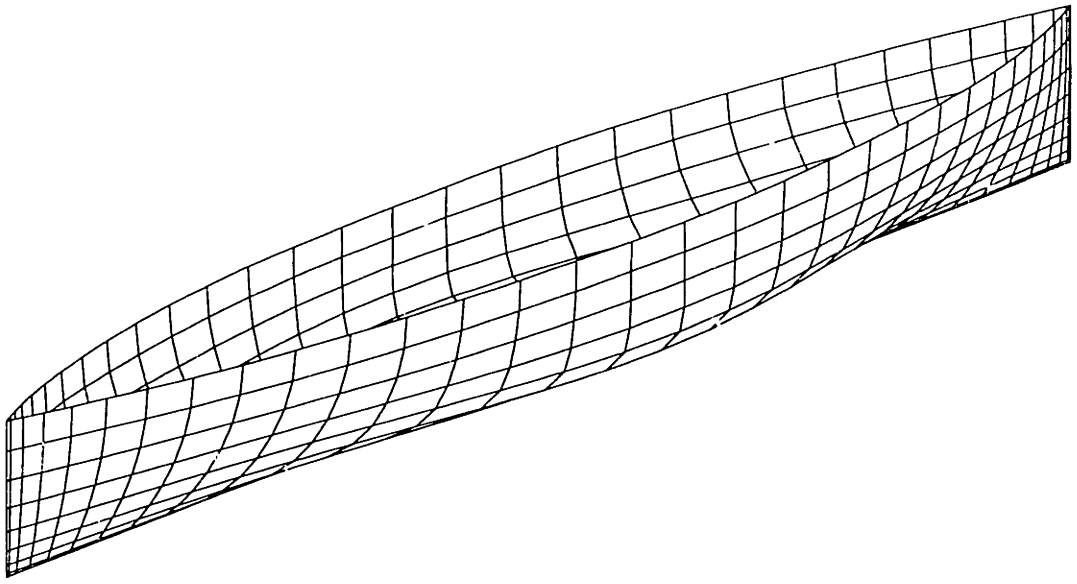

Figure 4-3: 256 panel discretization of the Wigley hull.

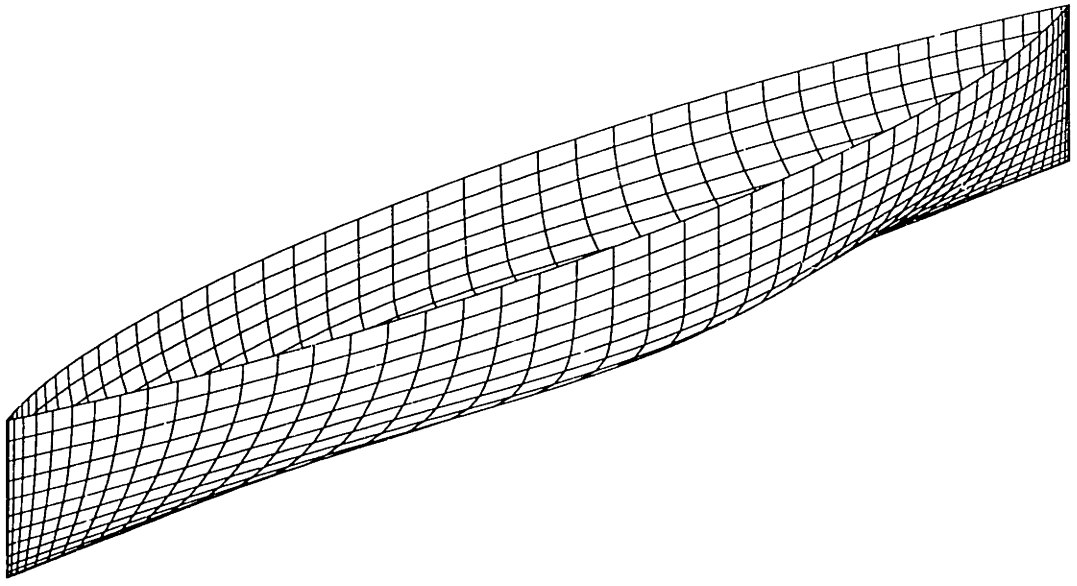

Figure 4-4: 576 panel discretization of the Wigley hull.

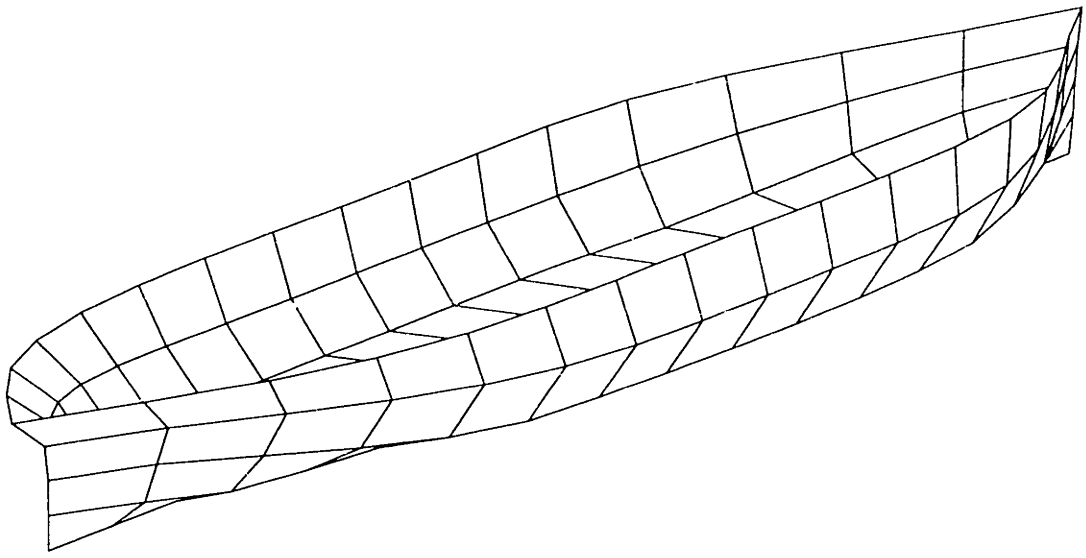

Figure 4-5: 64 panel discretization of the Series 60 hull.

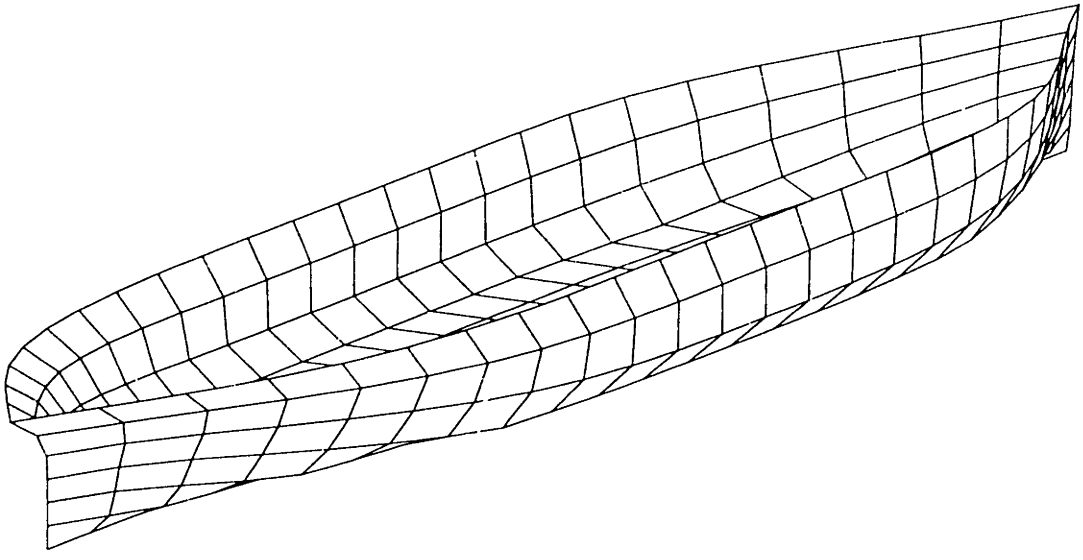

Figure 4-6: 144 panel discretization of the Series 60 hull.

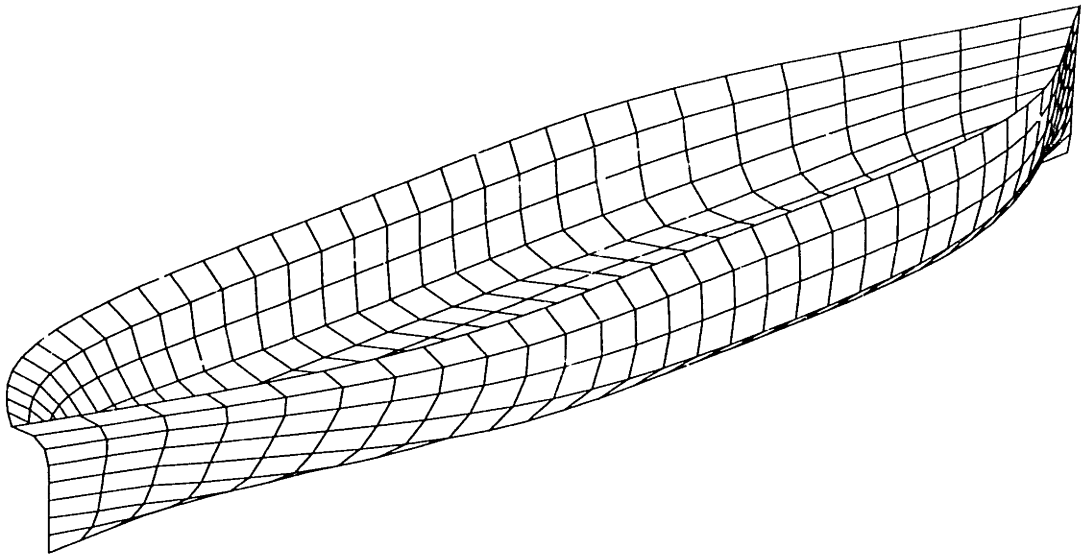

Figure 4-7: 256 panel discretization of the Series 60 hull.

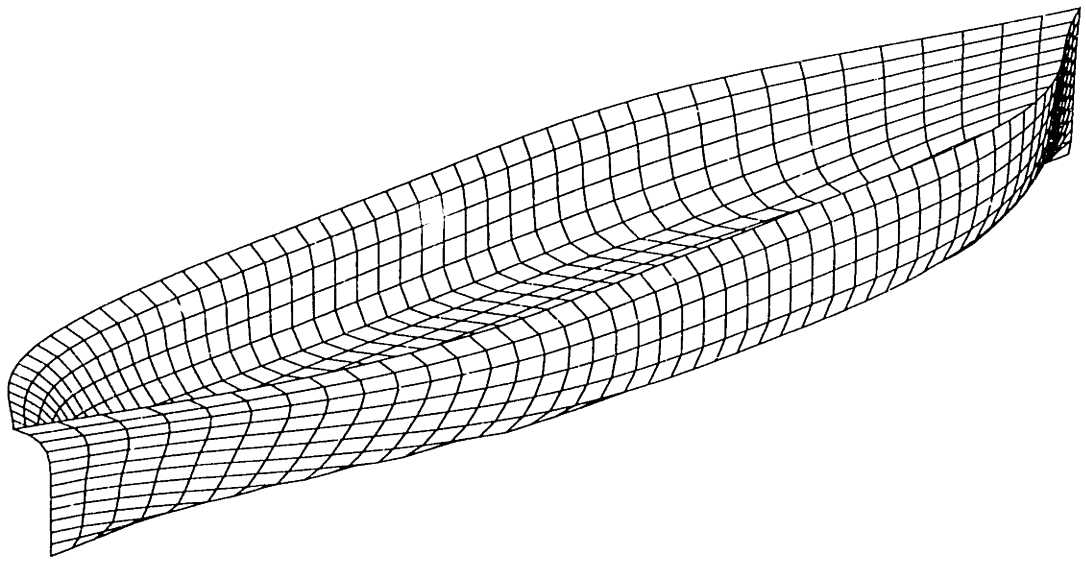

Figure 4-8: 576 panel discretization of the Series 60 hull.

4.2 Steady Forces

This section contains a comparison of the calculations of the steady resistance with experimental results for the Wigley hull at $F_n = 0.3$. Predictions of the steady sinkage and trim angle are also compared to experimentally measured results. The force coefficients appearing in the plots are defined by

$$C_r = -\frac{F_x}{\frac{1}{2}\rho U^2 S}, \qquad C_l = \frac{F_z}{\frac{1}{2}\rho U^2 S}, \qquad C_t = \frac{M_y}{\frac{1}{2}\rho U^2 S L}$$

where S is the submerged surface area of the hull. The sinkage depth and trim angle are calculated from the steady version of the equations of motion with the ship free to heave and pitch only:

$$\begin{aligned} C_{33}x_3 + C_{35}x_5 &= F_z \\ C_{53}x_3 + C_{55}x_5 &= M_y \end{aligned} \tag{4.1}$$

The experimental range of measured wave resistance was taken from the Proceedings of the First DTNSRDC Workshop on Ship Wave Resistance Computations [38], while the corresponding sinkage depths and trim angles are from the Proceedings of the Second meeting of the same Workshop [43].

All of the results plotted in these figures were calculated using the 144 panel discretization of the hull at a non-dimensional time step of $\Delta t = .05$. The calculations were truncated at a non-dimensional time of 15.0 and a least squares fit was made to the last 1/4 of a $\tau = 1/4$ period of the data (with the decay assumed to be $\propto 1/t$) to obtain the mean value.

4.3 Unsteady Forces

Figures 4-12 through 4-29 compare the unsteady radiation and diffraction forces calculated using T[MIT to experimental results. The comparisons are made using the appropriate frequency domain coefficients. Experimental results for the Wigley hull

are from Journée [20], and these plots include calculations made directly in the frequency domain using the Rankine panel method SWAN [40]. SWAN used a linearization about the double-body flow and so the calculations are not expected to agree perfectly. Experimental results for the Series 60 hull are from Gerritsma and Beukelman [12]. All of the TĪMIT calculations which appear in these figures were made using 256 panels on half of the hull, a non-dimensional time step size of 0.05, and a truncation point at 15..

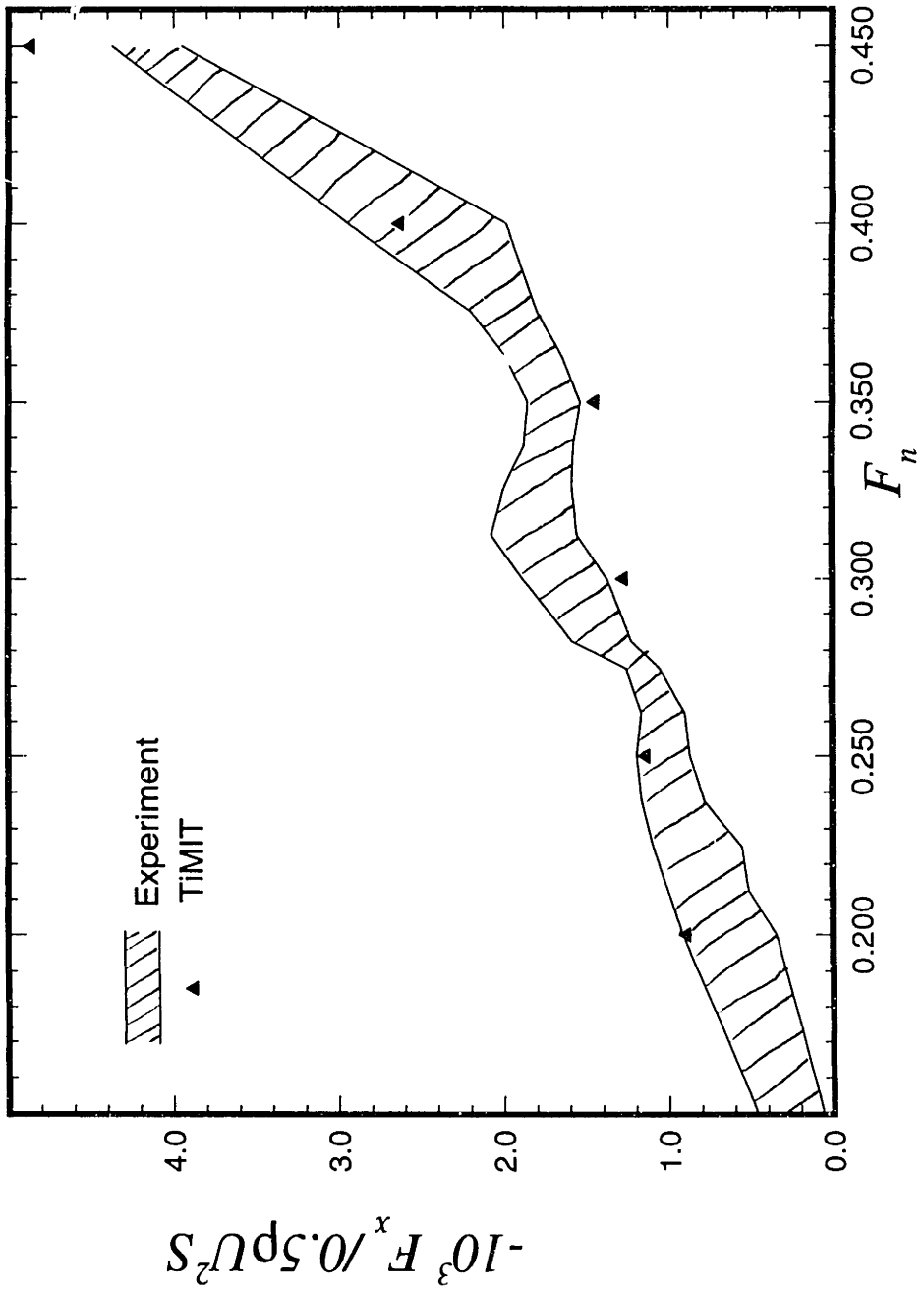

Figure 4-9: Wave resistance of the Wigley hull over a range of Froude numbers.

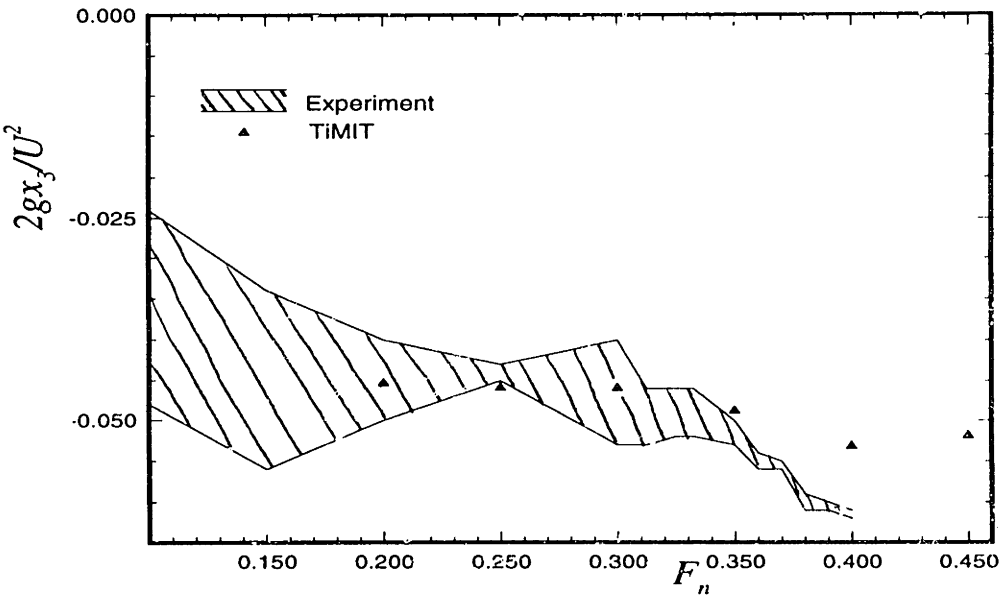

Figure 4-10: Sinkage of the Wigley hull over a range of Froude numbers.

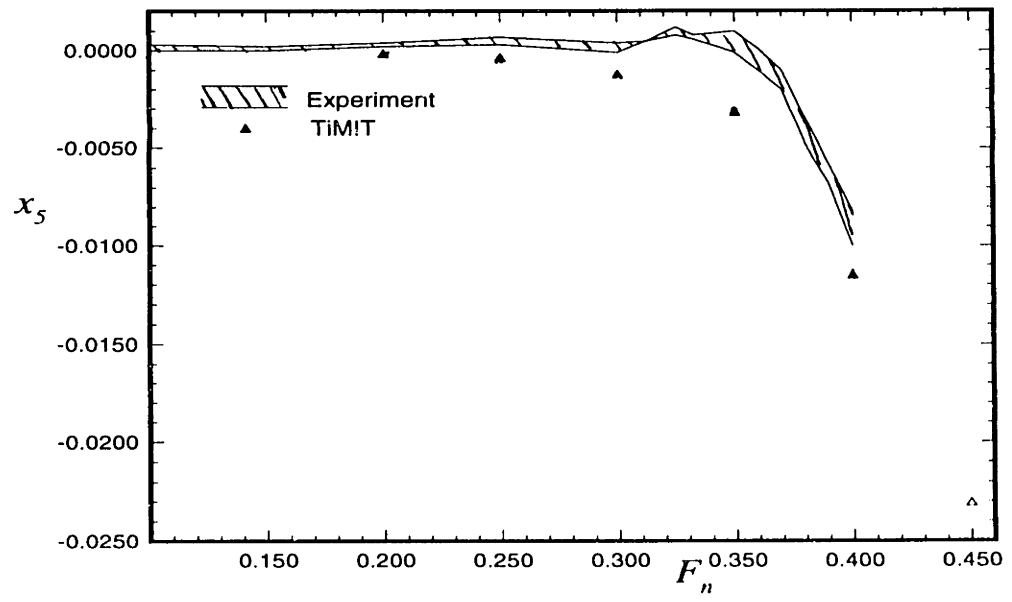

Figure 4-11: Trim angle of the Wigley hull over a range of Froude numbers.

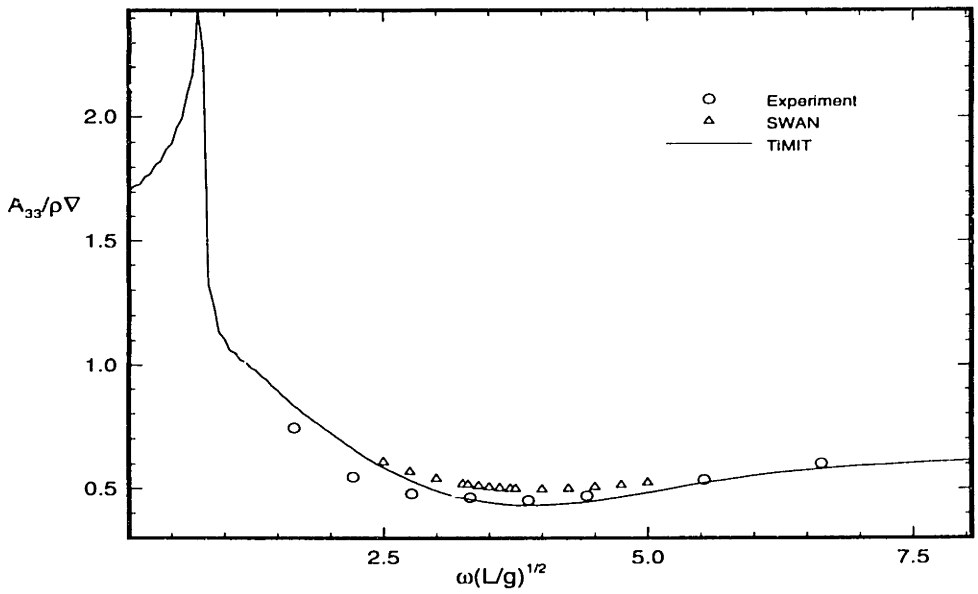

Figure 4-12: Heave-heave added mass coefficients for a Wigley hull at $F_n = 0.3$

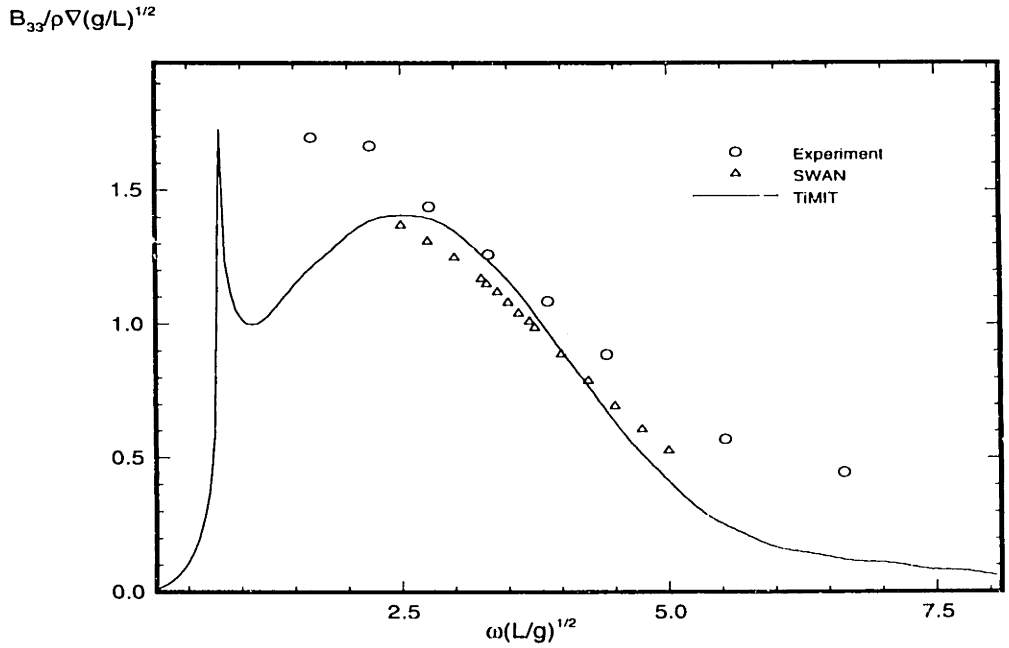

Figure 4-13: Heave-heave damping coefficients for a Wigley hull at $F_n = 0.3$

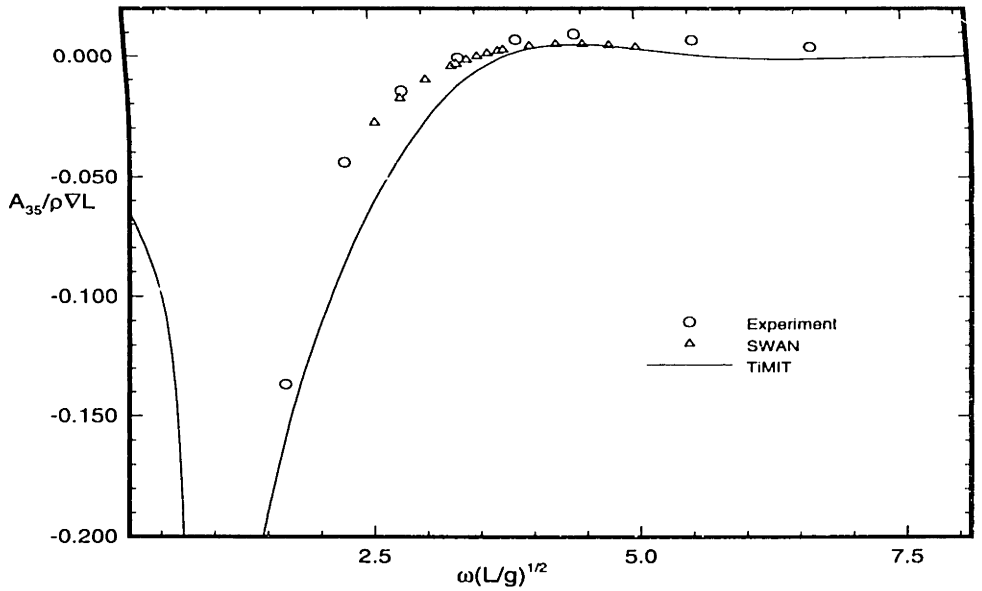

Figure 4-14: Heave-pitch added mass coefficients for a Wigley hull at $F_n = 0.3$

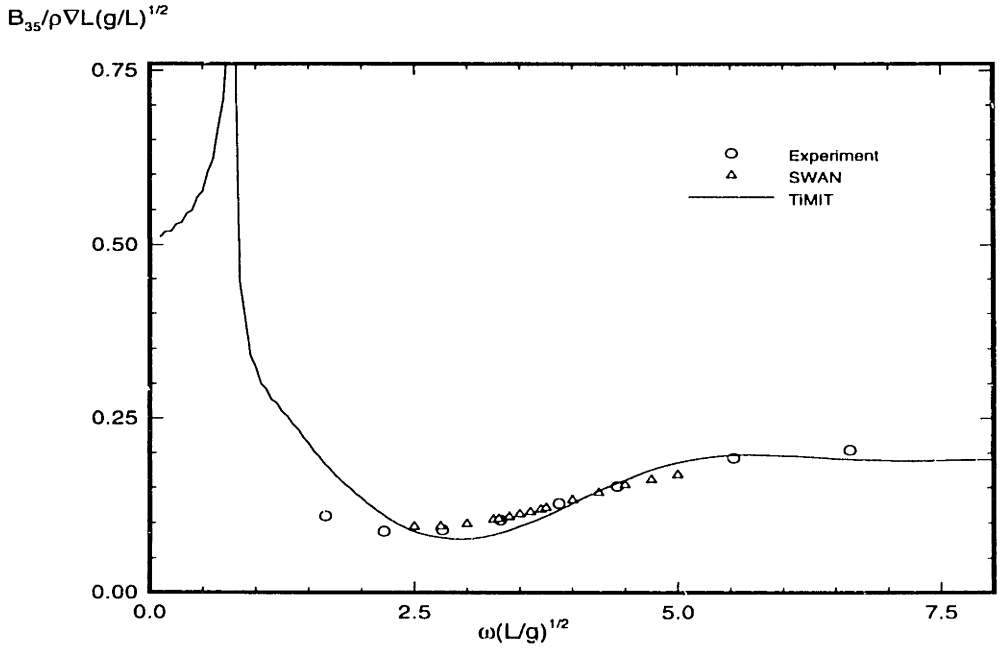

Figure 4-15: Heave-pitch damping coefficients for a Wigley hull at $F_n = 0.3$

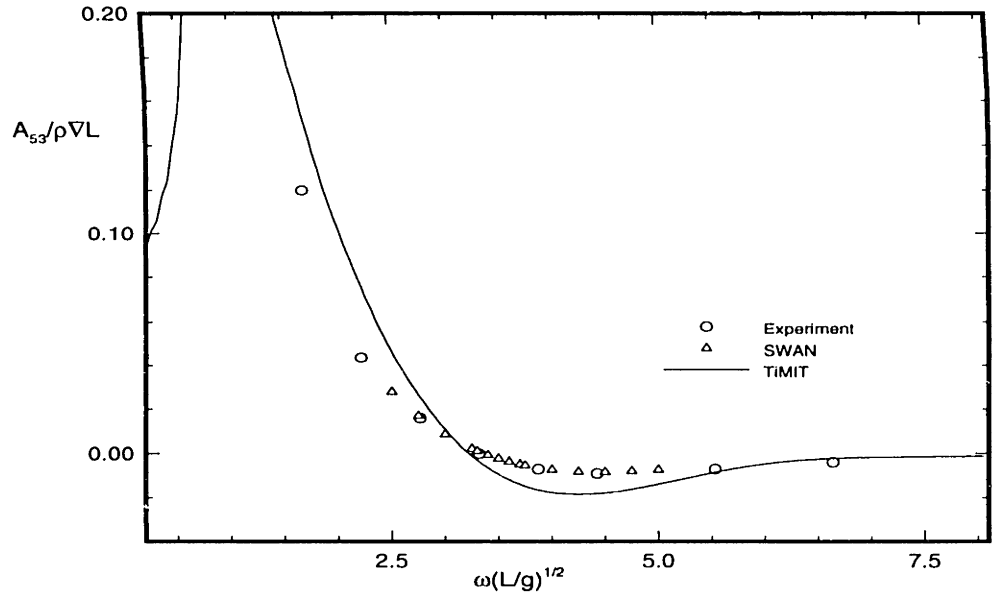

Figure 4-16: Pitch-heave added mass coefficients for a Wigley hull at $F_n = 0.3$

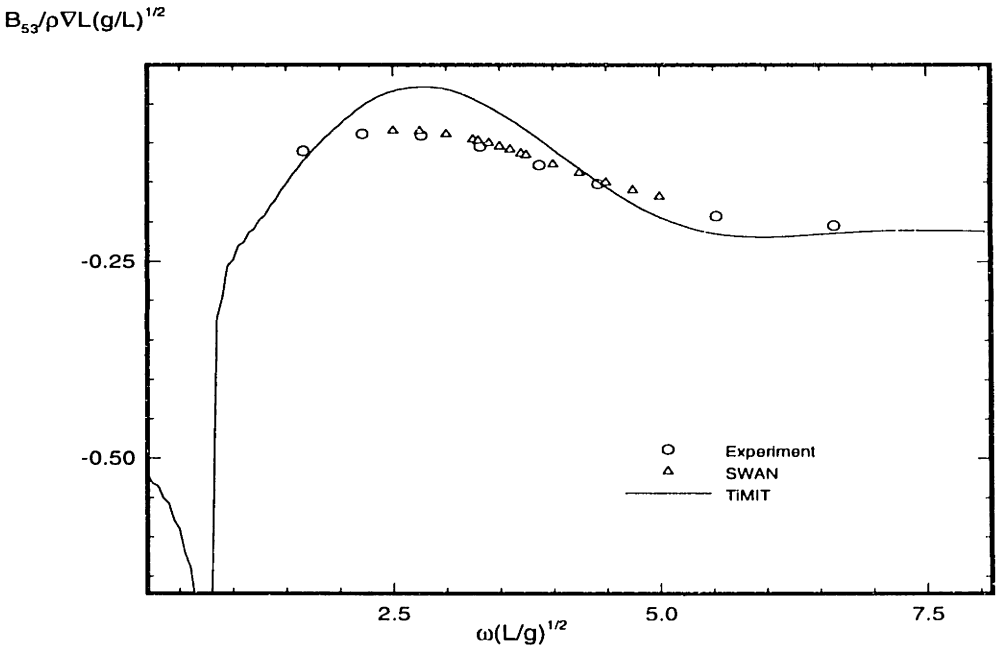

Figure 4-17: Pitch-heave damping coefficients for a Wigley hull at $F_n = 0.3$

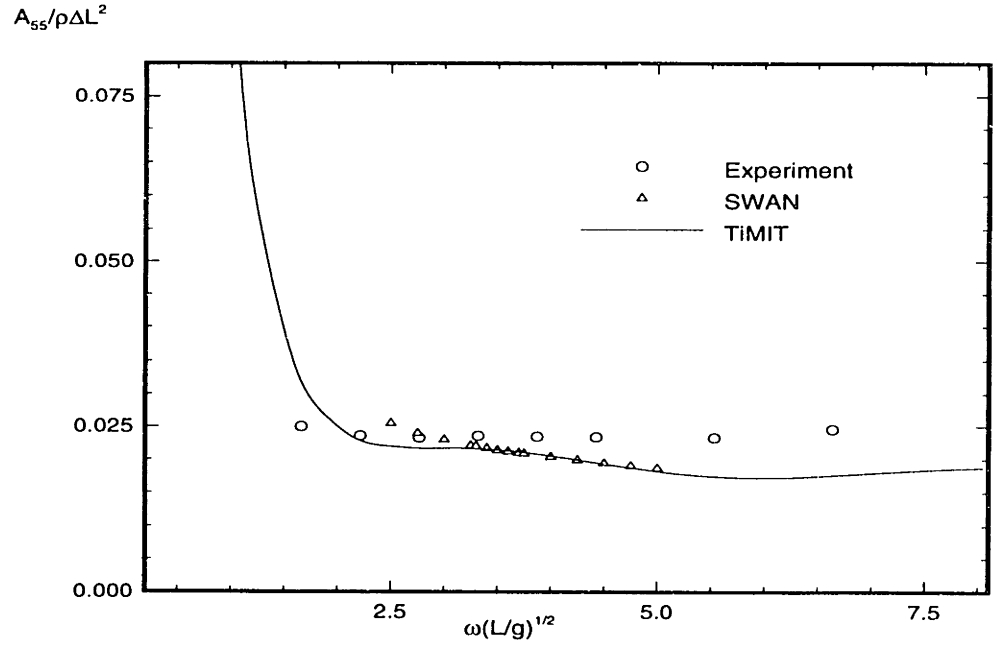

Figure 4-18: Pitch-pitch added mass coefficients for a Wigley hull at $F_n = 0.3$

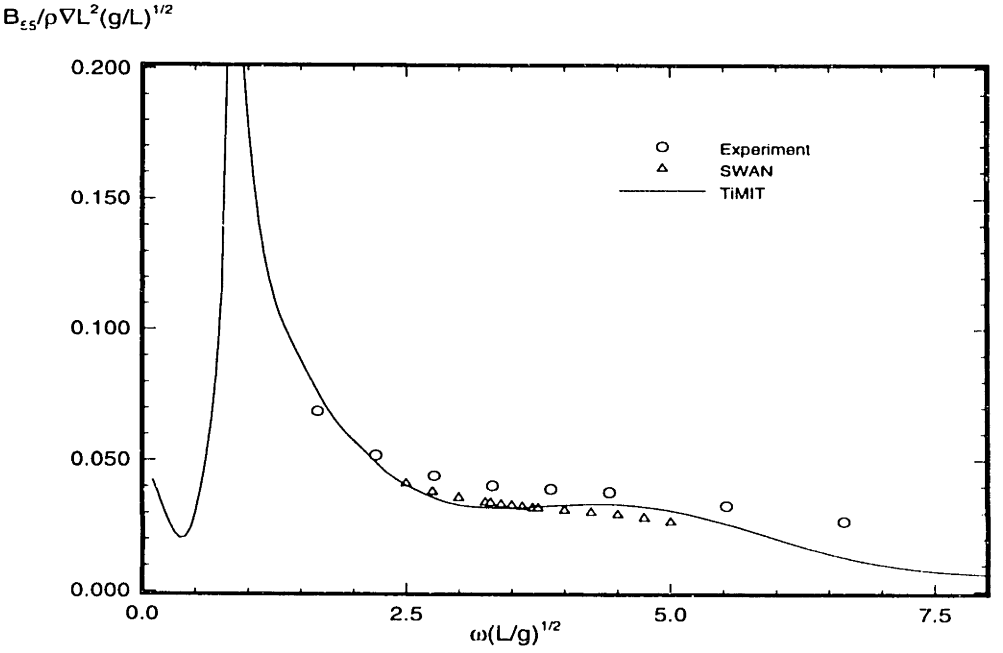

Figure 4-19: Pitch-pitch damping coefficients for a Wigley hull at $F_n = 0.3$

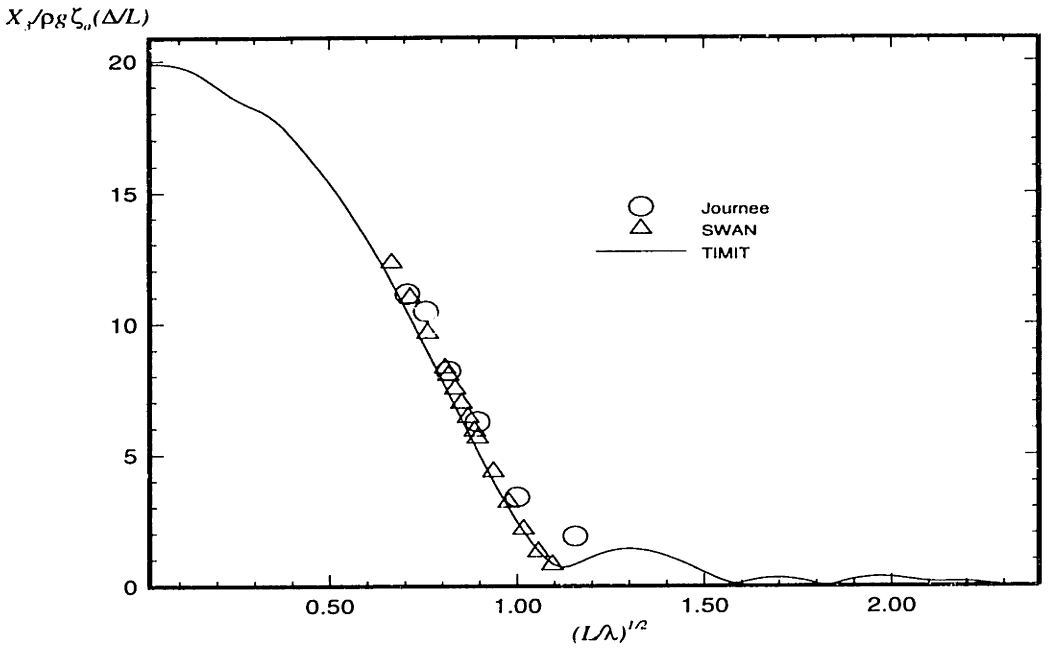

Figure 4-20: Heave exciting force coefficients for a Wigley hull at $F_n = 0.3$

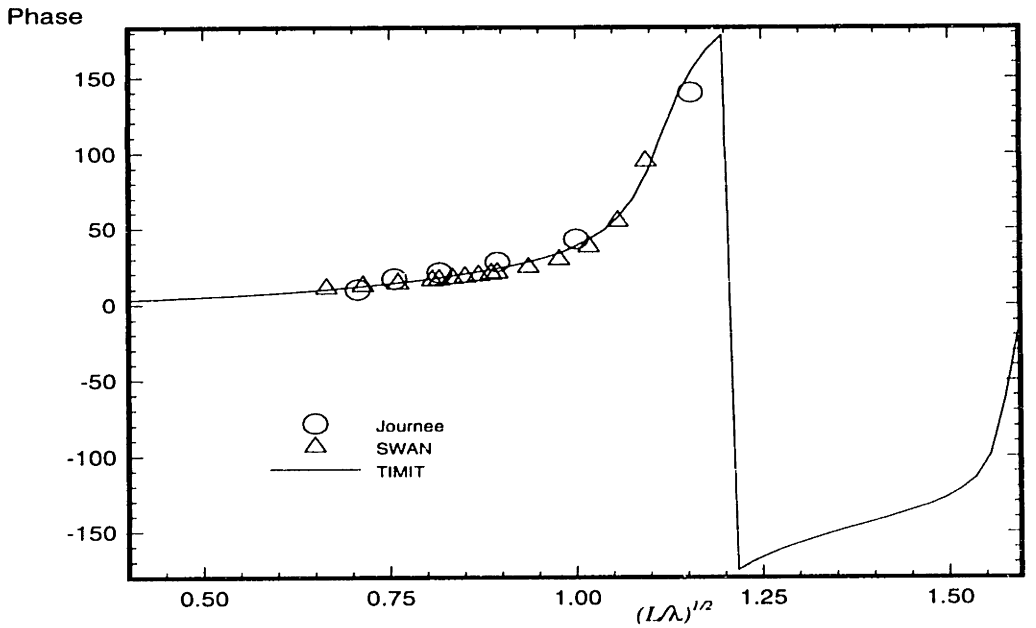

Figure 4-21: Heave exciting force phase angle for a Wigley hull at $F_n = 0.3$

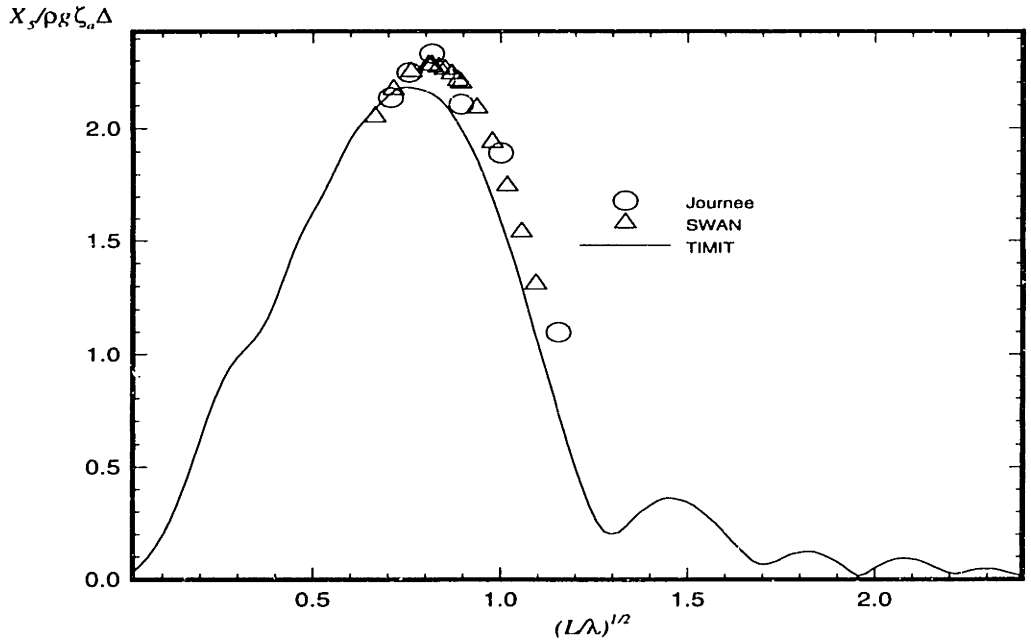

Figure 4-22: Pitch exciting force coefficients for a Wigley hull at $F_n = 0.3$

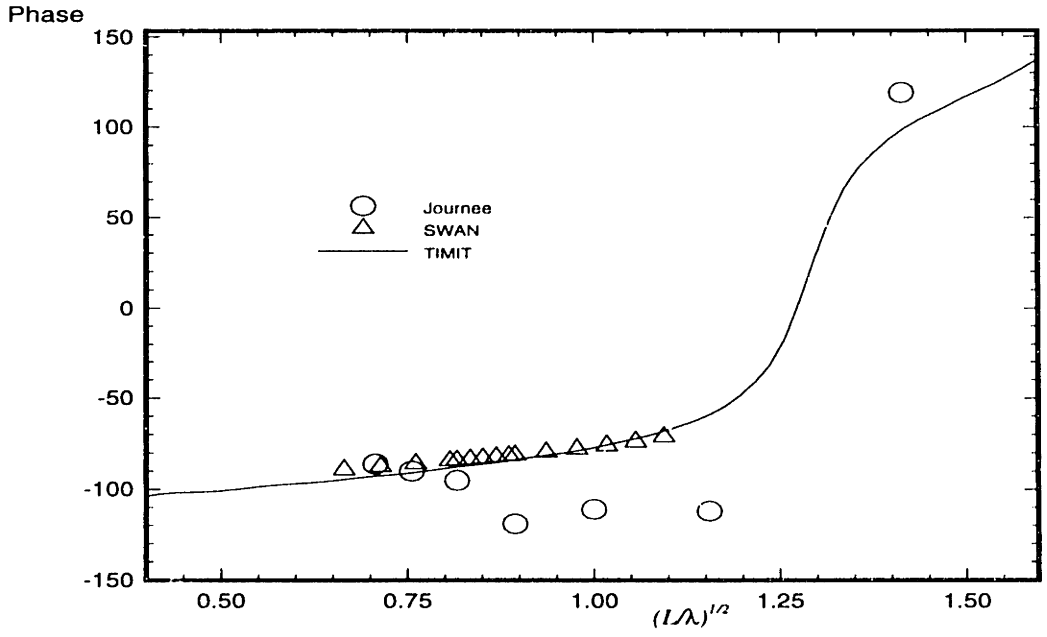

Figure 4-23: Pitch exciting force phase angle for a Wigley hull at $F_n = 0.3$

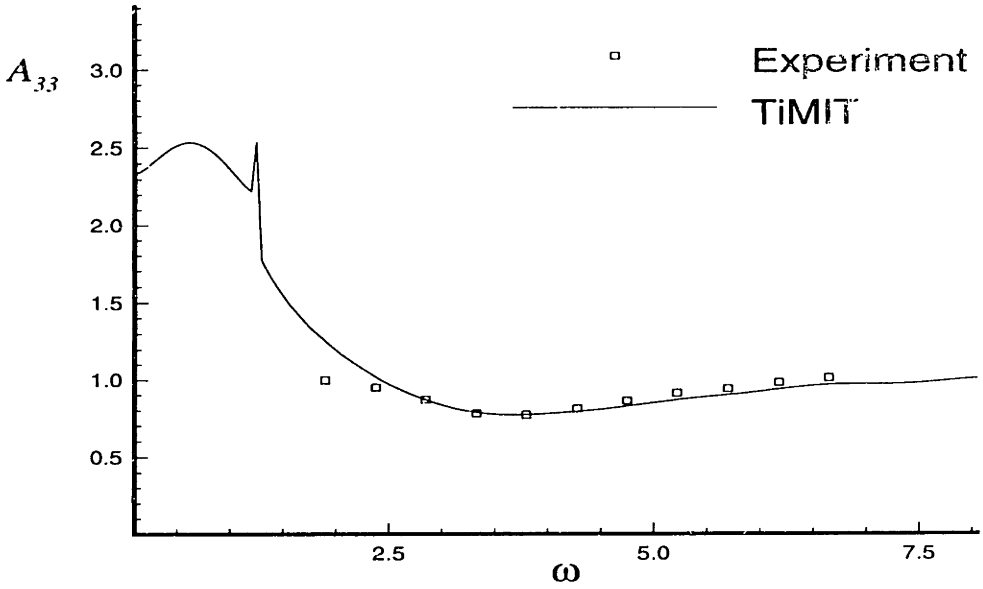

Figure 4-24: Heave-heave added mass coefficients for a Series 60 Block 70 hull at $F_n = 0.2$

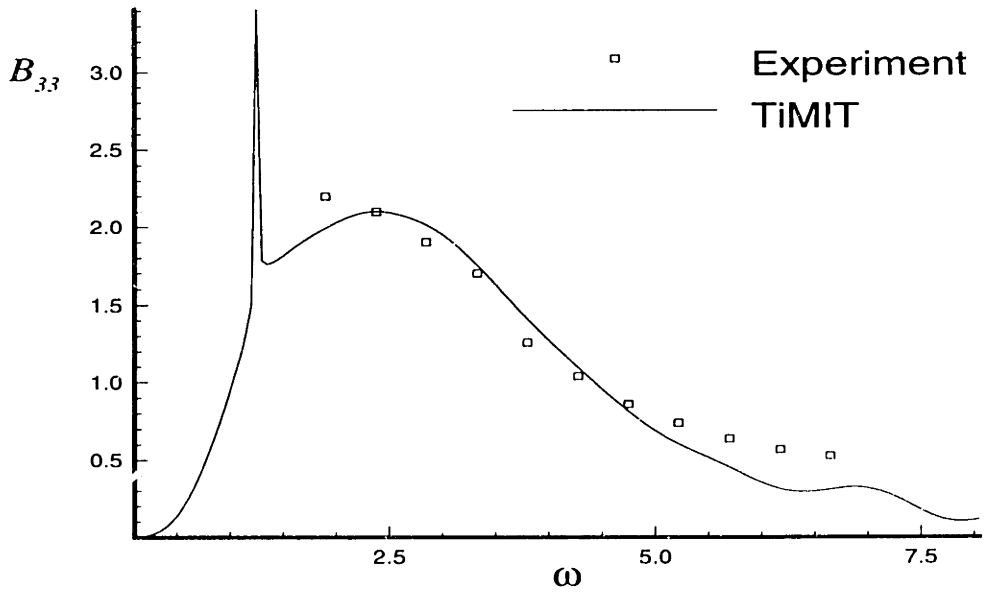

Figure 4-25: Heave-heave damping coefficients for a Series 60 hull at $F_n = 0.2$

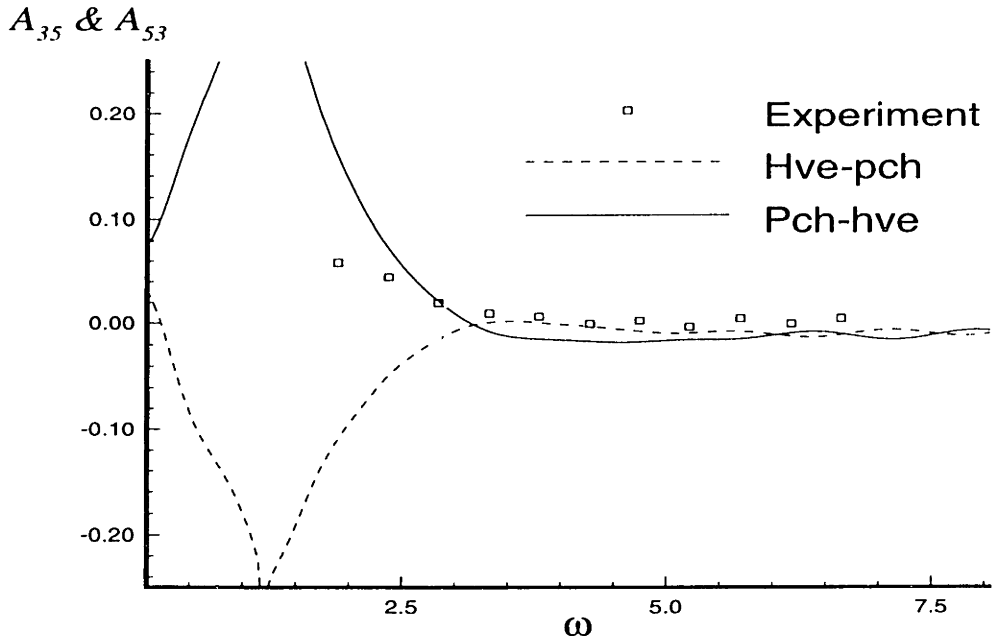

Figure 4-26: Cross-coupling added mass coefficients for a Series 60 Block 70 hull at $F_n = 0.2$

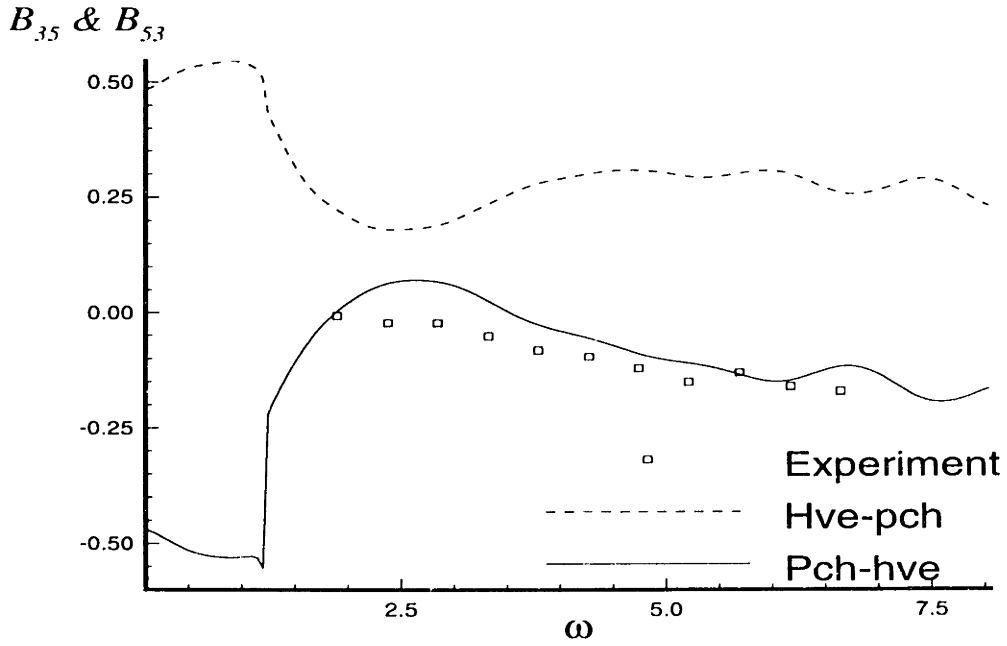

Figure 4-27: Cross-coupling damping coefficients in heave and pitch for a Series 60 Block 70 hull at $F_n = 0.2$

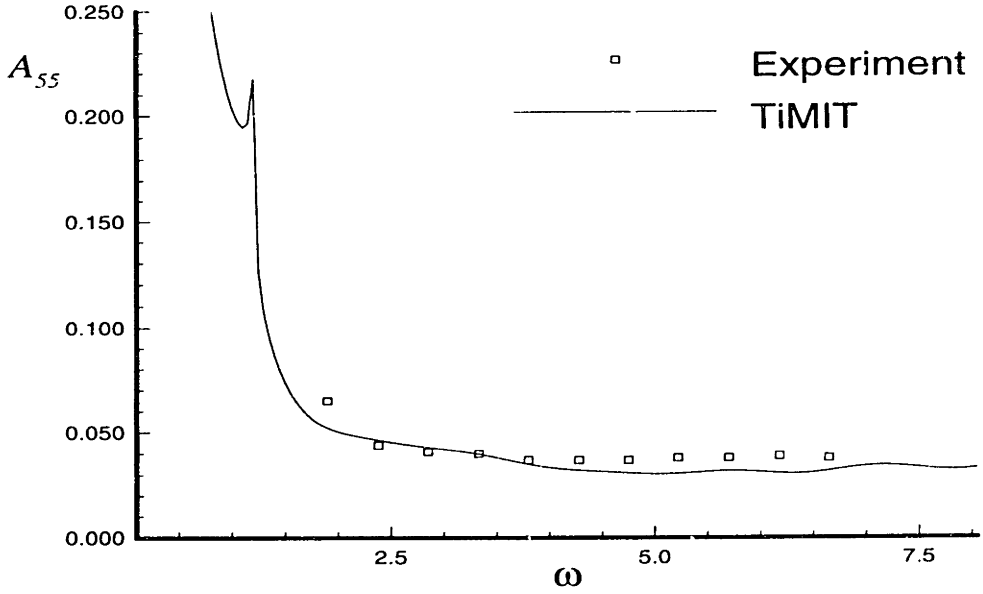

Figure 4-28: Pitch-pitch added mass coefficients for a Series 60 Block 70 hull at $F_n = 0.2$

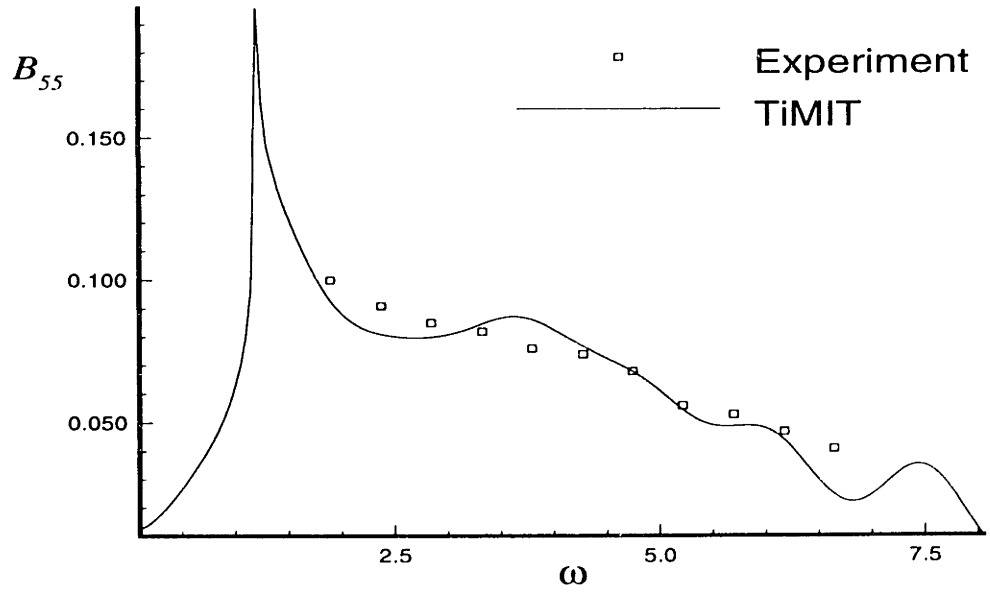

Figure 4-29: Pitch-pitch damping coefficients for a Series 60 hull at $F_n = 0.2$

4.4 Simulation

The results presented in this section are from a simulation of a Wigley hull at Froude number 0.3, encountering head seas with a Pierson-Moskowitz spectrum corresponding to 5 meters per second wind speed. The simulation is carried out by the temporal integration of the equations of motion, using a 4^{th} order explicit Runge-Kutta scheme. The top of Figure 4-30 shows a segment of the time history of the incident wave elevation as measured at the origin of the ship-fixed reference frame. The next two time histories in this figure are the heave and pitch responses of the ship respectively.

Validation of these time histories may be made by deducing the frequency-domain response-amplitude operators from the input and output signals:

$$RAO_j = \frac{|\tilde{x}_j(\omega)|}{|\tilde{\zeta}(\omega)|}, \tag{4.2}$$

where $\tilde{x}_j(\omega)$ and $\tilde{\zeta}(\omega)$ are obtained by taking the Fourier transforms of the output and input signals respectively. Figures 4-31 and 4-32 are plots of the frequency-domain response-amplitude operators compared to experimental results.

We find that the computation of the frequency-domain response-amplitude operators converges more slowly in the vicinity of resonance than at frequencies away from that region, as can be seen in Figures 4-31 and 4-32. This is expected since resonance occurs precisely because the determinant of the frequency-domain system of equations of motion becomes small, leading to poor conditioning of the linear system. The convergence of these results is also subject to the reduction of the size of the time-step and the increase of the order of the integration scheme used to solve the time-domain equations-of-motion. A fourth-order Runge-Kutta algorithm is a reasonable choice because it is robust and efficiency is not paramount in this calculation.

To quantify the relatively slow convergence around resonance, we have solved the equations of motion in the frequency domain using the frequency-domain coefficients presented in various figures shown in Section 4.3. In this particular case the condition number at the frequency of peak heave and pitch response is approximately twice the value for frequencies away from this peak. It is reasonable to expect that

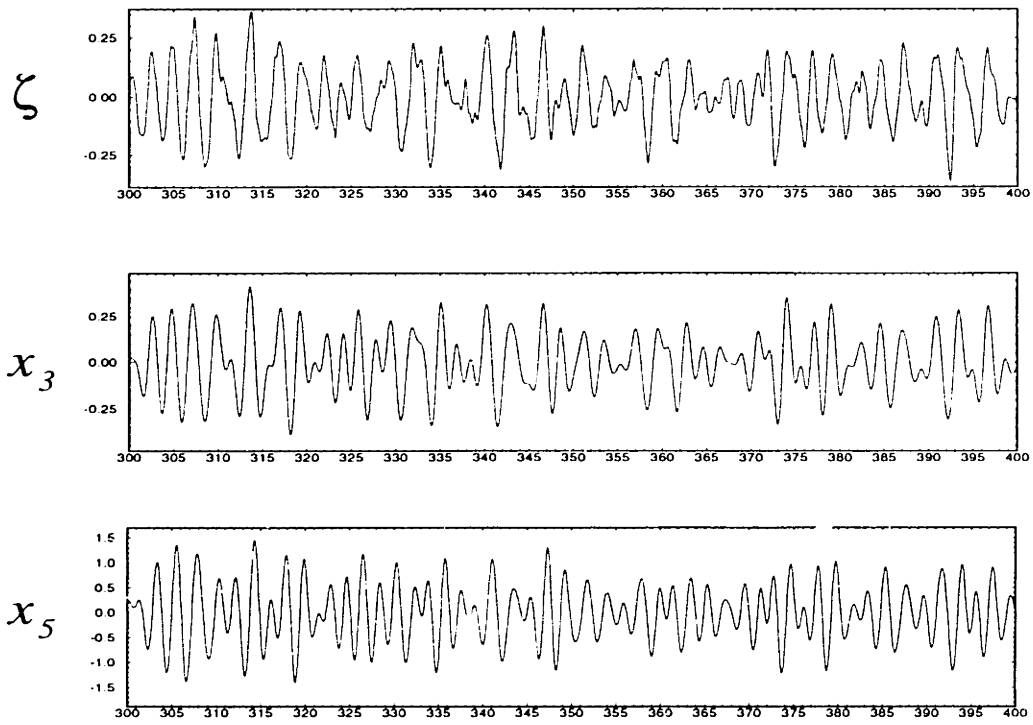

Figure 4-30: Time histories from a simulation of a Wigley hull at $F_n = 0.3$, $\beta = \pi$. From the top: incident wave elevation in the ship-fixed frame, heave response, pitch response.

accurate results in the time-domain can only be produced for temporal and spatial discretizations which are sufficiently fine to achieve convergence around resonance.

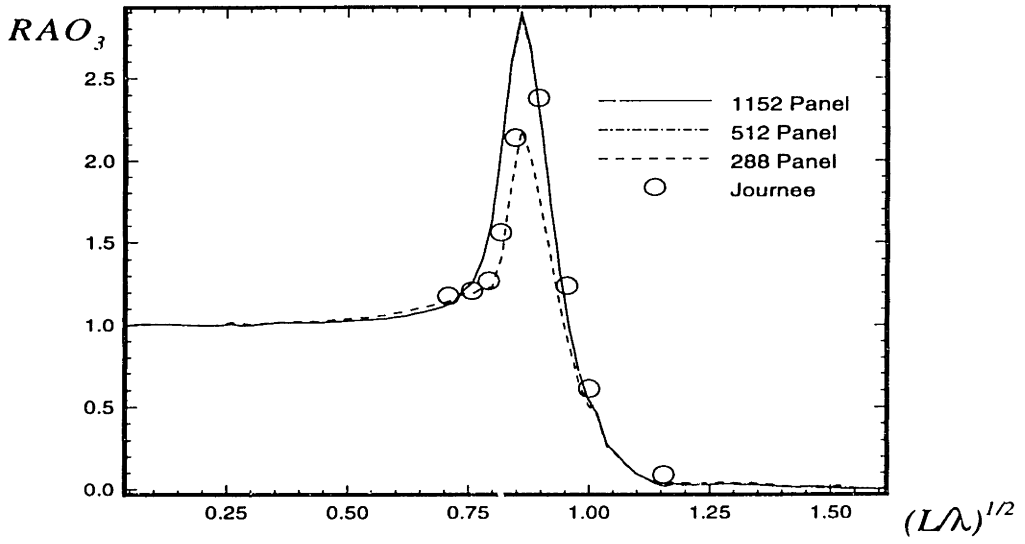

Figure 4-31: Wigley hull at $F_n = 0.3$, $\beta = \pi$, the heave response-amplitude operator.

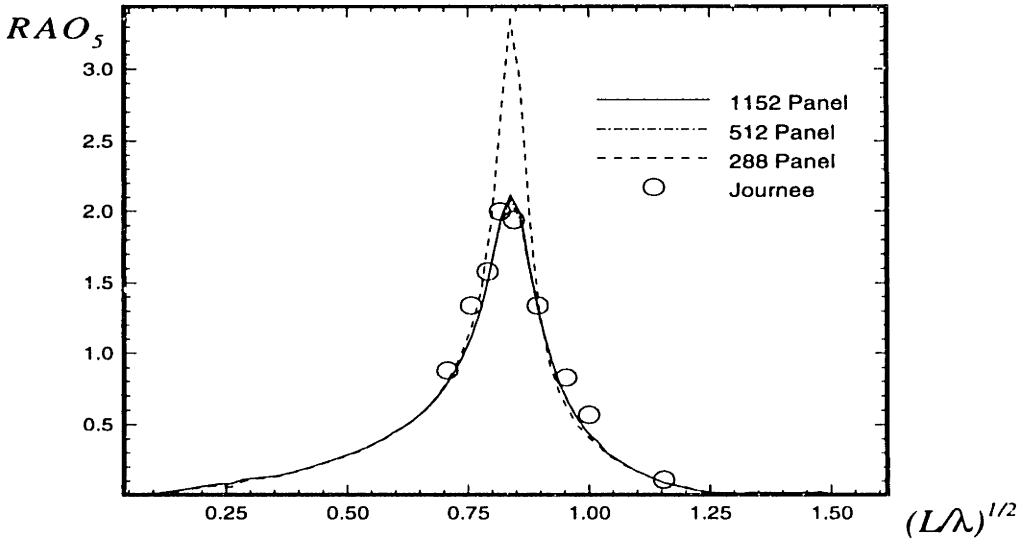

Figure 4-32: Wigley hull at $F_n = 0.3$, $\beta = \pi$, the pitch response-amplitude operator.

Chapter 5

Discussion

A numerical solution for predicting the flow around, and the motions of, a ship traveling in waves has been developed. The flow is assumed to be potential and the waves, as well as the body motions, are assumed to be small enough that a linearization of the boundary conditions about the incoming stream is justified. The resulting initial-boundary-value problem (the *Neumann-Kelvin* problem) is recast into integral equation form, using the transient free-surface Green function, and solved using a constant-strength planar-panel method.

A proof is proposed to show that solutions to the continuous integral equation are unique, and this argument applies as well to the source-only formulation as it does to the potential formulation. This is in contrast to the analogous, at zero speed, frequency domain equations which are known to have non-unique solutions at the irregular frequencies. A simple example is used to show that non-trivial homogeneous solutions to the transient integral equations are excluded by the initial conditions. Coarsely discretized numerical solutions of the transient integral equations do however show a non-physical oscillation in the solution. At zero forward speed this oscillation persists indefinitely in time and has a frequency content which is concentrated in narrow bands at the irregular frequencies, as is observed in calculations made directly in the frequency domain. At non-zero forward speed, the oscillation persists only as long as it takes the ship to travel one ship length (approximately) after the impulse. Compression of the oscillation in time leads to an expansion of its frequency content

until, at very high speeds, essentially the entire frequency spectrum becomes contaminated. Refinement of the spatial and temporal discretizations is shown to remove these errors from the solution although, in practice and especially at high speeds, it may be convenient to find a more efficient method of suppressing this behavior.

The radiation problem is presented in a generalized form, and techniques for continuing the forward-speed solution to large time and for obtaining an analytic Fourier transform of the asymptotics are developed. A close examination of the asymptotics of the numerical solution provides strong support for the theory that the linearized problem has (in general) a finite solution at the critical frequency corresponding to $\tau = 1/4$. The steady problem is posed as the steady-state limit of an impulsive acceleration of the ship to a forward speed U, making it identical to one of the radiation problems. A non-impulsive acceleration is also used to calculate the steady forces and the two results are in excellent agreement. Using an impulsive acceleration for this calculation is approximately six times faster however, since previously calculated Green function coefficients can be stored and re-used in this case. Source-only formulations are used in order to obtain robust calculations of fluid velocities and this is especially important in calculating the steady forces using a low-order panel method.

A procedure is developed which allows an improved approximation of the steady flow to be used in the unsteady body boundary conditions, without the need for numerical spatial derivatives of the potential over the body. Calculations of either the steady perturbation potential or the double-body potential are suggested as the obvious choices to use for this purpose. This requires a substantial increase in the computational effort but is a robust way of improving the satisfaction of the body boundary condition in a low-order panel method. Although i is not possible to obtain a similar improvement in the free-surface boundary condition, without abandoning the free-surface Green function, the prospect of analyzing ships with a full form provides some motivation to apply this procedure. Results using this technique are not presented as this work is preliminary.

A representative sample of calculations for both the steady and the unsteady forces on a ship in waves is included. Convergence of the calculations is shown, and these

point out that large errors can be expected in the steady forces when an overly coarse time discretization is used. Calculations using both the Wigley and the Series 60 hulls are in good agreement with experiments, as well as with calculations made using other linearized techniques. The Series 60 hull, like most real ships, has significant flare near the stern and this appears to magnify the non-physical oscillations in the solution.

Once the hydrodynamic coefficients for a particular hull have been calculated, the equations of motion can be solved in two ways: a time history of the incident wave elevation can be used to obtain time histories of the body motions by solving the transient equations of motion, or, time-harmonic motion can be assumed and the equations solved in the frequency domain. There are several reasons why it might be desirable to solve the equations directly in the time-domain: since time histories of the body and fluid motions are the result, this is the natural way to begin an analysis of the local flow by providing a boundary condition for a non-linear solution; non-linearities in the hydrostatic buoyancy and the roll damping forces, which are known to be significant in certain situations, can be included in obvious ways; and finally, one pseudo-random simulation can be Fourier transformed to obtain the entire response-amplitude operator (RAO). The thesis includes results from a sample simulation using the Wigley hull traveling at $Fn = 0.3$ in a Pierson-Moskowitz sea. A spectral analysis of these results produces RAO's which are in good agreement with experiment, as long as care is taken to integrate the equations of motion with great accuracy.

Suggestions for further research are the following. Most real ships have significant flare, yet this effect has been thrown out of the waterline integral, as well as the expression used to calculate the unsteady hydrodynamic forces. Including this effect should be investigated. This will require calculating girth-wise tangential derivatives of the potential numerically, and success will depend upon a careful discretization of the hull near the waterline. The effort involved in a transient calculation scales like the square of the total number of time steps used in the calculation and other time integration schemes should be investigated to determine whether the same accuracy can be achieved with less overall effort. The convergence of the solution is mainly determined by the irregular behavior of the solution which was demonstrated in Sec-

tion 3.6. For complicated geometries, and at high speeds, a substantial number of panels and a very small time step size are required to remove this effect. Experience with calculations made directly in the frequency domain suggests that it may be possible to removed these effects from the solution in other ways and this should be considered.

One of the most appealing aspects of the transient approach to predicting ship motions in a seaway is that it opens countless avenues for making further calculations. Particularly attractive is the idea of adding non-linear hydrostatics and non-linear roll damping to the simulation, while retaining the linearized hydrodynamic coefficients. Finally, to obtain truly non-linear solutions, it seems quite practical to consider the combination of a free-surface Green function exterior solution with a completely bounded interior region where Rankine singularities are used to satisfy the non-linear body and free-surface boundary conditions.

Appendix A

Derivation of the integral equations

A differential equation can always be recast in integral equation form, as long as the appropriate Green function exists. A Green function for the initial-boundary-value problem developed in Section 2.2 (without a body), is Equation (2.13) which is derived in Wehausen and Laitone [53] and is repeated here:

$$G(\vec{x};\vec{\xi},t-\tau) = G^{(0)} + H \tag{A.1}$$

where

$$G^{(0)}(\vec{x};\vec{\xi}) = \left(\frac{1}{r} - \frac{1}{r'}\right)$$

$$H(\vec{x};\vec{\xi},t-\tau) = 2\int_0^\infty dk\ \left(1 - \cos\left[\sqrt{gk}\,(t-\tau)\right]\right) \exp(kZ)\, J_0(kR),$$

$$\left.\begin{matrix} r \\ r' \end{matrix}\right) = \sqrt{(x-\xi)^2 + (y-\eta)^2 + (z \mp \zeta)^2}$$

$$Z = (z+\zeta)$$

$$R = \sqrt{(x-\xi)^2 + (y-\eta)^2}$$

and, J_0 is the Bessel function of zero order. It is straightforward to verify that this function satisfies the Laplace equation (except when $\vec{x} = \vec{\xi}$ where it is a delta function of strength 4π), the linearized free-surface boundary condition, and the initial conditions at $(t-\tau) = 0$. This is true in either the earth-fixed or the ship-fixed frames of reference and with respect to either the variables $(\vec{x}, t)$ or $(\vec{\xi}, \tau)$. We will begin in the earth-fixed coordinates.

A.1 An Integral Equation in Earth-Fixed Coordinates

This derivation of the body-exact integral equation follows Korsmeyer [25]. Apply Green's second identity to the time derivative of the total velocity potential, $\Phi_\tau(\vec{\xi}_0, \tau)$ and the above Green function, $G(\vec{x}_0; \vec{\xi}_0, t-\tau)$, (the spatial arguments will be dropped at this point for brevity)

$$\begin{aligned} \iiint_{\mathcal{V}(\tau)} d\mathcal{V}[\Phi_\tau(\tau)\,\nabla^2 G(t-\tau) - G(t-\tau)\,\nabla^2\Phi_\tau(\tau)] &= \\ \iint_{S(\tau)} d\vec{\xi}[\Phi_\tau(\tau)\,G_{n_\xi}(t-\tau) - G(t-\tau)\,\Phi_{\tau n_\xi}(\tau)] &= 0 \end{aligned} \qquad \text{(A.2)}$$

As illustrated in Fig. 2-1, the complete boundary surface S is composed of four elements,

$$S(t) = S_b(t) + S_f(t) + S_\infty + S_\epsilon$$

where S_ϵ is a small sphere of radius ϵ which excludes the point $\vec{x}$ from the fluid domain. The integral over S_∞ gives no contribution, since G_n, $\Phi_n \to 0$ as $R \to \infty$. If the point $\vec{x_0}$ is taken to lie on the body boundary, then the integral over S_ϵ becomes $2\pi\Phi_\tau$. This leaves

$$\begin{aligned} 2\pi\,\Phi_\tau(\tau) \quad &+ \iint_{S_b(\tau)} d\vec{\xi}\,[\Phi_\tau(\tau)\,G_{n_\xi}(t-\tau) - \Phi_{\tau n_\xi}(\tau)\,G(t-\tau)] \\ &+ \iint_{S_f(\tau)} d\vec{\xi}\,[\Phi_\tau(\tau)\,G_{n_\xi}(t-\tau) - \Phi_{\tau n_\xi}(\tau)\,G(t-\tau)] = 0. \end{aligned} \qquad \text{(A.3)}$$

By applying the divergence and transport theorems to equation (A.3) this may be written as

$$\begin{aligned}
&\frac{d}{d\tau}\int\int_{S_b(\tau)} d\vec{\xi}\,[\Phi G_n - G\Phi_n] - \int\int_{S_b(\tau)} d\vec{\xi}\,(\Phi G_{\tau n} - G_\tau \Phi_n) \\
&+\frac{d}{d\tau}\int\int_{S_f(\tau)} d\vec{\xi}\,[\Phi G_n - G\Phi_n] - \int\int_{S_f(\tau)} d\vec{\xi}\,(\Phi G_{\tau n} - G_\tau \Phi_n) \\
&\qquad\qquad +2\pi\,\Phi_\tau = 0. \qquad\qquad (A.4)
\end{aligned}$$

Now integrate over the entire time history, from t_0 to t,

$$\begin{aligned}
&\int\int_{S_b(t)} d\vec{\xi}\,[\Phi(t)G_n(0) - G(0)\Phi_n(t) - \Phi(t_0)G_n(t-t_0) + G(t-t_0)\Phi_n(t_0)] \\
&\qquad\qquad - \int_{t_0}^{t} d\tau \int\int_{S_b(\tau)} d\vec{\xi}\,(\Phi G_{\tau n} - G_\tau \Phi_n) \qquad (A.5) \\
&+\int\int_{S_f(t)} d\vec{\xi}\,[\Phi(t)G_n(0) - G(0)\Phi_n(t) - \Phi(t_0)G_n(t-t_0) + G(t-t_0)\Phi_n(t_0)] \\
&\qquad\qquad - \int_{t_0}^{t} d\tau \int\int_{S_f(\tau)} d\vec{\xi}\,(\Phi G_{\tau n} - G_\tau \Phi_n) \\
&\qquad\qquad +2\pi\,(\Phi(t) - \Phi(t_0)) = 0
\end{aligned}$$

Terms involving $\Phi(t_0)$ and $G(0)$ in the integral over the free-surface vanish due to initial conditions and the definition of $G^{(0)}$. Other terms in equation (A.5) may be related to each other by writing Green's second identity for the functions $\Phi(t_0)$ and $G(t-t_0)$, (as before the integral over S_ϵ gives $2\pi\Phi$ if the point $\vec{x}$ is taken to lie on the body surface)

$$\begin{aligned}
-2\pi\,\Phi(t_0) = &\int\int_{S_b(t)} d\vec{\xi}\,[\Phi(t_0)G_n(t-t_0) - G(t-t_0)\Phi_n(t_0)] \\
&- \int\int_{S_f(t)} d\vec{\xi}\,G(t-t_0)\Phi_n(t_0) \qquad\qquad (A.6)
\end{aligned}$$

Using this in equation (A.5) gives,

$$\begin{aligned}
2\pi\Phi(t) \;+&\int\int_{S_b(t)} d\vec{\xi}\,[\Phi(t)G_n(0) - G(0)\Phi_n(t)] - \int_{t_0}^{t} d\tau \int\int_{S_b(\tau)} d\vec{\xi}\,(\Phi G_{\tau n} - G_\tau \Phi_n) \\
&+\int\int_{S_f(t)} d\vec{\xi}\,\Phi(t)G_n(0) - \int_{t_0}^{t} d\tau \int\int_{S_f(\tau)} d\vec{\xi}\,(\Phi G_{\tau n} - G_\tau \Phi_n) = 0 \qquad (A.7)
\end{aligned}$$

Consider just the convolution integral over the free-surface,

$$I_{S_f} = -\int_{t_0}^{t} d\tau \iint_{S_f(\tau)} d\vec{\xi}\, (\Phi G_{\tau n} - G_\tau \Phi_n) \tag{A.8}$$

and apply the free-surface boundary condition to replace $\frac{\partial}{\partial n}$ with $-\frac{1}{g}\frac{\partial^2}{\partial \tau^2}$.

$$= \frac{1}{g}\int_{t_0}^{t} d\tau \iint_{S_f(\tau)} d\vec{\xi}\, \frac{\partial}{\partial \tau}(\Phi G_{\tau\tau} - G_\tau \Phi_\tau) \tag{A.9}$$

By looking down on the free-surface, i.e. the $z = 0$ plane, it is possible to write a two dimensional version of the transport theorem as follows,

$$\frac{d}{dt}\iint_{S_f(t)} d\vec{\xi}\, f = \iint_{S_f(t)} d\vec{\xi}\, \frac{\partial}{\partial t} f + \int_{C(t)} dl\, f\, \vec{U}\cdot\vec{n}_{2D} \tag{A.10}$$

where $C(t) = \Gamma(t) + C_\infty$ is the boundary of the free-surface. After applying this to equation (A.9) and using the boundary and initial conditions satisfied by Φ and G,

$$I_{S_f} = -\iint_{S_f(t)} d\vec{\xi}\, \Phi(t) G_n(0) - \frac{1}{g}\int_{t_0}^{t} d\tau \int_{\Gamma(\tau)} dl\, [\Phi G_{\tau\tau} - \Phi_\tau G_\tau]\vec{U}\cdot\vec{n}_{2D} \tag{A.11}$$

Finally, this may be combined with equation (A.7) to give an integral equation for the total velocity potential of a body with arbitrary speed $\vec{U}(t)$, in a reference frame which is fixed in space:

$$2\pi\Phi + \iint_{S_b(t)} d\vec{\xi}\, \left[\Phi G_n^{(0)} - G^{(0)}\Phi_n\right] - \int_{t_0}^{t} d\tau \iint_{S_b(\tau)} d\vec{\xi}\, (\Phi H_{\tau n} - H_\tau \Phi_n)$$
$$-\frac{1}{g}\int_{t_0}^{t} d\tau \int_{\Gamma(\tau)} dl\, [\Phi H_{\tau\tau} - \Phi_\tau H_\tau]\vec{U}(\tau)\cdot\vec{n}_{2D} = 0. \tag{A.12}$$

Here the definition of the Green function has been used to split it into its time-dependent and time-independent parts.

Equation (A.12) is often referred to as the *body non-linear* or the *body exact* formulation of the transient ship motions problem. The source formulation of this equation (B.4) is used for the special case of a non-impulsive acceleration of the ship to a steady forward speed in Section 3.7.1.

A.2 Steady Forward Speed

For the case of a ship moving with constant speed U_0 in the positive x_0 direction it is convenient to transform from stationary coordinates, $\vec{x_0}$, to the steadily translating frame of reference, $\vec{x}$. The only subtle point involved in this transformation is to recognize that the time derivative of a function in a moving system of coordinates is the substantial derivative of the same function in stationary coordinates, *i.e.*

$$\frac{\partial}{\partial t} f(\vec{x},t) = \frac{D}{Dt} f(\vec{x}_0,t) = \frac{\partial}{\partial t} f(\vec{x}_0,t) + \vec{U}(t) \cdot \vec{\nabla} f(\vec{x}_0,t).$$

Thus, the equivalent integral equation in translating coordinates is obtained upon making the following substitutions:

$$\vec{U} = (U_0, 0, 0), \qquad dl\, \vec{U} \cdot \vec{n}_{2D} = U_0\, n_1\, dl$$

$$S_b(t) = \bar{S}_b, \;\; \Gamma(t) = \bar{\Gamma}$$

$$x_0 = x + U_0 t, \; y_0 = y, \; z_0 = z, \; \vec{\nabla}_{x_0} = \vec{\nabla}_x$$

$$\frac{\partial}{\partial t} \rightarrow \frac{\partial}{\partial t} - U_0 \frac{\partial}{\partial x}.$$

With these substitutions, equation (A.12) becomes

$$\begin{aligned} 2\pi\Phi + \int\int_{\bar{S}_b} d\vec{\xi} \left[\Phi G_n^{(0)} - G^{(0)}\Phi_n\right] - \int_{t_0}^{t} d\tau \int\int_{\bar{S}_b} d\vec{\xi} \left(\Phi H_{\tau n} - H_\tau \Phi_n\right) \\ - \frac{U_0}{g} \int_{t_0}^{t} d\tau \int_{\bar{\Gamma}} n_1 dl \left[\Phi\left(H_{\tau\tau} - U_0 H_{\tau\xi}\right) - H_\tau\left(\Phi_\tau - U_0 \Phi_\xi\right)\right] \\ = -\frac{U_0}{g} \int_{t_0}^{t} d\tau \int\int_{\bar{S}_b} d\vec{\xi} \left[\Phi G_{\xi n} - G_\xi \Phi_n\right] \\ + \frac{U_0^2}{g} \int_{t_0}^{t} d\tau \int_{\bar{\Gamma}} n_1 dl \left[G_\xi\left(\Phi_\tau - U_0\Phi_\xi\right) - \Phi\left(G_{\xi\tau} - U_0 G_{\xi\xi}\right)\right]. \end{aligned} \tag{A.13}$$

If the waterline is traversed in the counter-clockwise direction, then $n_1 dl = -d\eta$, and the waterline term on the right hand side of equation (A.13) may be related through

Stokes' theorem to an integral over the free-surface:

$$\frac{1}{g}\int_{\Gamma} d\eta\ \left[G_{\xi}\left(\Phi_{\tau}-U_0\Phi_{\xi}\right)-\Phi\left(G_{\xi\tau}-U_0 G_{\xi\xi}\right)\right]=\int\int_{S_f} d\vec{\xi}\ \left[\Phi G_{\xi n}-G_{\xi}\Phi_n\right] \qquad \text{(A.14)}$$

Further, by applying Green's second identity to the functions $\Phi(\tau)$, and $G_{\xi}(t-\tau)$ (G_{ξ}, being a harmonic function) and integrating in time, it becomes clear that the entire right hand side of equation (A.13) vanishes, leaving:

$$\begin{aligned} 2\pi\Phi(\vec{x},t)+\int\int_{\bar{S}_b} d\vec{\xi}\ \left[\Phi(\vec{\xi},t)G_n^{(0)}(\vec{x},\vec{\xi})-G^{(0)}(\vec{x},\vec{\xi})\Phi_n\right](\vec{\xi},t) \qquad \text{(A.15)}\\ -\int_{t_0}^{t} d\tau\ \int\int_{\bar{S}_b} d\vec{\xi}\ \left[\Phi(\vec{\xi},\tau)H_{\tau n}(\vec{x},\vec{\xi},t-\tau)-H_{\tau}(\vec{x},\vec{\xi},t-\tau)\Phi_n(\vec{\xi},\tau)\right]\\ -\frac{U_0}{g}\int_{t_0}^{t} d\tau\ \int_{\bar{\Gamma}} n_1 dl\ \Big(\Phi(\vec{\xi},\tau)\left[H_{\tau\tau}(\vec{x},\vec{\xi},t-\tau)-U_0 H_{\tau\xi}(\vec{x},\vec{\xi},t-\tau)\right]\\ -H_{\tau}(\vec{x},\vec{\xi},t-\tau)\left[\Phi_{\tau}(\vec{\xi},\tau)-U_0\Phi_{\xi}(\vec{\xi},\tau)\right]\Big)=0\\ \vec{x}\in\bar{S}_b. \end{aligned}$$

The potential in the moving coordinates only differs from the potential in the stationary coordinates by the free-stream potential:

$$\Phi(\vec{x}_0,t)=\Phi(\vec{x},t)+U_0\,x.$$

Appendix B

Derivation of Source-Only Formulations

B.1 Source-Only Integral Equations

Consider a fictitious fluid domain which is interior to the body and bounded by $\bar{S}_b$ and an interior free-surface S_i. Define a potential $\Phi'(\vec{x},t)$ which solves the same boundary-value problem as Φ but in this interior domain. If the derivation of Equation A.15 is repeated for Φ', the only difference is that the vector normal to the body boundary is now pointing into the fluid domain and the result is

$$-2\pi\Phi'(\vec{x},t)+\int\int_{\bar{S}_b} d\vec{\xi}\,\left[\Phi' G_n^{(0)}-G^{(0)}\Phi'_n\right]-\int_{t_0}^{t} d\tau\,\int\int_{\bar{S}_b} d\vec{\xi}\,\left[\Phi' H_{\tau n}-H_\tau\Phi'_n\right] \quad \text{(B.1)}$$
$$-\frac{U_0}{g}\int_{t_0}^{t} d\tau\,\int_\Gamma n_1 dl\,\left[\Phi'\left(H_{\tau\tau}-U_0 H_{\tau\xi}\right)-H_\tau\left(\Phi'_\tau-U_0\Phi'_\xi\right)\right]=0$$

Now subtract Equation (B.1) from Equation (A.15), let $\Phi'=\Phi$ on $\bar{S}_b$, and define a source strength on the body as $\sigma(\vec{x},t)=\frac{1}{4\pi}(\Phi_n-\Phi'_n)$:

$$\Phi(\vec{x},t)=\int\int_{\bar{S}_b} d\vec{\xi}\,\sigma\,G^{(0)}+\int_{t_0}^{t} d\tau\,\int\int_{\bar{S}_b} d\vec{\xi}\,\sigma\,H_\tau \quad \text{(B.2)}$$
$$+\frac{U_0}{g}\int_{t_0}^{t} d\tau\,\int_\Gamma n_1 dl\,H_\tau\left[\left(\Phi_\tau-\Phi'_\tau\right)-U_0\left(\Phi_\xi-\Phi'_\xi\right)\right]$$

Since $\Phi = \Phi'$ on $\bar{S}_b$ for all time, $\Phi_t = \Phi'_t$. The x-derivative of the potential on the waterline can be written in a coordinate system with unit vectors $(\hat{n}, \hat{l}, \hat{s})$ which are tangent to and normal to the hull at the waterline:

$$(\Phi_\xi - \Phi'_\xi) = (\Phi_n - \Phi'_n)(\hat{n} \cdot \hat{\imath}) + (\Phi_l - \Phi'_l)(\hat{l} \cdot \hat{\imath}) + (\Phi_s - \Phi'_s)(\hat{s} \cdot \hat{\imath})$$

where $\hat{\imath}$ is the unit vector in the x-direction. Since $\Phi = \Phi'$ everywhere on the hull, the tangent l- and s-derivatives are also equal, and we are left with the following first-kind integral equation for the source-strength if the potential is known:

$$\Phi(\vec{x}, t) = \int\int_{\bar{S}_b} d\vec{\xi}\, \sigma(t)\, G^{(0)} + \int_{t_0}^{t} d\tau \int\int_{\bar{S}_b} d\vec{\xi}\, \sigma(\tau)\, H_t(t-\tau) - \frac{U_0^2}{g} \int_{t_0}^{t} d\tau \int_{\bar{\Gamma}} n_1^2 dl\, \sigma(\tau) H_t(t-\tau) \qquad \vec{x} \in \bar{S}_b \tag{B.3}$$

where we have used the relation $H_\tau = -H_t$.

The same technique can be applied to the body-exact integral equation (A.12) and the result is:

$$\Phi(\vec{x_0}, t) = \int\int_{S_b(t)} d\vec{\xi_0}\, \sigma(t)\, G^{(0)} + \int_{t_0}^{t} d\tau \int\int_{\bar{S}_b(\tau)} d\vec{\xi_0}\, \sigma(\tau)\, H_t(t-\tau) - \frac{1}{g} \int_{t_0}^{t} d\tau \int_{\Gamma(\tau)} n_1^2 dl\, U^2(\tau)\, \sigma(\tau) H_t(t-\tau) \qquad \vec{x} \in \bar{S}_b. \tag{B.4}$$

Here it is important to note that we have used the fact that

$$\frac{D}{Dt}(\Phi - \Phi') = (\Phi_t - \Phi'_t) + \vec{U}(t) \cdot (\nabla\Phi - \nabla\Phi') = 0$$

on the moving body surface $S_b(t)$, which means that (because the tangential derivatives of Φ and Φ' are equal)

$$(\Phi_t - \Phi'_t) = -(\vec{U} \cdot \vec{n})\, \sigma.$$

In practice the gradients of these equations are used to solve for the source strength, and in turn the fluid velocities, as discussed in Section 2.5.

B.2 Decomposition of the Radiation Source Strength

If radiation fluid velocities are of interest then it will be convenient to develop a decomposition of the source strength corresponding to the decomposed radiation potential of Section 2.8. An impulsive acceleration will be used as an example. As discussed in Section 2.8, the impulsive acceleration radiation potential can be decomposed into

$$\phi_k^{(2)} = \mathcal{N}_k h(t) + \mathcal{M}_k r(t) + \psi_k^{(2)} h(t).$$

We assume an analogous decomposition of the source strength so that

$$\sigma_k^{(2)} = \alpha_k h(t) + \beta_k r(t) + \gamma_k^{(2)} h(t) \tag{B.5}$$

where

$$\mathcal{N}_k(\vec{x}) = \int\int_{\bar{S}_b} d\vec{\xi}\, \alpha_k G^{(0)}, \qquad \mathcal{M}_k(\vec{x}) = \int\int_{\bar{S}_b} d\vec{\xi}\, \beta_k G^{(0)}, \tag{B.6}$$

and an integral equation for γ_k is obtained by substituting the decomposition of the source strength into Equation (2.15) and using the decomposition of the source strength appearing in Equation (B.5) along with the relations in Equation (B.6). The result is

$$\begin{aligned} \psi^{(2)}(\vec{x},t) = & \int\int_{\bar{S}_b} d\vec{\xi}\, \gamma_k(t)\, G^{(0)} \\ & + \int_0^t d\tau \int\int_{\bar{S}_b} d\vec{\xi}\, [\alpha_k + \beta_k \tau + \gamma_k(\tau)]\, H_t(t-\tau) \\ & - \frac{U_0^2}{g} \int_0^t d\tau \int_\Gamma n_1^2 dl\, [\alpha_k + \beta_k \tau + \gamma_k(\tau)]\, H_t(t-\tau). \end{aligned} \tag{B.7}$$

Again the gradients of these equations will allow calculations of the corresponding fluid velocities to be made.

Appendix C

Absence of Homogeneous Solutions to the Integral Equation

In this appendix we consider the fluid motions due to a two dimensional rectangular "barge" of infinite draft in order to show that the initial conditions make it impossible to construct a non-trivial homogeneous solution to the transient integral equation from the homogeneous solutions to the time-harmonic integral equation.

C.1 The Time-Harmonic Problem

Consider a two-dimensional barge of length $2L$ and infinite draft, with the coordinate system centered at the center of the barge on the free surface and with z positive upwards. A time-harmonic exterior solution to this problem can be written in integral equation form as

$$2\pi\tilde{\phi}(\vec{x},\omega) + \int\int_{\bar{S}_b} d\vec{\xi}\, \tilde{\phi}(\vec{\xi},\omega)\, \tilde{G}_{n_\xi}(\vec{x},\vec{\xi},\omega) = \int\int_{\bar{S}_b} d\vec{\xi}\, \tilde{\phi}_n(\vec{\xi},\omega)\, \tilde{G}(\vec{x},\vec{\xi},\omega) \qquad \vec{x} \in \bar{S}_b, \quad \text{(C.1)}$$

where the two-dimensional Green function is

$$\tilde{G} = \ln\frac{r}{r'} - 2\int dk \frac{e^{kZ}}{k-K}\cos\left[k(x-\xi)\right].$$

A homogeneous solution to this integral equation can be constructed by consid-

ering a fictitious flow interior to the barge defined by the potential $\tilde{\phi}'$. An integral equation representation for this potential is

$$-2\pi\tilde{\phi}'(\vec{x},\omega)+\int\int_{\bar{S}_b}d\vec{\xi}\;\tilde{\phi}'(\vec{\xi},\omega)\,\tilde{G}_{n_\xi}(\vec{x},\vec{\xi},\omega)=\int\int_{\bar{S}_b}d\vec{\xi}\;\tilde{\phi}'_n(\vec{\xi},\omega)\,\tilde{G}(\vec{x},\vec{\xi},\omega);\qquad \vec{x}\in\bar{S}_b. \tag{C.2}$$

If a homogeneous Dirichlet condition is imposed upon this potential, then the left hand side of Equation (C.2) vanishes, and

$$\int\int_{\bar{S}_b}d\vec{\xi}\;\tilde{\phi}'_n(\vec{\xi},\omega)\,\tilde{G}(\vec{x},\vec{\xi},\omega)=0.$$

This shows that, given a non-trivial eigensolution $\tilde{\phi}'$, there exists a distribution of normal velocity over the body surface with an exterior eigensolution which solves the homogeneous form of Equation (C.1).

The potential $\tilde{\phi}'$ satisfies the eigenvalue problem:

$$\begin{aligned}
\nabla^2\tilde{\phi}' &= 0 \quad \text{in } \mathcal{V}' \\
-\omega^2\tilde{\phi}'+g\tilde{\phi}'_z &= 0 \quad \text{on } z=0 \\
\tilde{\phi}' &= 0 \quad \text{on } \bar{S}_b \\
\nabla\tilde{\phi}' &\to 0 \quad \text{as } z\to-\infty,
\end{aligned} \tag{C.3}$$

where $\mathcal{V}'$ is the volume of fluid interior to the barge. The eigensolutions to this problem can be obtained using separation of variables, and they are

$$\tilde{\phi}'_i=\Re\{C_{(i+\frac{1}{2})}\cos(k_{(i+\frac{1}{2})}x)\,e^{k_{(i+\frac{1}{2})}z}e^{i\omega_{(i+\frac{1}{2})}t}+C_i\sin(k_ix)e^{k_iz}e^{i\omega_it}\}, \tag{C.4}$$

$$\omega^2=gk,\qquad k=\begin{cases}k_{(i+\frac{1}{2})}=\frac{(i+\frac{1}{2})\pi}{L}\\ k_i=\frac{i\pi}{L}\end{cases}\qquad i=0,1,...,\infty,$$

where C_i and $C_{(i+\frac{1}{2})}$ are complex constants and ω_i and $\omega_{(i+\frac{1}{2})}$ are the irregular frequencies for this geometry.

C.2 The Transient Problem

If it were possible to construct out of these time-harmonic eigensolutions a solution to the corresponding transient interior problem, then this transient interior solution could be used to force an exterior potential satisfying the homogeneous form of the transient integral equation. This is not possible however, because of the initial conditions, as is shown in the following.

Consider an interior flow which satisfies the following initial-boundary-value problem:

$$\begin{aligned} \nabla^2\phi' &= 0 && \text{in } \mathcal{V}' \\ -\omega^2\phi' + g\phi'_z &= 0 && \text{on } z = 0 \\ \phi' &= 0 && \text{on } \bar{S}_b \\ \nabla\phi' &\to 0 && \text{as } z \to -\infty \\ \phi'(x,0,0) &= \phi'_t(x,0,0) && = 0 \end{aligned} \tag{C.5}$$

Clearly the individual eigensolutions (C.4) do not satisfy the initial conditions, but it might be thought that a suitable combination might do so. To show that this is not possible, we propose a solution to this initial-boundary-value problem of the form

$$\phi'(x,z,t) = \sum_{i=0}^{\infty} \tilde{\phi}'_i \tag{C.6}$$

The function ϕ' satisfies all of the conditions in Equation (C.5) except for the initial conditions, so the coefficients $C_{(i+\frac{1}{2})}$ and C_i must be chosen to allow these conditions to be satisfied, *i.e.*:

$$\begin{aligned} &\sum_{i=0}^{\infty}[C^R_{(i+\frac{1}{2})}\cos(k_{(i+\frac{1}{2})}x) + C^R_i \sin(k_i x)] = 0 \\ &\sum_{i=0}^{\infty}[C^I_{(i+\frac{1}{2})}\cos(k_{(i+\frac{1}{2})}x) + C^I_i \sin(k_i x)] = 0 \\ &\qquad\qquad -L < x < L. \end{aligned} \tag{C.7}$$

[Superscript R and I indicate the real and the imaginary parts of the coefficient respectively.] Equation (C.7) defines Fourier series representations of two functions each of which is identically zero over the interval. Due to the orthogonality of the sine and cosine functions this is only possible if each coefficient is zero [17], thus the associated time-harmonic homogeneous solutions must be trivial in the transient integral equation.

Although this example considered a special geometry, we expect the initial conditions to rule out a non-trivial homogeneous solution in general.

Bibliography

[1] M. Abramowitz and I. A. Stegun. *Handbook of Mathematical Functions.* Dover Press, New York, 1964.

[2] H. Adachi and S. Ohmatsu. On the influence of irregular frequencies in the integral equation solutions to the time-dependent free surface problems. *J. Soc. Nav. Arch. Japan*, 146, 1979.

[3] R. F. Beck and A. R. Magee. Time domain analysis for predicting ship motions. In *Proc. IUTAM Symp. Dynamics of Marine Vehicles & Structures in Waves*, London, U.K., 1990.

[4] V. Bertram. A Rankine source approach to forward speed diffraction problems. In *Proc. 5th Intl. Workshop on Water Waves and Floating Bodies*, Manchester, U.K., 1990.

[5] H. B. Bingham, F. T. Korsmeyer, J. N. Newman, and G. E. Osborne. The simulation of ship motions. In 6^{th} *Intl. Conf. on Numerical Ship Hydro*, Iowa City, Iowa, 1993. University of Iowa.

[6] J.-M. Clarisse. *Numerical applications of the generalized method of steepest descents.* PhD thesis, MIT, Cambridge, MA, 1992.

[7] W. E. Cummins. The impulse response function and ship motions. *Schiffstecknik*, 9:101–109, 1962.

[8] T. Dagan and G. Miloh. Flow past oscillating bodies at resonant frequency. *Proc. 13th Symp. Naval Hydro.*, pages 355–373, 1980.

[9] N. Daoud. Potential flow near to a fine ship's bow. Technical Report 177, The Department of Naval Architecture and Marine Engineering, The University of Michigan, Ann Arbor, Michigan, 1975.

[10] Department of Ocean Engineering, Massachusetts Institute of Technology, Cambridge. *WAMIT; A radiation-diffraction panel program for wave-body interactions*, 1988.

[11] William Froude. On the rolling of a ship. *Trans. Inst. Naval Arch.*, 2:180–227, 1861.

[12] J. Gerritsma and W. Beukelman. Distribution of damping and added mass along the length of a ship model. Technical Report 21, Shipbuilding laboratory, Technological University - Delft, Delft, The Netherlands, 1963.

[13] J. Grue and E. Palm. Wave radiation and wave diffraction from a submerged body in a uniform current. *J. Fluid Mech.*, 151:257–278, 1985.

[14] M. D. Haskind. Two papers on the hydrodynamic theory of heaving and pitching of a ship. Technical Report 1-12, The Society of Naval Architects and Marine Engineers, 601 Pavonia Ave., Jersey City, New Jersey, 1953.

[15] T. H. Havelock. The resistance of a submerged cylinder in accelerated motion. *Quart. J. Mech. Appl. Math.*, 2:419–427, 1949.

[16] John L. Hess and A.M.O. Smith. Calculation of nonlifting potential flow about arbitrary three-dimensional bodies. *J. Ship Research.*, 8:22–44, 1964.

[17] F.B. Hildebrand. *Advanced calculus for applications.* Prentice-Hall, Inc., Englewood Cliffs ,N.J., 1976.

[18] M. A. Jaswon and G. T. Symm. *Integral equation methods in potential theory and elastostatics.* Academic Press, New York, 1977.

[19] F. John. On the motion of floating bodies II. *Comm. Pure and App. Math*, 3:45–101, 1950.

[20] J. M. J. Journée. Experiments and calculations on four Wigley hull forms. Technical Report 909, Delft University of Technology, Ship Hydromechanics Laboratory, Delft, The Netherlands, 1992.

[21] Oliver D. Kellog. *Foundations of potential theory.* Dover Press, New York, 1953.

[22] B. W. King. Time-domain analysis of wave exciting forces on ships and bodies. Technical Report 306, The Department of Naval Architecture and Marine Engineering, The University of Michiga , \nn Arbor, Michigan, 1987.

[23] B. W. King, R. F. Beck, and A. R. Magee. Seakeeping calculations with forward speed using time domain analysis. In *Proc. 17th Symp. Naval Hydro.*, The Hague, Netherlands, 1988.

[24] F. T. Korsmeyer. *The first- and second-order transient free-surface wave radiation problems.* PhD thesis, Massachusetts Institute of Technology, Cambridge, Massachusetts, 1988.

[25] F. T. Korsmeyer. Derivation of the body-exact integral equation. Unpublished Note, 1991.

[26] F. T. Korsmeyer. The time domain diffraction problem. In *The Sixth International Workshop on Water Waves and Floating Bodies*, Woods Hole, Massachusetts, 1991.

[27] F. T. Korsmeyer, C. H. Lee, J. N. Newman, and P. D. Sclavounos. The analysis of wave effects on tension leg platforms. In *OMAE Conference*, Houston, Texas, 1988.

[28] B. V. Korvin-Kroukovsky. Investigation of ship motions in regular waves. *Trans. Soc. Nav. Archit. Mar. Eng.*, 63:386–435, 1955.

[29] C. H. Lee and P. D. Sclavounos. Removing the irregular frequencies from boundary integral equations in wave-body interactions. *J. Fluid Mech.*, 207:287–418, 1989.

[30] S. J. Liapis. *Time domain analysis of ship motions.* PhD thesis, The Department of Naval Architecture and Marine Engineering, The University of Michigan, Ann Arbor, Michigan, 1986.

[31] S. J. Liapis. Time domain analysis of ship motions. Technical Report 302, The Department of Naval Architecture and Marine Engineering, The University of Michigan, Ann Arbor, Michigan, 1986.

[32] M. J. Lighthill. *Fourier Analysis and Generalised Functions.* Cambridge University Press, Cambridge, 1958.

[33] W. M. Lin and D. K. P. Yue. Numerical solutions for large-amplitude ship motions in the time domain. In *Eighteenth Symp. on Nav. Hydro.*, Ann Arbor, Michigan, 1990.

[34] W. M. Lin and D. K. P. Yue. Time-domain analysis for floating bodies in mild-slope waves of large amplitude. In *8th Intl. Workshop Water Waves & Floating Bodies*, St. John's, Newfoundland, 1993.

[35] Y. Liu and D. K. P. Yue. On the solution near the critical frequency for an oscillating and translating body in or near a free surface. *J. Fluid Mechanics*, 254:251–266, 1993.

[36] Y. Liu and D. K. P. Yue. On the time dependence of the wave resistance of a body. *Submitted for publication*, 1994.

[37] H. Maruo. Modern developments of the theory of wave-making resistance in the non-uniform motion. *The Society of Naval Architects of Japan, 60th anniversary series*, 2:1–87, 1957.

[38] J.H. McCarthy editor. Overview of results. In *First Workshop Ship Wave-Resistance Computations*, David Taylor Naval Ship Research Center, Bethesda, MD, 1979.

[39] D. E. Nakos, D. E. Kring, and P. D. Sclavounos. Rankine panel methods for time-domain free surface flows. In *6th Intl. Conf. Num. Ship Hydro.*, U. Iowa, Iowa City, 1993.

[40] D. E. Nakos and P. D. Sclavounos. Ship motions by a three dimensional Rankine panel method. In *Eighteenth Symp. on Nav. Hydro.*, Ann Arbor, Michigan, 1990.

[41] J. N. Newman. The theory of ship motions. *Advances in Applied Mechanics*, 18:[illegible]-283, 1978.

[42] J. N. Newman. The approximation of free-surface Green functions. In P. A. Martin and G. R. Wickham, editors, *Wave Asymptotics*, pages 107–135. Cambridge University Press, 1992.

[43] F. Noblesse editor. Summary of the cooperative experiment on Wigley parabolic model in Japan. In *Second Workshop Ship Wave-Resistance Computations*, David Taylor Naval Ship Research Center, Bethesda, MD, 1983.

[44] T. F. Ogilvie. Recent progress toward the understanding and prediction of ship motions. In *The Fifth Symposium on Naval Hydrodynamics*, pages 3–128, Bergen, 1964.

[45] T. F. Ogilvie and E. O. Tuck. A rational strip theory for ship motions, part 1. Technical Report 013, The Department of Naval Architecture and Marine Engineering, The University of Michigan, Ann Arbor, Michigan, 1969.

[46] T.F. Ogilvie. Singular-perturbation problems in ship hydrodynamics. *Adv. Appl. Mech.*, 17:91–188, 1977.

[47] P.H. Roberts. Thomas Henry Havelock 1877-1968 Section II. Scientific Work. *Biographical Memoirs of Fellows of The Roy. Soc.*, 17:327–377, November, 1971.

[48] Johan E. Romate. *The numerical simulation of non-linear gravity waves in three-dimensions using a higher order panel method.* PhD thesis, Twente University, The Netherlands, , 1989.

[49] N. Salvesen, E.O. Tuck, and O. Faltinsen. Ship motions and sea loads. *Soc. Nav. Archit. Mar. Eng., Trans.*, 78:250–287, 1970.

[50] J. J. Stoker. *Water Waves.* Interscience Publishers, Inc., New York, 1957.

[51] Sir W. Thompson (Lord Kelvin). On ship waves. *Proc. Inst. Mech. Eng.*, Popular lectures iii:482, Aug. 3, 1887.

[52] J. V. Wehausen. Effect of the initial acceleration upon the wave resistance of ship models. *Journal of Ship Research*, pages 38–50, 1964.

[53] J. V. Wehausen and E. V. Laitone. Surface waves. In *Handbuch der Physik*, pages 446–778. Springer, 1960.